

ALGERIAN DEMOCRATIC AND POPULAR REPUBLIC
MINISTRY OF HIGH EDUCATION AND SCIENTIFIC
RESEARCH



UNIVERSITY BROTHERS MENTOURI CONSTANTINE 1

FACULTY OF SCIENCES EXACTES

PHYSICS DEPARTMENT

Order N°:112/D3c/2018

Series:10/Phy/2018

THESIS

PRESENTED FOR LMD DOCTORAT DEGREE REQUIREMENT

SPECIALITY " Physics of Materials and Applications".

THEME

***Study of the order disorder transitions and the mechanical properties in the
metallic alloys (AuCu and AuCuAg)***

By

Imene LAMIRI

Defended on : 12/11 /2018

Jury committee:

President :	M.Boucheur	Prof.	Univ. Brothers Mentouri Constantine 1
Advisor :	D.Hamana	Prof.	Univ. Brothers Mentouri Constantine 1
Examiners :	S.Achour	Prof.	ENP - Constantine
	S. Belhas	Prof.	Univ. of Batna Hadj Lakhder
	L.Hadjadj	Prof.	Univ. Brothers Mentouri Constantine 1
	L.Chetibi	M.C.A.	ENP - Constantine

*To my parents Leloucha and Mohand
and my brother Elias
and my sisters Miled, Wafa
and especially Farah.*

Acknowledgements

For most, I would like to express my sincere gratitude to my advisor Prof. **Djamel Hamana** for the all the direction of this thesis. Moreover, all the members of Material Science and Application research unit in the university of Constantine.

A special acknowledgement for the (**PNE**) scholarship that allowed me to collaborate with two efficient research groups in Spain and Switzerland.

A special acknowledgement for Prof. **Santiago García Granda** and Prof. **José Rubén García Menéndez** for their co-supervision and continuous support. For **Mohammed Said Mohammed Abdelbaky**, for his efficiency, presence and enthusiasm during all this work. A special gratefulness for Dr. **David Martínez Blanco** for his great contribution, patience, motivation and scientific support. And all the research group **SYSTAM** in university of Oviedo.

I would like also to thank warmly Prof. **Daniele Mari** and Dr. **Iva Tkalcec** for their support, collaboration, guidance and knowledge. Furthermore, all the members of the mechanical spectroscopy group in Ecole Polytechnique de Lausanne (**EPFL**).

My thanks are addressed to Prof. **M.Boucheur** who has accepted to chair my thesis jury.

My sincere thanks are addressed to Prof. **S.Belhas** for here kind acceptance to make a part of the jury.

My worm thanks go to Prof. **S.Achour** who agreed to be the examiner of this work. I also thank him for his kindness, his availability, his advice and his patience, through discussions that I had with him.

I address my thanks to Dr. **L.Chetibi** who agreed to review this work and for her guidance and counseling during the work.

I would like also to thank warmly Prof **L. Hadjadj** for his acceptance to judge this work.

Contents

General introduction	1
I: Phase transformations and order-disorder transitions.....	4
Introduction	4
1.1. The solid solution	4
1.2. Types of solid solutions	5
1.2.1. Substitutional Solid Solutions.....	5
1.2.2. Interstitial Solid Solutions	7
1.3. Intermetallic compounds	8
1.4. Definition of the phase transformations.....	8
1.5. Types of phase transformations in solid state	9
1.5.1. Diffusional transition.....	9
1.5.2. Diffusionless transition	9
1.5.3. Dilational (dilatational) transition	10
1.6. Order - disorder transitions.....	10
1.6.1. Definition and basic concepts.....	10
1.6.2. Characteristics of order disorder transformation	14
1.6.3. The order degree parameters	14
1.6.4. Variation of the order parameter with the temperature.....	16
1.6.5. The atomic model of the interface between an ordered phase and another disordered	17

1.6.6. Different steps of the order disorder transformation	18
1.6.7. The ordering and antiphase boundaries (APB)	20
1.6.8. Superdislocations	23
1.6.9. The Influence of the order on the physical properties of the alloys	27
II: Characteristics and ordering process in AuCu and AuCuAg systems	30
Part I: Order-disorder transitions in the AuCu binary system	
<i>Introduction</i>	30
2.1.1. The order in AuCu system.....	30
2.1.2. Equilibrium phase diagram of AuCu binary system	31
2.1.3. The ordered phase AuCu	33
2.1.4. The ordered phase Au ₃ Cu.....	34
2.1.5. The ordered phase AuCu ₃	34
2.1.6. Stability of AuCu ₁₁ phase	35
2.1.7. Types of boundaries in Au-Cu binary system	36
2.1.7.1. The structure AuCu ₁₁	36
2.1.7.2. The structure AuCu ₃	37
2.1.8. Vacancies effect on the order processes	38
2.1.8.1. Punctual defects "vacancies"	38
2.1.8.2. Identification of vacancies	39
2.1.8.3. Trapping of vacancies during quenching.....	40
2.1.8.4. Accelerated diffusion by quenching.....	40

2.1.8.5. Ordering of quenched alloys	40
Part II: Order-disorder transitions in the AuCuAg ternary system	
Part III: Mechanical behavior of gold alloys	
2.III.1. Some previous mechanical results for AuCu and AuCuAg systems: .	45
2.III.2. Zener Relaxation near Order-Disorder Transitions	46
III: Materials and Experimental Techniques	
3.1. Studied alloys and applied heat treatments.....	49
3.2. The used characterization techniques.....	50
3.2.1. Electron probe microanalysis (EPMA).....	50
3.2.2. Differential Scanning Calorimetry (DSC).....	51
3.2.3. Dilatometric analysis	52
3.2.4. Scanning Electron Microscopy (SEM).....	53
3.2.5. Scanning Tunneling Microscopy (STM)	55
3.2.6. X-Ray Photoelectron Spectroscopy (XPS).....	57
3.2.7. X-Ray Diffraction (XRD)	59
3.2.8. Forced torsion pendulum	61
3.2.9. Quantitative elemental depth profile analysis.....	63
IV: Results and discussions.....	
Part I: Kinetic study of the metastable phase in 12-carat compositions	
4.1.1. Results of previous experiments on AuCu equiatomic system	64
4.1.2. DSC and Dilatometric studies.....	65

4.I.2. Morphological study (SEM and STM).....	70
4.I.2.1. SEM study from the disordered state	70
4.I.2.2. SEM study from the ordered state.....	78
4.I.3. STM study	799
4.I.4. Further techniques	80
Conclusion of the part I	81

Part II: Trial for characterization of the metastable phase at low temperature in 18 carat binary gold alloys Au-25wt.%Cu

4.II.1. DSC and dilatometric results	84
4.II.2. Morphological study	87
4.II.3. X-Ray Photoelectron Spectroscopy (XPS)	93
4.II.4. Quantitative elemental depth profile analysis	96
4.II.5. Electrical Resistance study.....	96
Conclusion of the part II	98

Part III: Investigation of the order -disorder phase transition series in 18 carat binary gold alloys Au-25wt.%Cu by in-situ temperature XRD and mechanical spectroscopy

4.III.1. In-situ XRD structural study.....	99
4.III.2. Discussion of the structural results	1133
4.III.2.1. Upon heating.....	113
4.III.2.2. Upon cooling	114
4.III.3. Mechanical study.....	114

4.III.4. Discussion of the mechanical results	117
4.III.4.1. Upon heating.....	117
4.III.4.2. Upon cooling	118
Conclusion of the part III	118

**Part IV: Extra structural results for the ternary 18-carat composition Au-7wt.%Cu-
18wt.%Ag**

General conclusion.....	121
-------------------------	-----

General introduction

In the history, metals stand for a very special class of materials, because metals are stable enough to remain solid at room temperature. Therefore, metals have long been used to understand the nature of materials. Part of the advantages for metals in scientific research is due to some of their simple atomic arrangements or crystal structures. Metals are frequently mixed to improve their properties, mechanically or physically. By mechanical properties, we mean to make the materials harder and stronger.

Order and disorder in materials are omnipresent in nature in minerals, polymers, glasses, metal alloys, and the like. In physics of Materials, order-disorder transformation has been studied for a long time in different intermetallic systems [1]. Tamman in 1919 [2] has guess for the first time the existence of order; Bain in 1923 [3], Johansson et Linde en 1925 [3] have shown this transformation by X-ray diffraction (XRD). In 1934 Bragg and Williams described this transition observed in Cu-Zn alloys by the existence of a state in which groups of atoms are ordered in a crystal lattice [4]. Basing on the spectrum of DRX, they were able to show that below a certain temperature of transition the atoms are ordered on two different sub-lattices which interpenetrate [4].

Since the dawn of human civilization, gold has been one of the most appealing and sought-after elements of the periodic system. With its high corrosion resistance the defining quality of noble metals it suggested itself as the base material or protective coating of works and ornaments created to stand the test of time. Its distinctive color stands out against the grayish monotony displayed by most metals (the only other exceptions being copper and caesium). These properties combined with its rarity qualifies gold as a precious metal, a perception that, to the casual observer, is further reinforced by its high specific weight. Historically, gold has therefore become a standard for monetary exchange and reserve assets in many parts of the world. In the industrial age, gold found many a new application: in electronics for its good conductivity and chemical passivity; in optics for its excellent reflectivity of infrared light; and, more recently, in organic chemistry for the catalytic

properties of gold nanoparticles [5]. However, to this day the lion share of gold has been and is being used for jewelry production. It accounted for 58% (2137.5 tonnes) of global gold demands in 2008, and even 68% during the two preceding years. The jewelry demand is roughly matched by the annual output of today's gold mines worldwide[6].

Pure gold, with a Vickers hardness of only 20 to 30 HV [7] (depending on purity), is too soft for almost all jewelry purposes as the final product would easily deform and show poor resistance to wear. It must thus be alloyed to achieve reasonable hardness values, ideally 300 HV or more in the finished product. To reassure customers, these gold alloys are hallmarked with their fineness (mass of gold per thousand) or caratage (24 carat equaling 100 weight-percent). In many countries legislation restricts tradable gold alloys to certain compositions. Most high-quality jewelry is therefore made of 18-carat gold, an international standard cartage combining high value with good resistance to tarnish, corrosion, and wear[8].

Yellow gold alloys have a long tradition in jewelry, watch-making and dental prosthesis. Most "golden" rings or watches are made from the 18-carat alloy containing 12.5 weight-% of each copper and silver, which imitates the color of pure gold. The phase diagram of Au–Cu–Ag has been studied for almost 100 years[9]. It is a ternary alloy system of particular interest as it inherits the immiscibility gap from the binary silver–copper alloys as well as the tendency to form ordered phases from gold–copper. Both mechanisms, phase separation (into a silver-rich and a copper-rich phase) and atomic ordering (within the copper-rich phase), may lend the alloy a much desired property: age-harden ability[10]. An age-hardenable material offers the advantage that the jeweler can work or machine the product in a soft and ductile state (the annealed and quenched solid solution), and eventually finish the product by means of a simple heat treatment rendering the material hard and resistant. However, even in the finished product the material must meet certain requirements as to its ductility. If it is too brittle, certain elements, like clockwork springs or watchstrap pins, may not withstand the stresses they are subject to in everyday situations, and break or crack. It is therefore important to control the phase transformation process for any given alloy, which requires knowledge of transition temperature and transition times.

The goal of this thesis is to contribute to a fundamental understanding of phase transitions in 18-carat and 12-carat binary and ternary gold alloys by studying the order disorder transitions and dynamic processes at the microstructural level. The methods of choice for this endeavor is in-situ structural study (XRD) and mechanical spectroscopy. The in-situ XRD to understand the phase transitions upon the thermal cycles, and the mechanical spectroscopy as experimental technique that probes the mechanical response of a specimen (deformation/strain) to a periodic external excitation (applied stress). Mechanical spectroscopy being sensitive to point defect relaxations, grain boundary sliding and dislocation motion, it can yield data on atomic diffusion as well as the mobility of the two mediators of plastic deformation, grain boundaries and dislocations. While the primary objective is to present a comprehensive interpretation of the structural transitions and mechanical spectra, further emphasis will be placed on implications with regard to the order-disorder transitions, namely the determination of the mechanical properties of the alloys. Both studies, may be exploited to optimize material properties such as hardness and ductility. In addition, we used two essential methods very sensitive to the order state: dilatometry and differential scanning calorimetry (DSC). Complimentary techniques have been used to clarify some details during the study, using SEM, STM, XPS, and MFM.

Thesis outline

The **first chapter** presents a brief review on the literature about the phase transitions in general with focus on order-disorder transitions.

The **second chapter**, presents a brief review on the literature about the characteristics and ordering process in AuCu and AuCuAg systems

In chapter three, the alloys studied and the materials used in the measurements as well as the experimental techniques are described. The focus is set on structural and mechanical spectroscopy.

Chapter four, presents the experimental results.

***I: Phase transformations and order-disorder
transitions***

Introduction

Two types of order can be found in solid materials "structural order" and "magnetic order"[11]. The structural order is based on the phenomenon of ordering Atoms or molecules, whereas the magnetic order is related to the spontaneous ordering of the magnetic moments (without an external magnetic field)[11]. This study is interested with the structural order.

The use properties of metals and alloys are determined in large part by the morphology and degree of dispersion of constitutive phases, i.e. by the microstructure. Today, mastering the microstructures in order to optimize this or that property can be achieved by suitable thermal or thermomechanical treatments, that are based on the possibilities of structural transformations.

Understanding the various aspects of phase transformations becomes necessary for mastering the technology of metallic materials. Among the most interesting solid-state phase transformations that have long attracted a good number of researchers we are interested with the order-disorder transformation.

1.1. The solid solution

When two metals are completely soluble in the liquid and in the solid state, it means that they form a solid solution. In other words, when homogeneous mixtures of two or more kinds of atoms (of metals) occur in the solid state, they are known as solid solutions. The more abundant atomic form is referred as solvent and the less abundant atomic form is referred as solute [12].

The chemical composition (the elements of which it is made and their relative proportions) and crystalline structure (the three-dimensional arrangement of its constituent atoms or ions) are the two most fundamental properties that characterize and distinguish an alloy from other alloys. Thus, a given mineral has a specific composition that in part defines it.

Most alloy crystal structures can have an extensive substitutions between certain elements among specific sites and can thus exhibit extensive variation in chemical composition; in this case it is called a solid solution.

It is convenient to think of the alloy structure as a collection of crystallographic sites with specific linkages and arrangements; in which variable but specific elemental constituents, can reside, this is in cases where solid solutions occur. Indeed, Klein and Hurlbut (1999) state that "a solid solution is a mineral structure in which specific atomic site(s) are occupied in variable proportions by two or more different chemical elements (or groups) [13].

1.2. Types of solid solutions

Two types of solid solutions are distinguishable : (a) Substitutional solid solutions. (b) Interstitial solid solutions.

1.2.1. Substitutional Solid Solutions

The solid solution is a substitutional solid solution when the atoms of the solvent or parent metal are replaced in the crystal lattice by atoms of the solute metal. As an example, copper atoms may substitute with nickel atoms without disturbing the F.C.C. structure of nickel Fig.1.1(a). In the substitutional solid solutions, the substitution can be either disordered or ordered. Fig.1.1(b), shows disordered substitutional solid solution. In this case, the solute atoms have substituted disorderly for the solvent atoms on their lattice site. Fig.1.1(c) shows an ordered substitutional solid solution. In this case, the solute atoms have substituted in an orderly manner for the solvent atoms on their lattice site.

-Hume Rothery rules for the formation of substitutional solid solutions

Hume Rothery formulated certain rules which govern the formation of substitutional solid solutions by studying a number of alloy systems, [12]. As following:

(a) Crystal structure factor: For complete solid solubility, the two elements should have the same type of crystal structure i.e., both elements should have either F.C.C. or B.C.C. or H.C.P. structure [12].

(b) Relative size factor: When the difference of the size (atomic radii) between two elements increases the solid solubility becomes more restricted. For extensive solid solubility the difference in atomic radii of two elements should be less than about 15 percent. In case the relative size factor is more than 15 percent, solid solubility is limited. For example, both silver and lead have F.C.C. structure and the relative size factor is about 20 percent. Therefore the solubility of lead in solid silver is about 1.5 percent and the solubility of silver in solid lead is about 0.1 percent. Copper and nickel are completely soluble in each other in all proportions. Because they have the same (F.C.C) crystal structure but differ in the atomic radii with about 2 percent [12].

(c) Chemical affinity factor: when the two metals have lesser chemical affinity, the solid solubility is favored. In general, two metals have greater chemical affinity when they are widely separated in the periodic, and so, they more likely will form some type of compound instead of solid solution.

(d) Relative valence factor: The dissolutions of a metal of high valence in a metal of low valence is greater than the dissolutions of a metal of low valence in a metal of high valence. For example in aluminium-nickel alloy system, nickel (lower valence) dissolves 5 percent aluminium but aluminium (higher valence) dissolves only 0.04 percent nickel [12].

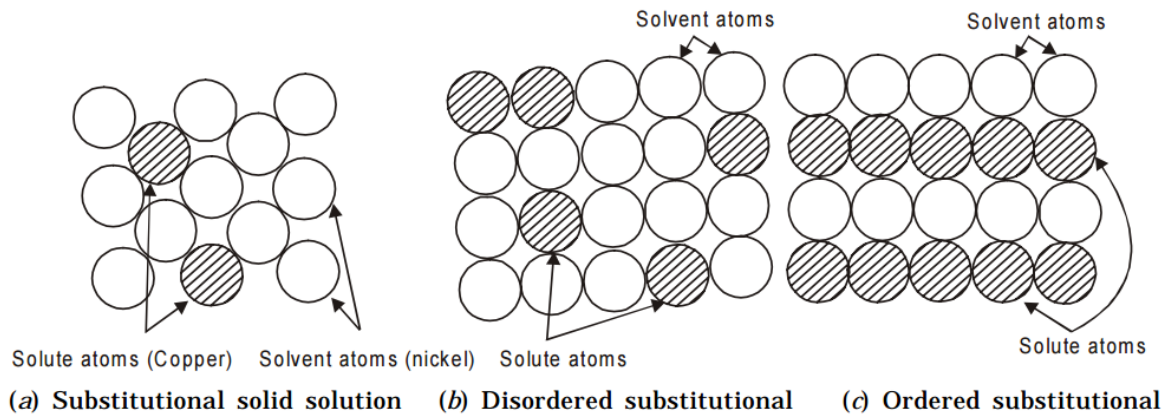


Fig. 1.1. Substitutional Solid Solutions [12].

1.2.2. Interstitial Solid Solutions

The solute atom does not displace a solvent atom in case of interstitial solid solutions, it rather enters in one of the holes or interstices between the solvent atoms. An excellent example is iron-carbon system which is shown in Fig.1.2 [12].

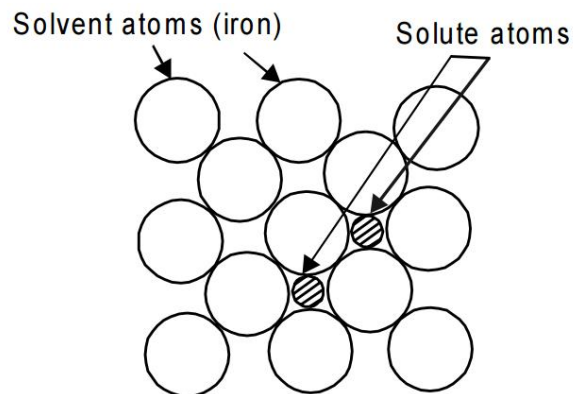


Fig.I.2. Interstitial solid solution [12]

1.3. Intermetallic compounds

When, one metal (for example magnesium) has chemical properties which are strongly metallic and the other metal (for example antimony, tin or bismuth) has chemical properties which are only weakly metallic, then, they form intermetallic compounds. Examples of intermetallic compounds are Mg_2Sn , Mg_2Pb , Mg_3Sb_2 and Mg_3Bi_2 . These intermetallic compounds have higher melting point than either of the parent metal. This higher melting point indicates the high strength of the chemical bond in intermetallic compounds. Therefore, for high temperature structural applications the ordered intermetallic compounds have attracted much interest [14,15,16,17]

1.4. Definition of the phase transformations

A phase is the homogeneous arranged portion of atoms. And it constitutes the system. A phase is physically distinguished by its state: gas, liquid or solid. It is homogeneous on a macroscopic scale for constant composition. Finally, a phase can be separated from the rest of the system, which means that the extensive quantities vary continuously within the phase, while the discontinuities are present at phase boundaries. Under these conditions, if the thermal equilibrium stability criteria are satisfied, the phase remains stable and homogeneous, and has specific properties to this state.

We call phase transformation (or phase transition) the formation (disappearance), within a system, of at least one phase or disappearance (formation) of at least one phase. Where this phase transformation means a change in the properties of the studied system, caused by the variation of an external particular parameter (temperature, pressure) or by the application of stress [18].

These transformations can be caused by either variations in the intensive parameters (T, P) that is imposed to the system, or from extensive quantities (S, V), by exchange with the external environment.

1.5. Types of phase transformations in solid state

The phase transformation of a solid to another solid state is subject to the same rules that the transformation from liquid to solid state. Solidification "requires a supercooling to form stable germs, and the growth of the phase, at an important exception, is dependent on the diffusion. The presence of internal surfaces and imperfections facilitates greatly the germination.

1.5.1. Diffusional transition

They are transformations that allow a new phase to form by breaking the atomic bonds of the mother phase and the disordered redistribution of the atoms, within the solid, that move randomly over long distances [18]. Thus, it is a transition that requires the rearrangement of atoms, ions, or molecules in a manner that cannot be accomplished by a cooperative atomic displacement; it may require the movement of atoms, ions, or molecules over distances significantly larger than a unit cell. Example: The transition of graphite (hexagonal sheets of three-coordinated carbon atoms) to diamond (infinite three-dimensional framework of four-coordinated carbon atoms) at high temperature and pressure [19].

1.5.2. Diffusionless transition

A transition that does not involve long-range diffusion of atomic species over distances significantly greater than a typical interatomic distance [19]. They are also called, athermal transformations; they do not require a diffusion of atoms over a long distance but the displacement of a large number of these atoms, with faint amplitude (interatomic distance). In these transformations there is no change in the chemical composition and they generally spread independently of the time. Moreover the amount of phase formed depends only on the temperature level. It is noted that the displacive transformation may exist at any temperature during heating or very rapid cooling [18]. Thus, in some way it is non thermally activated transition.

1.5.3. Dilational (dilatational) transition

A transition in which the crystal structure is dilated (or compressed) along one (or more) crystallographic direction(s) while the symmetry about that direction is retained. Examples:

- (i) The transition of a CsCl-type structure to a rock salt structure in which dilation occurs along the three-fold axis.
- (ii) The transition at T_D in quenched NiS in which volume expansion occurs without change of symmetry on going from a metallic state ($T > T_D$) to a semiconducting state ($T < T_D$)

1.6. Order - disorder transitions

1.6.1. Definition and basic concepts

In a pure metal A, a foreign atoms B can be added without changing the crystal structure of the basic metal A, we obtain the solid solution A-B. In alloys considered here, the atoms of element B in solution in the metal A are placed in substitution of the atoms A on the lattice nodes. Consider now an ordered alloy comprising the elements A and B having a different steric hindrance. The regular arrangement of the atoms A and B on the lattice should be made in such a manner as to obtain a structure as compact as possible. In general, there is a possibility of order, if from the energetic point of view, the interatomic bonds A-B are favored over A-A and B-B bonds: is the alloying effect [18].

An alloy would be chemically disordered for an infinitely high temperature. Namely, the arrangement of the atoms on the lattice would be completely random. In this case, the configuration of a binary alloy consisting of atoms A and B is defined by a probability of pairs AB equal to the atomic fractions C_A and C_B .

In the ideally ordered case, the crystal structure of an alloy close to the composition AB, AB₂, AB₃, ..., has sub-lattices α , β , ..., totally occupied with atoms of a given species: the alloy is said to be large distance ordered (LDO) [1]. The

Fig.1.3 shows an example of a large distance ordered alloy, with the composition AB.

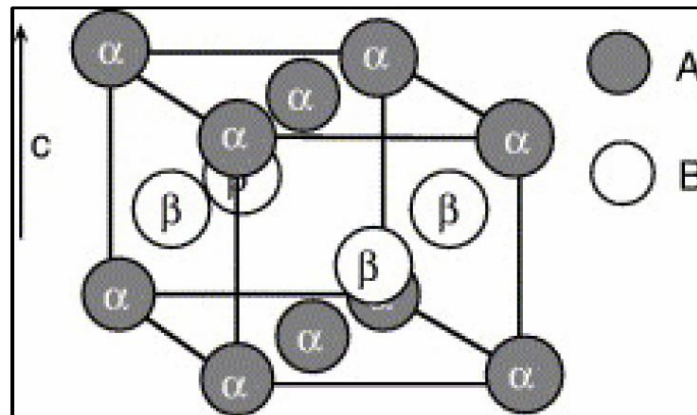


Fig.1.3. Cell of $L1_0$ structure, with the two types of sites (α and β) that are occupied by the atoms A and B. The axis c represents the direction of the modular composition in large ordered structures distance [20].

Assuming that we have an equal number of different atoms A and B on the one hand, with two types of sites α and β on the other hand. Each site α is surrounded only by β sites and vice versa (Fig.1.4). The identical sites (α or β) are the next closest neighbors. If energy of interaction between two neighboring atoms V_{AB} is lower than the average interaction energy between atoms of the same species $(V_{AA} + V_{BB}) / 2$, one should expect to find the system completely ordered at very low temperature ; all the A atoms occupy the α sites and the B atoms occupy the β sites because this arrangement corresponds to the lowest energy for the system. At high temperature the system becomes more and more disordered [4].

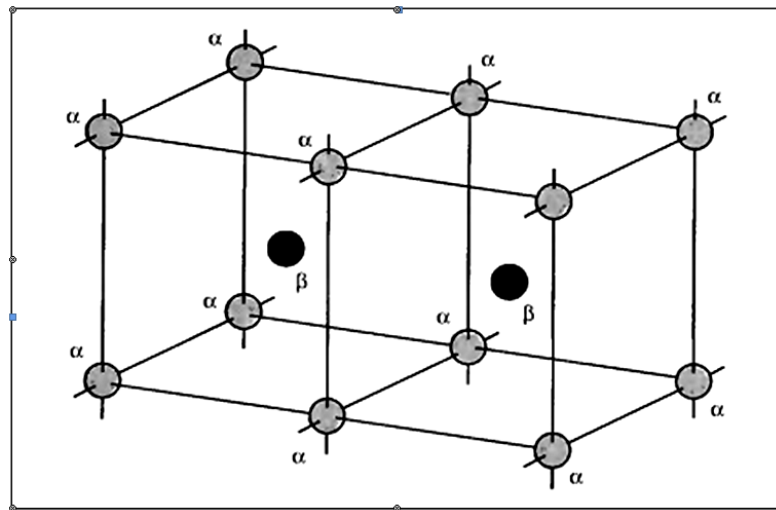


Fig.1.4. Ordered structure of binary alloy [4].

Some alloys, chemically ordered, exhibit a chemical order-disorder transition. For these alloys, the chemical order will be destroyed at high temperature by thermal agitation which causes a permanent exchange of atoms between the sites. Thus, the ordered structure disappears above a temperature, called critical temperature T_c . Also we can observe ordered structures at low temperature which, if the temperature is raised, will be progressively destroyed. It is then necessary to measure a parameter evaluating the order state compared to the perfectly ordered state, it is noted η .

The transition is said to be of the first order; If the order parameter is continuous. Otherwise, the transition is said to be of the second order (fig.1.5) [21]. Where, the second order transitions are quite rare and special.

In general, the order-disorder transitions can be of first or second order in the thermodynamic sense. During the first-order transformations, the volume and enthalpy of the system change in a discontinuous manner, the sudden variation of the enthalpy corresponding to the latent heat of transformation. The transition takes place by germination and growth of a new phase which coexists with the mother

phase. The quantities such as the composition and the parameter of order change locally in the germination sites, and the transformation is continued by the growth of these germs. On the other hand, during the second-order transformations there is no discontinuous change of the enthalpy and therefore there is no latent heat involved in this type of transition and the state of order changes continuously in the alloy. All the material is in an intermediate state between the old and the new phase and there is no phase coexistence.

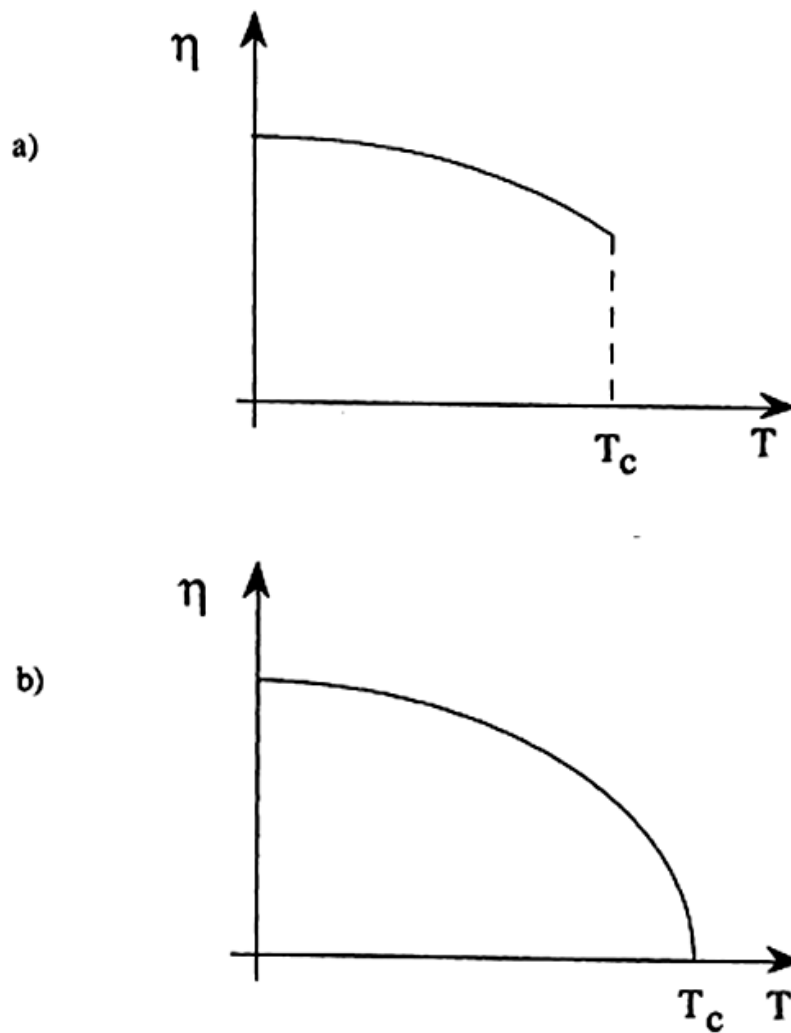


Fig1.5. Evolution of order parameter with the temperature, First order transition (a), Second order transition (b)[21].

1.6.2. Characteristics of order disorder transformation

According to the previous explanations we can summarize the characteristics of the order-disorder transformation as follows [11]:

- ❖ The order implies a periodicity or a symmetry of atomic arrangements;
- ❖ The order can be quantified in terms of long range order parameter;
- ❖ The ordered structures are stable at low temperatures and become disordered at high temperatures.

The first two characteristics involve the experimental possibility to measure the order directly by means of an in situ diffraction method and to identify the order-disorder transition.

The last characteristic can be simply understood from thermodynamics. The stability of the order at low temperatures means that the internal energy of the ordered state is less than the internal energy of the disordered state. At high temperatures, order is destroyed (formation of disorder) whose free energy is now minimal above a critical temperature.

1.6.3. The order degree parameters

Numerous metal alloys are in the form of solid solutions, the various atoms being distributed more or less randomly on the sites of a crystal lattice. The third principle of thermodynamics predicts that at low temperature, these alloys are ordered or form a multiphase mixture of ordered phases.

In solid solutions, atoms are never totally distributed randomly, atoms of the same nature tend locally to segregate or to be ordered. This is because the interaction potentials between pairs of atoms differ according to the nature of the atoms concerned ($V_{AA} \neq V_{AB} \neq V_{BB}$). This is very often called a local order or a short-range order (SRO): this order is indeed localized at interatomic distances where the atomic arrangement is irregular in space. Intuitively, one imagines that this SRO decreases when raising the temperature, or on the contrary increases and leads to a phase

transition to a long-rang order (LRO) when it is lowered and the density of the atoms is the same in all the Directions [22].

Long range order which can be defined quantitatively in several manners, characterizes how different types of sites are occupied by different atom types. Therefore, all long range ordered structures can be described using a set of sub-lattices.

The most widely used model for treating long-range order is that of Bragg-William which considers a binary alloy containing N_A atoms of A, N_B atoms of B and two sub-lattices (α) and (β). He defined the long-range order parameter as follows:

$$S = (P_A^\alpha - N_A)/(1-N_A) = (P_B^\beta - N_B)/(1-N_B) \dots\dots\dots(1.1)$$

Where P_A^α (P_B^β) is the probability of finding on average an A (B) at an α (β) site and N_A (N_B) is the atomic fraction A (B) in solution for an alloy in the ordered state, namely all the atoms A (B) occupy the n_α (n_β) sites α (β), $P_A^\alpha = 1$ et $S = 1$.

In the totally disordered state the probability of finding an atom A (B) on one site α (β) is equal to the atomic fraction where $S = 0$ [23].

The short rang order which remains above the transition temperature (T_c) is characterized by Warren - Cowley parameters α_j [24] between j^{th} neighbors:

$$\alpha_j = 1 - \frac{P_{AB}^j}{c_B} \dots\dots\dots(1.2)$$

P_{AB}^j is the probability of finding an atom B in the j^{th} neighbor of a given atom A. In the completely disordered state, $P_{AB}^j = N_B$ and α_j is equal to zero for all j. For an ordered alloy at short range, the parameter α_j tends rapidly to zero when j increases (dominant effect of the first neighbors). For the first coordination layer, α_1 is negative for a tendency to order, and positive for a tendency to segregation. In the case of a perfectly ordered state at long rang, the α_j take a periodic sequence of values. For

example, for a structure of the D_{2h}^{25} (Pt₂Mo, Ni₂Cr) type, α_j is alternately equal to $-1/4$, 0 and $+1/4$.

1.6.4. Variation of the order parameter with the temperature

Because of the interchange between two atoms in a completely ordered configuration requires a well-defined increase in energy. The quantity ν must be equal to zero when the disorder becomes complete where there is no distinction between the ordered and the disordered sites.

In this manner (ν) is assumed to be related to the long range order parameter by the relation:

$$\nu = \nu_0 \cdot S \dots \dots \dots (1.3)$$

Where : ν_0 is a constant representing the interchange energy of an atom pair in perfectly ordered structure.

The decrease in the energy of the quantity (ν) when the disorder increases is responsible on the progression of the disorder process as the temperature increases, until the long range order parameter reaches the zero at a critical temperature T_c .

The curve giving the variation of the long-range order parameter S as a function of the temperature (Fig.1.6) shows that S decreases progressively until the critical temperature T_c where it abruptly drops to zero [25].

The variation of the short-range order parameter with the temperature is given also in the previous figure (Fig.1.5). It is noticed that it decreases with the increase of the temperature up to a value T_c where it abruptly drops until a low value called residual which decreases subsequently with the increase in temperature [23, 26, 27].

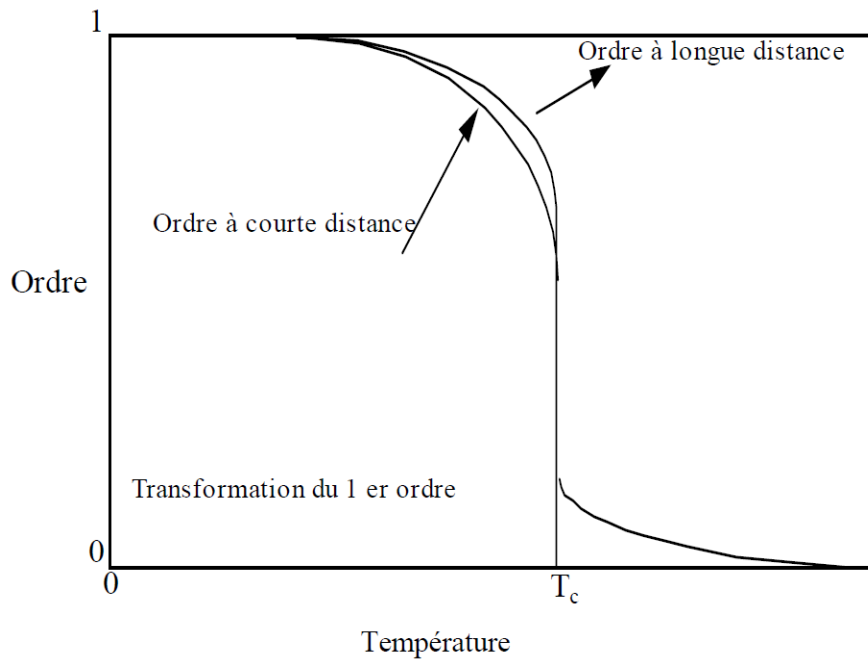


Fig.1.6. Short and long rang order for an alloy AB_3 with first order transformation [25].

1.6.5. The atomic model of the interface between an ordered phase and another disordered

The interphase wall concept was introduced for the first time by Vander Waals in 1894 to explain the behavior of fluids [28], but can also be used to describe interphase joints between all states of matter.

A mathematical formula for the diffusion of interphase joints was developed by Cahn and Hilliard in 1958 to explain experimental observations of the behavior of the germination in solids [29]. This formula requires the use of the coefficient of the energy gradient and is currently used in several fields: materials science, physics, mathematics, fluid mechanics and biology.

Figure.1.7 shows a type of diffusion on the interphase joint between an ordered phase α and the other disordered β of the compositions of 50% at. A and 50% at. B. The long-range order is represented in the α phase and it gradually changes through the thickness L to the short-range order until the disorder of the disordered phase β ; It also shows the change in the concentration of the element A in each perpendicular plane of the interphase joint, shown below the atomic model presented [30].

The composition and the degree of order can change through the thickness L and these variations have been observed directly at the atomic level at the temperature used, using a high resolution transmission electron microscope.

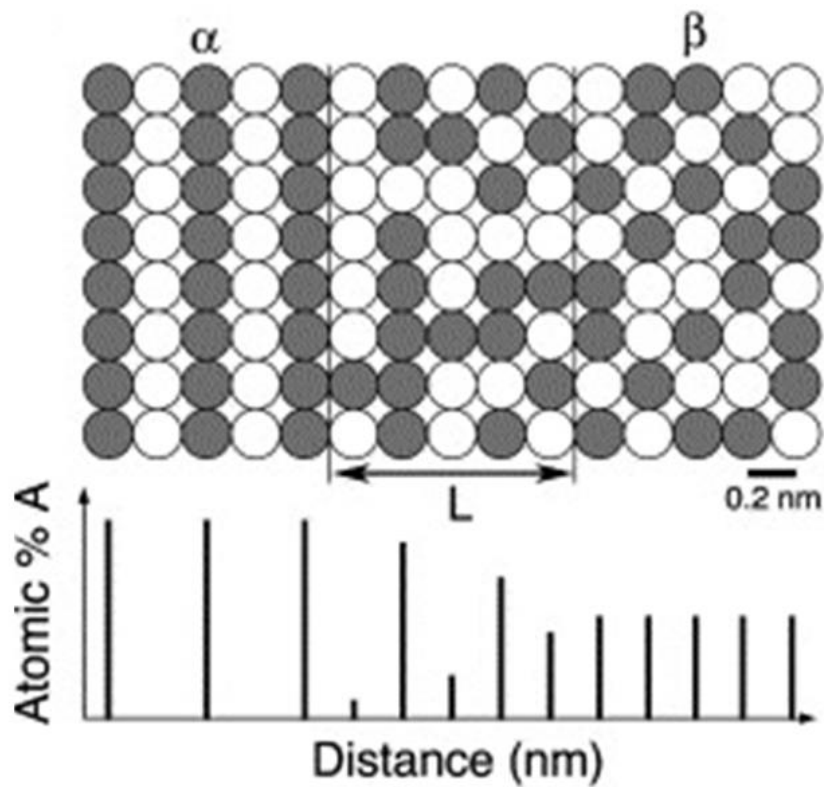


Fig.1.7. Atomic model and concentration profil of an interphase joint between an ordered phase (α) and another disordered (β)[30].

1.6.6. Different steps of the order disorder transformation

The simplest order-disorder transformation is carried out in four steps. Starting from the perfectly disordered alloy at high temperature and gradually lowering the temperature, we observe successively [31]:

- ❖ The formation of the short-range order over T_C ,
- ❖ The germination and growth of the ordered phase below T_C ,
- ❖ The increase of the degree of long range order of the ordered phase,
- ❖ The coalescence of antiphase domains (APhSD).

a- The germination and growth of the ordered phase

A disordered alloy quenched at a temperature below T_c is in a state where the order is generally at short range, implying that the ordering may extend to a few nearby neighbors. Therefore, a structure with a short-range order can be considered as an ordered structure with small ordered domains [31]. Such ordered domains of supercritical size play the role of the germs of the ordered phase. Thus the transformation can be considered as starting with a constant number N_0 of ordered domains and extending by the growth of these ordered domains in all directions.

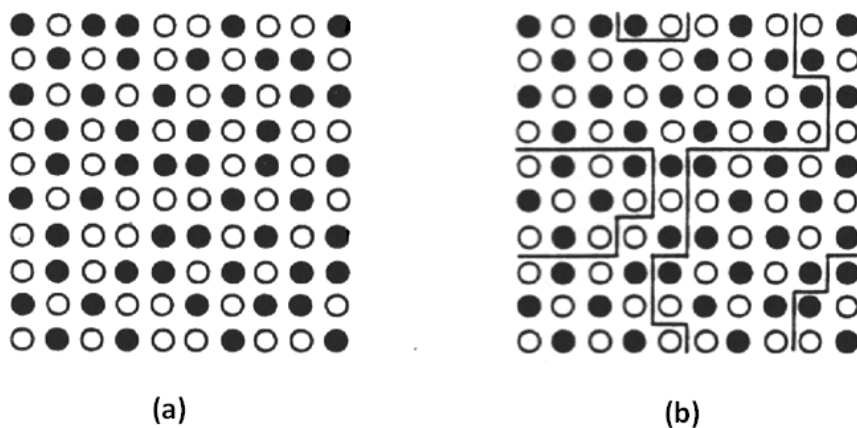


Fig.1.8. (a) Solid solution A-50at%B with short range order, (b) perfect order region tracing in the solution shown in (a)[32].

b-The increasing of the order degree

The degree of order at long range in the ordered domains which germinate and grow is generally less than 1. Thus, the degree of order in these domains continues to increase with time even during their growth. The mechanism of ordering requires a diffusional transfer of atoms from the wrong positions to the right positions. Ordering is therefore a homogeneous reaction [31].

c-The coalescence of the antiphase domains

The antiphase domains grow in a disordered material. This process ends when the order parameter reaches the value 1 where one obtains a material completely formed by ordered domains. The following process is the coalescence of these ordered domains. The first process is similar to the primary recrystallization, ie : the absorption of a deformed microstructure by free of stress crystal. The second process is similar to secondary recrystallization, in the sense that individual domains grow at the expense of neighboring domains in such a way that the total surface of the anti phase boundaries is reduced [33].

1.6.7. The ordering and antiphase boundaries (APB)

From the disordered state, if the temperature is lowered below T_C , the germination of ordered domains begins at several points of the crystal (nucleation phase). These small ordered regions develop by consuming the disordered matter (growth phase). They grow until they meet and thus form domains separated by walls called antiphase boundary walls (APB).

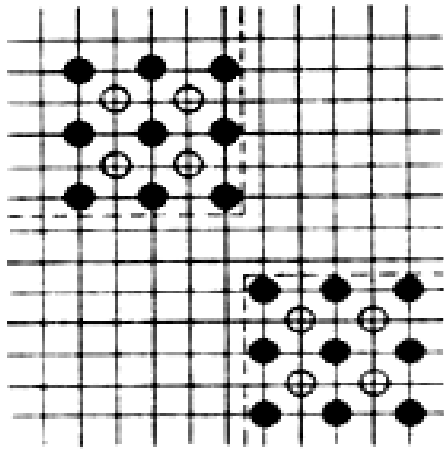
In a domain where the alloy is ordered, let us consider a plane of same atom, for example pure A, at the level of an antiphase wall, it can become a plane A-B: there is a shift of the structure. The crystal is thus formed of ordered domains, limited by antiphase boundrie, where the ordered sequence is offset from the neighboring domain.

The antiphase boundary is a defect of order, independent of the geometry of the basic lattice, it is not limited to particular crystallographic planes. An antiphase

boundary can be characterized by changes in the bonds, with its first neighbors, of an atom of the boundary comparing to its environment in the elementary cell. The energy of the boundary depends also, in a first approximation, on the type and the number of these changes.

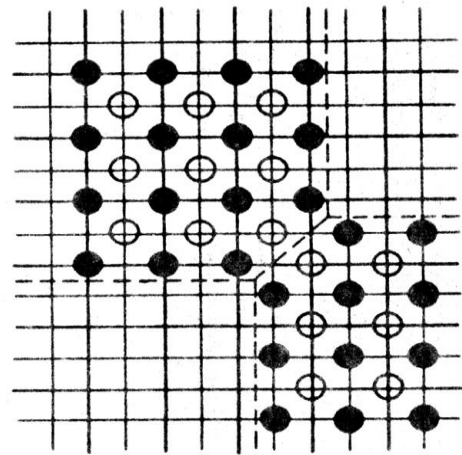
The interactions between second neighbors are generally ten times smaller than those between first neighbors. Therefore, these antiphase boundaries have a low energy (zero in the approximation to the first neighbors). The energy of an antiphase boundary depends on its orientation. Since the system seeks to minimize its energy, we can find a priori preferred directions for the antiphase boundaries.

Figure.1.9 shows a schematic diagram of the nucleation and growth of the ordered domains. The disordered lattice is represented by crossed lines, within this lattice, two sub-lattices are indicated by large and fine lines. These ordered domains grow until they gather and separate by antiphases boundaries [34].



Step I

Step II



Step III

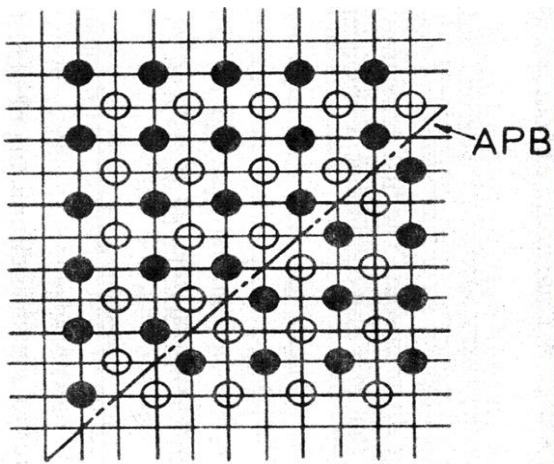


Fig.1.9. The formation of an antiphase boundary (APB) [34].

1.6.8. Superdislocations

The notion of superdislocation is better illustrated in the two-dimensional model (Fig.1.10), whose atoms are arranged in two directions. Generally, when the order appears, each type of atom occupies a type of site of the crystal lattice. This separating the atoms into sub-lattices where each of them is preferentially surrounded of the other type. When an entire dislocation in the disordered state moves in the ordered state, it does not change the geometry of the crystal, but it produces an interface along the sliding plane, whose atomic distribution is irregular [35]. This type is called "antiphase boundaries" [35,36]. The passage of a second dislocation of the same vector of Burgers, and in the same plane of sliding reconstitutes the order destroyed by the first dislocation.

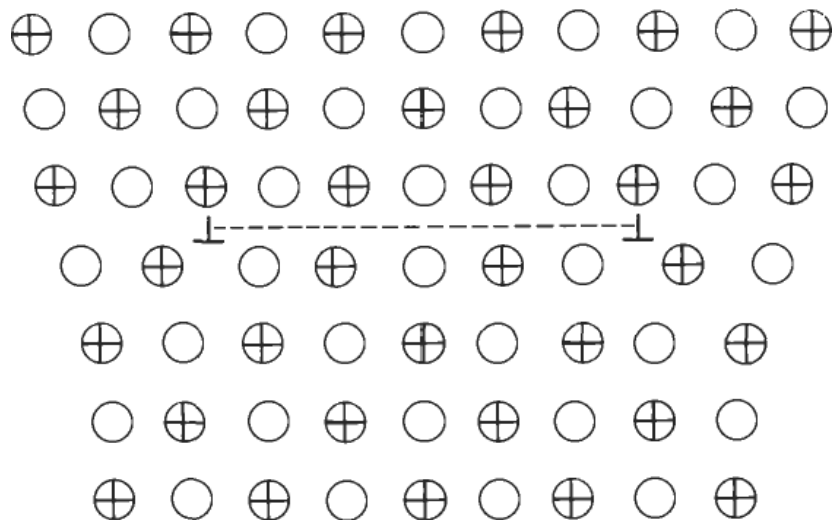


Fig.1.10. Superdislocations in an ordered two-dimensional structure [36].

The two dislocations and the antiphase boundary related, are called "Superdislocations" [36 , 37] (Fig.1. 10). The distance between these two dislocations that limit the antiphase boundary can be determined by the balance between the antiphase boundary energy, and the repulsion between these two dislocations [37, 38]. Due to the energetic considerations, each of the dislocations can dissociate into two partial dislocations of Shockley, limiting a stacking fault ribbon. Thus, the antiphase boundary leads to the Configuration shown in Figure.1.11 [36].

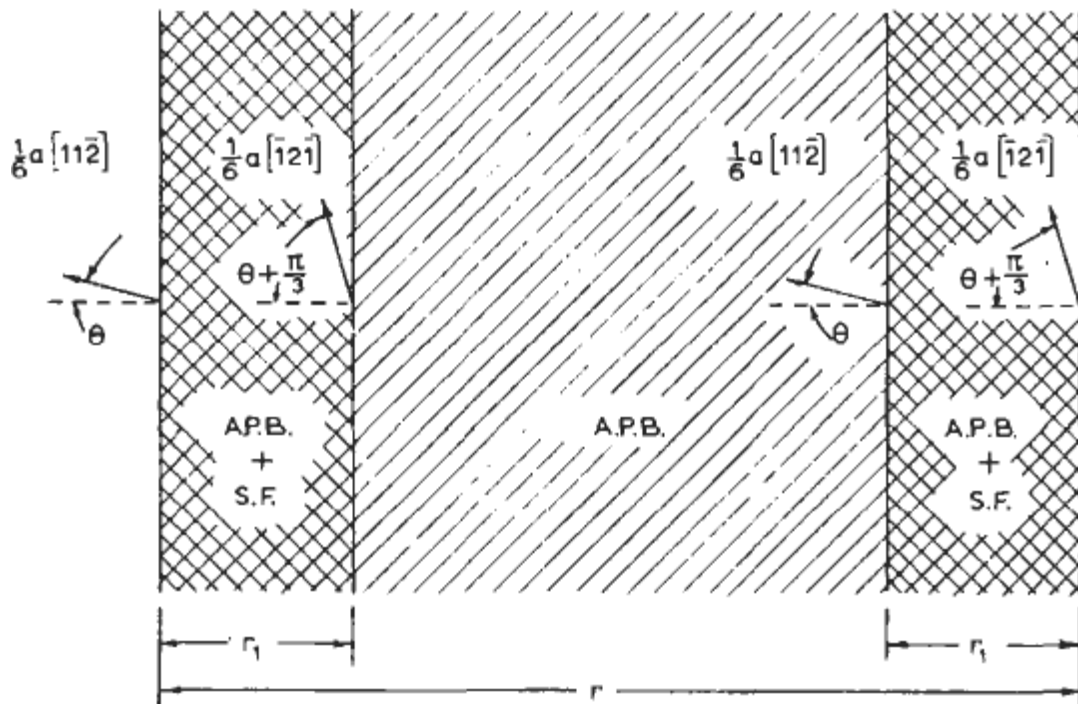


Fig.1.11. Dissociation of dislocations limiting antiphase boundaries[36].

Kear et al. [39] analyzed the structure $L1_2$ in the case where the energy of the antiphase boundary is higher, and the dissociation of the dislocations into two partial will be observed.

$$\frac{1}{2} a [01\bar{1}] \rightarrow \frac{1}{6} a [11\bar{2}] + \frac{1}{6} a [12\bar{1}].$$

This is the case of the Cu_3Au alloy whose combination of the two faults and the antiphase boundary creates an extension of the superdislocations along the direction $\langle 110 \rangle$; this can only be observed with TEM (Fig.1.12)[40], but can be schematized as shown in Figure.1.13.

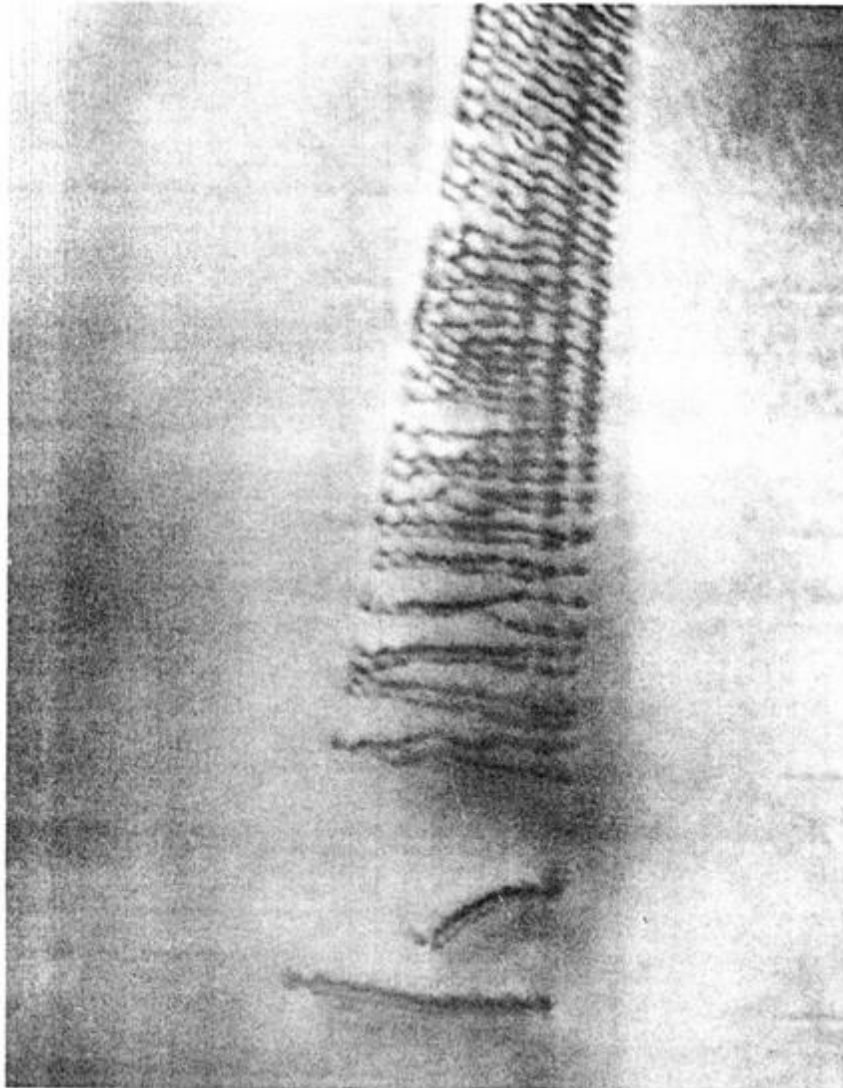


Fig.1.12. Observation of TEM superdislocations in the Cu_3Au alloy [40].

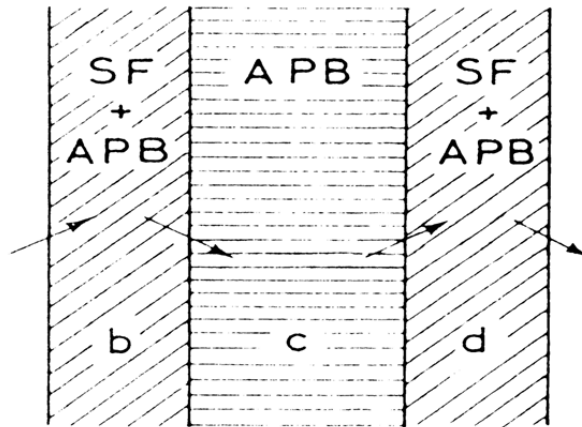


Fig.1.13. Schematisation of superdislocation structure of the orderd phase AuCu₃[36].

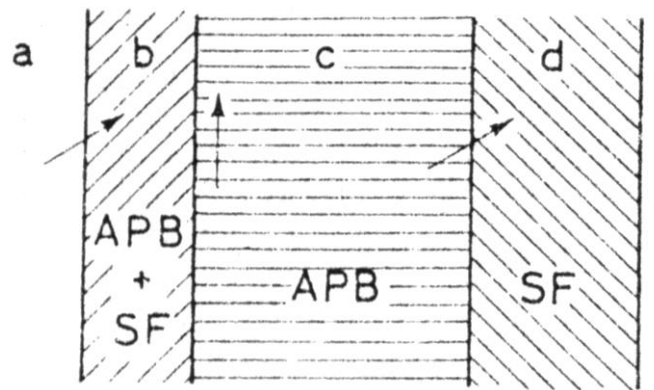


Fig.1.14. Schematisation of superdislocation structure of the orderd phase AuCu_I[36].

For the CuAuI alloy, there are two types of dislocations not equivalent in the sliding plane (111) due to distortions of the CFC lattice. According to Marcinkowski and al. [40] one of the types of dislocations do not form superdislocations, on the other hand the other types form asymmetric superdislocations.

Figure.1.14 schematizes the structure of the superdislocations in the CuAu alloy where there are three types of ribbon limiting partial dislocations; The first type which is to the left represents a combination of stacking fault and the antiphase boundary,

the second type in the middle represents an antiphase boundary and the third type which is to the right represents a ribbon of stacking fault [36].

We can also observe the coupling of the dislocations in the ordered alloys at short range. The local order was distorted by the passage of the first dislocation, a second dislocation is attracted by the first of its set because of the decrease of energy. The order is completely restored if the structure is perfectly ordered (Figure.1.10), this is not the case if the order is at short range[18].

1.6.9. The Influence of the order on the physical properties of the alloys

The existence of a superstructure can be traduced also with a modification of the most of the physical properties of the alloys; [23] Herein citation of some properties.

1.6.9.1. Mechanical properties

The superstructure is manifested by a greater resistance to plastic deformation, the passage of a dislocation destroying the order (Fig.1.14 (a)) [41]. Dislocations must in fact move in pairs; the second restoring the order destroyed by the first. Between the two dislocations there is an antiphase boundary ribbon (Fig.1.14 (b)). The mechanical properties are modified (especially due to the deviated slides).

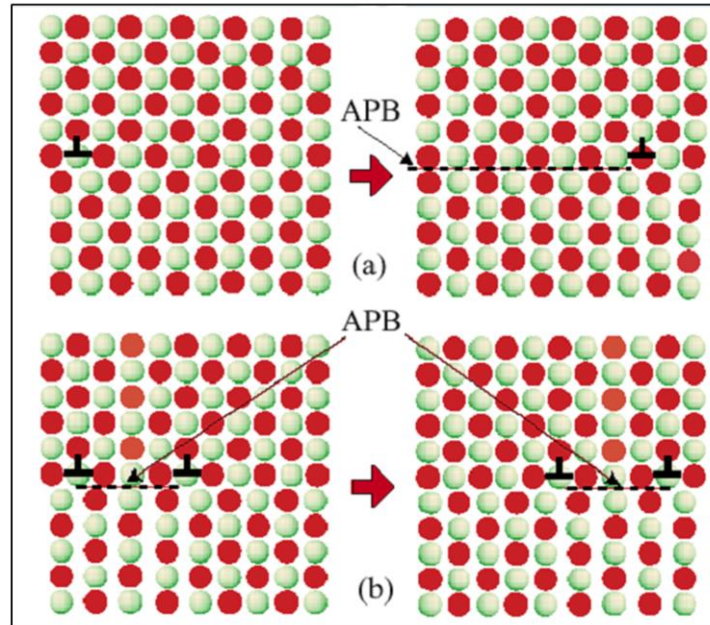


Fig.1.14. Orderd solution, antiphase boundy limited with dislocations [41] :

- (a) The passage of a dislocation creates antiphase boundaries which are energetically expensive.
- (b) The dislocations must circulate in pairs to cancel this effect, which is energetically expensive in the level of the field of elastic stress.

1.6.9.2. Electrical resistivity

The electrical resistivity originates in the diffusion of electronic waves by the lattice defects, including thermal vibrations. In a disordered structure, the waves will be more strongly diffused than in an ordered solution. The appearance of the order should therefore not show a drop in electrical resistivity, which is what is observed experimentally (Fig.1.15 (a)) [23]. Figure.1.15 (b) shows the resistivity of a disordered alloy which exhibits a parabolic variation as a function of the solute concentration, passing through a maximum for a composition close to the equiatomic concentration.

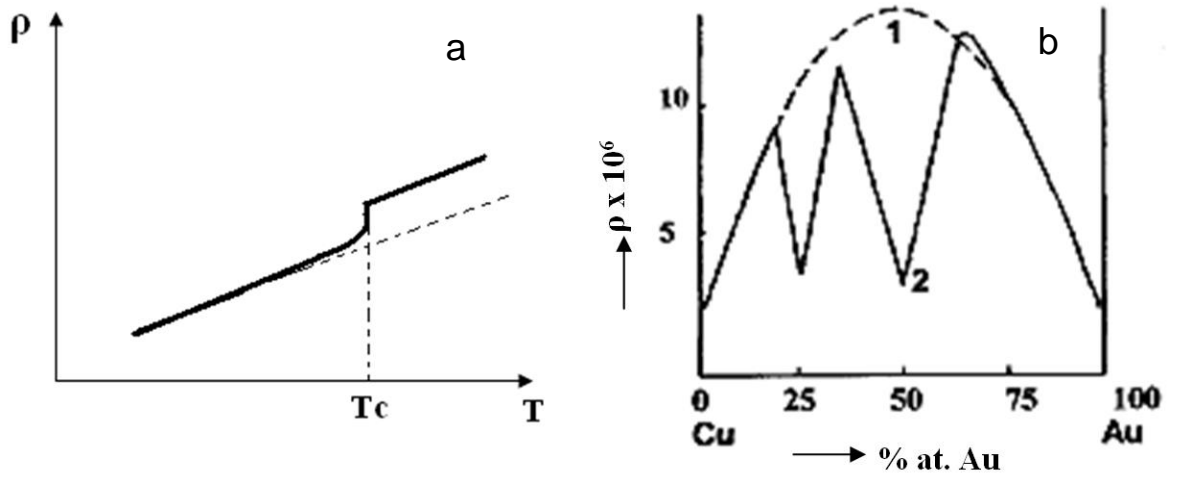


Fig.1.15. (a) Variation of the resistivity with temperature during an order-disorder transformation [23]. (b) electrical resistivity of AuCu alloys: 1-after quenching from 650 ° C (disordered state), 2- after annealing at 200 ° C (ordered state) [23].

***II: Characteristics and ordering process in AuCu
and AuCuAg systems***

2 Characteristics and ordering process in AuCu and AuCuAg systems

Introduction

Recently, many interests have been devoted on the order-disorder transitions study in different materials. Although the Cu-Au system is one of the first in which various order-order and order-disorder transformations have been observed [11], the study of gold alloys continues to attract many researchers because of different questions asked around its equilibrium diagram. The mechanical study have also recently attracted a lot of interest since gold alloys have a big importance in jewelry and horology industry.

Part I: Order-disorder transitions in the AuCu binary system.

2.1.1. The order in AuCu system

In gold copper alloys, a disordered structure could be obtained by simple quenching of the alloy. Nevertheless, this structure is not stable during machining steps, annealing, or also sometimes the drying after the quenching, and evaluate in ordered structure. This evolution can lead to a local hardness and , followed by, a cracking of the piece due to the effect of a gradient of the dilatation coefficient [42]. Furthermore, some pieces of big dimensions do not cool down rapidly over the entire volume, and the non-homogeneity of the hardness appears, causing, in the same manner, crack and machining difficulties. At the end, some alloys evaluate spontaneously, by aging, to an ordered structure.

Gold-copper alloys form a solid solution, which is significantly harder than the same alloys forming a disordered solid solution. Where, the alloys that present a

high hardness can hardly be shaped. This is the reason that makes the disordered structure more advantageous, from the machinability point of view [42].

2.1.2. Equilibrium phase diagram of AuCu binary system

Among the phase diagrams which remain incomplete and which are currently studied, the phase diagram of the Cu-Au system. It shows a series of order-disorder transformations in the solid state. Copper and gold form continuous series of solid solutions at high temperatures, but different superstructures exist at low temperatures for stoichiometric compositions well defined: Cu_3Au , CuAu and CuAu_3 . The most recent version of this diagram is presented in Figure.2.1 [43]

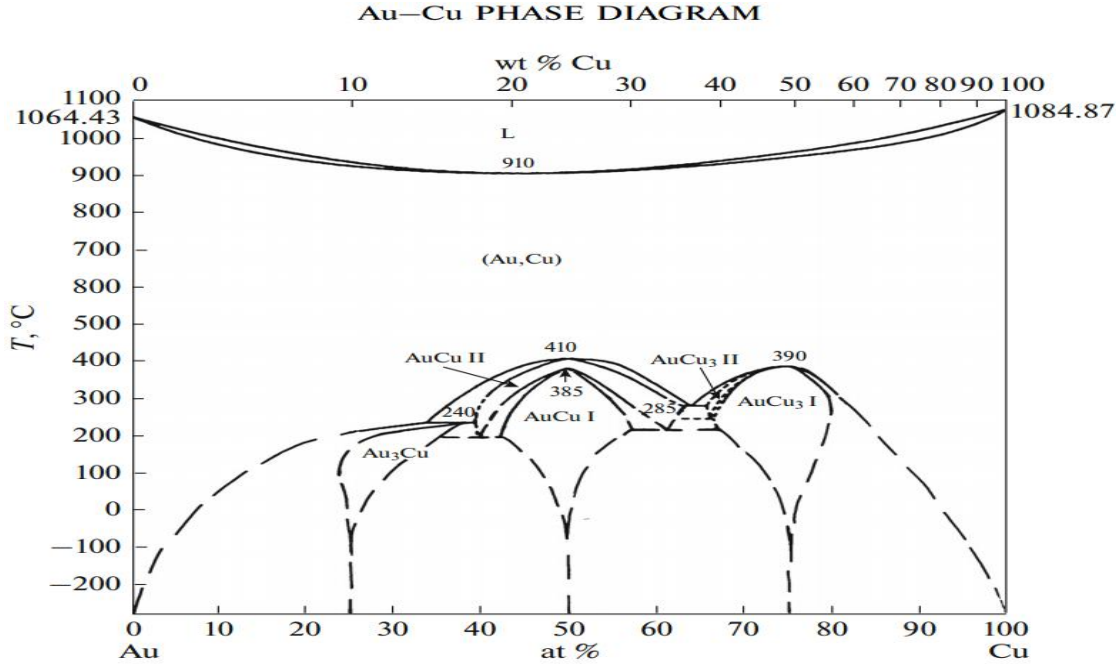


Fig.2.1. AuCu binary phase diagram [43].

Some compositional details about the binary phase diagram are represented in Tab.2.1.

Phase	Composition, % .at. Cu	Groupe d'espace	Type de structure	prototype
(Au,Cu)	0 à 100	$Fm\bar{3}m$	A1	Cu
Au ₃ Cu	10 à 38.5	$Pm\bar{3}m$	L1 ₂	AuCu ₃
AuCu (I)	42 à 57	$Pm\bar{3}m$	L1 ₀	AuCu
AuCu (II)	38.5 à 63	$Imma$...	AuCu (II)
AuCu ₃ (I)	67 à 81	$Pm\bar{3}m$	L1 ₂	AuCu ₃
AuCu ₃ (II)	66 à ?	$P4mm$...	Cu ₃ Pd

Tab.2.1. Structural details of the occurred phases in the binary Au Cu phase diagram [44].

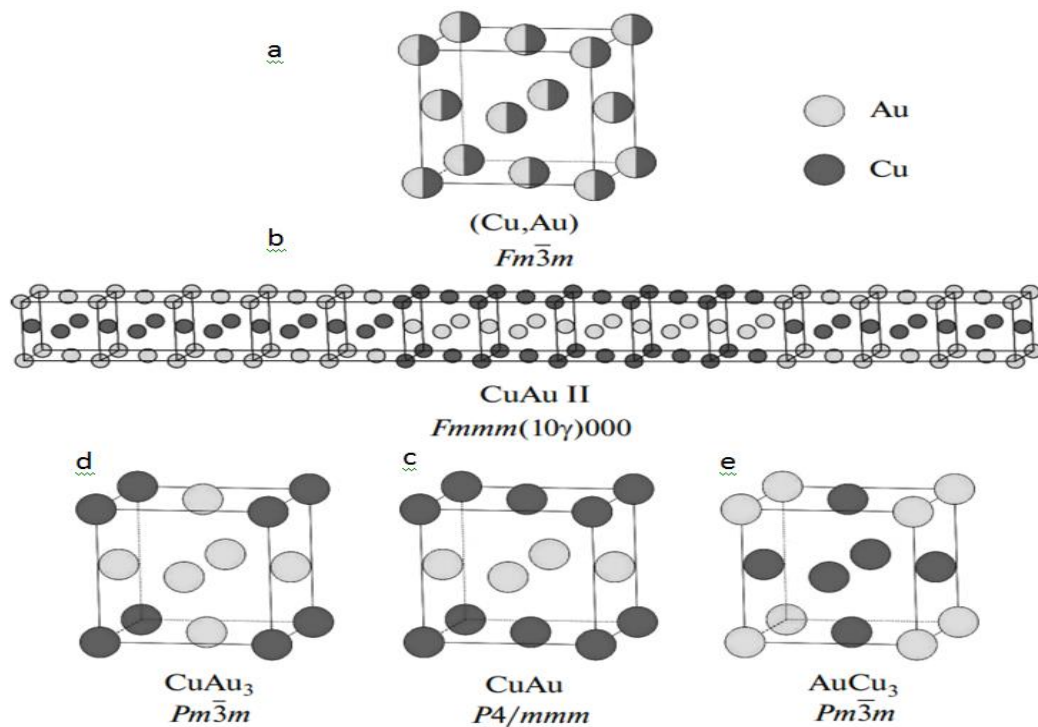


Fig.2.2. Crystal structures of the phases that can be formed in Au-Cu system [43].

2.1.3. The ordered phase AuCu

The CuAu alloy represents a good test for different models and approaches to describe phase changes in stoichiometric alloys [45]. This alloy is well known with two successive solid-solid transformations as follow (Fig.2.1):



- At high temperature, above $T_{C1} = 683\text{K}$ ($410\text{ }^\circ\text{C}$), the equilibrium structure is the disordered phase A1 of CFC structural system (Fig.2.2 (a)) with lattice parameter $a = 0.387\text{ nm}$ [27, 46, 47].
- Below 683K ($410\text{ }^\circ\text{C}$), a long rang order occurs. Between $T_{C1} = 683\text{K}$ ($410\text{ }^\circ\text{C}$) and $T_{C2} = 658\text{K}$ ($385\text{ }^\circ\text{C}$).
- A structure with a high periodicity CuAu II (Fig.2.2 (b)) described by a pseudo-orthorhombic cell with lattice parameters: $a = 0.3979\text{ nm}$, $b = 0.3963\text{ nm}$ and $c = 0.3678\text{ nm}$ [27, 46, 47].
- Below $T_{C2} = 658\text{K}$ ($385\text{ }^\circ\text{C}$), the equilibrium state is the ordered phase of the tetragonal face centered structure CuAuI ($L1_0$) (Fig. 2.2 (c)) with lattice parameters $a = 0.395\text{ nm}$ and $c = 0.368\text{ nm}$ [27, 46, 47].

The crystallographic structures of the two phases $L1_0$ and A1 are well defined but that of the CuAu II phase is less clear. It is a periodic antiphase (PAP) structure disproportionate (Incommensurate) produced from the tetragonal phase $L1_0$ with a periodicity due to the stacking of the phase $L1_0$ along the axes a and b [48]. So this structure derives from the $L1_0$ structure by forming antiphase boundaries which repeat every five cells giving a large orthorhombic cell and the antiphase boundaries are perpendicular to one direction [27].

2.1.4. The ordered phase Au₃Cu

The Au₃Cu phase is like the AuCu₃ phase except that below 463K (190 °C). the structure is Cubic but this time the Cu atoms are at the tops of the cube, and those of gold in the center of the faces (Fig.2.2 (d)).

For this alloy Batterman has shown that a long-range order exists below the critical temperature $T_C = 472K$ (199 °C) but not for compositions greater than CuAu₃ [27].

2.1.5. The ordered phase AuCu₃

This alloy has been the subject of numerous investigations because of its relationship with the improvement of electronic properties for technological applications concerning catalysts, coating and value devices [49]. Above $T_c = 663K$ (390 °C) the disordered phase A1 (of symmetry Fm-3m) face-centered cubic structure (CFC) occurs. Where, the atoms Cu and Au occupy the sites of the crystalline lattice in statistic manner, of probability 3/4 and 1/4 respectively.

Below 663K (390 °C) the ordered phase AuCu₃ is formed in L1₂ structure (of symmetry Pm-3m) Where the atoms of a species are found at the summits of the cube and those of the other species at the center of the faces, which corresponds to the stoichiometric composition AuCu₃ [27]. Each atom Au is surrounded by 12 Cu first neighbors, but each Cu has for first neighbors 8 Cu and 4 Au (Fig.2.3) [50, 51]. Where there will be segregation of atoms and the symmetry of the cell will no longer be CFC, but simply cubic (Fig.2.3) [27].

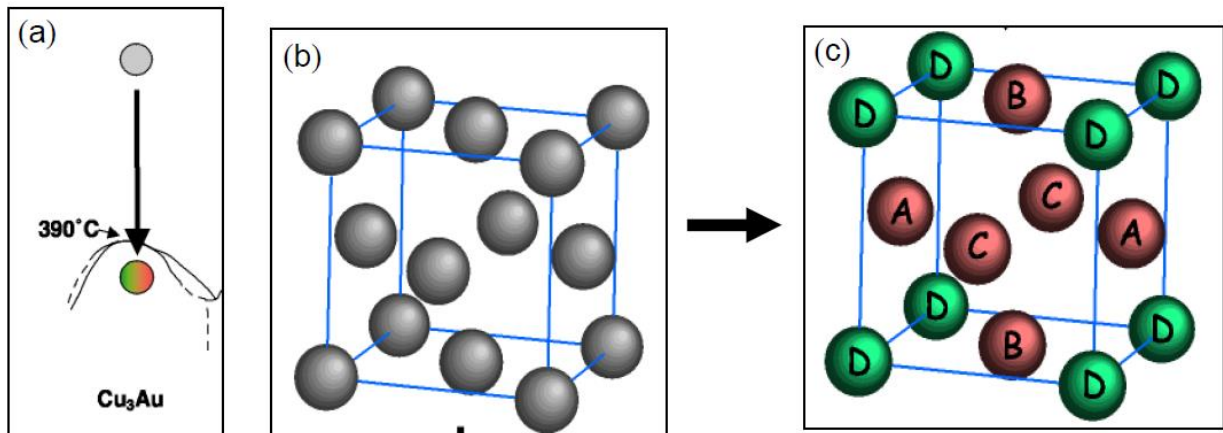


Fig.2.3. Disorder-order transition in AuCu₃(a): A1 (Fm-3m)(b) to L1₂ (Pm-3m)(c) [51].

2.1.6. Stability of AuCuII phase

The crystallographic structure of the two phases L1₀ and A1 is well defined but that of the CuAu II phase is less clear. It is a stable structure between almost 663K (390°C) and almost 683K (410°C) (see phase diagram). It derives from the quadratic structure L1₀ by formation of antiphase boundaries of vector $\frac{1}{2}(a^{-}+c^{-})$, these boundaries are repeated every five cells (Fig.2.4) [52]. This large cell is orthorhombic [52] and the antiphase boundaries are perpendicular to one direction.

In this sense this phase represents a semi-ordered structure, which reflects its intermediate thermodynamic position in the transition series between the ordinate structure L1₀ and the disordered structure A1.

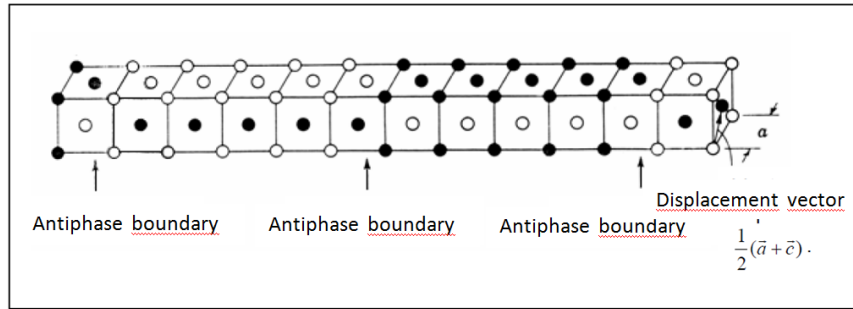


Fig.II.4. Construction of the quadratic cell of AuCuI [52].

2.1.7. Types of boundaries in Au-Cu binary system

2.1.7.1. The structure AuCuI

The AuCuI phase is well known with a tetragonal structure. The antiphase boundary results when a plane of Cu atoms in the first crystal is followed by a plane of Au atoms in the second (Fig.2.5), and the possible displacement vectors are: $\frac{1}{2} [0 \bar{1} 1]$ or $\frac{1}{2} [10\bar{1}]$, n is in the direction $\langle 100 \rangle$. For the first vector the boundary is obviously conservative ($R \cdot n = 0$); The second displacement leads to the insertion (or the extraction) of a lamella family of planes (100), and since this latter has the same chemical composition of the matrix so the boundary remains always conservative. The non conservative antiphase boundaries occur along the two planes (110) or $(1\bar{1} 0)$ (Fig.2.5).

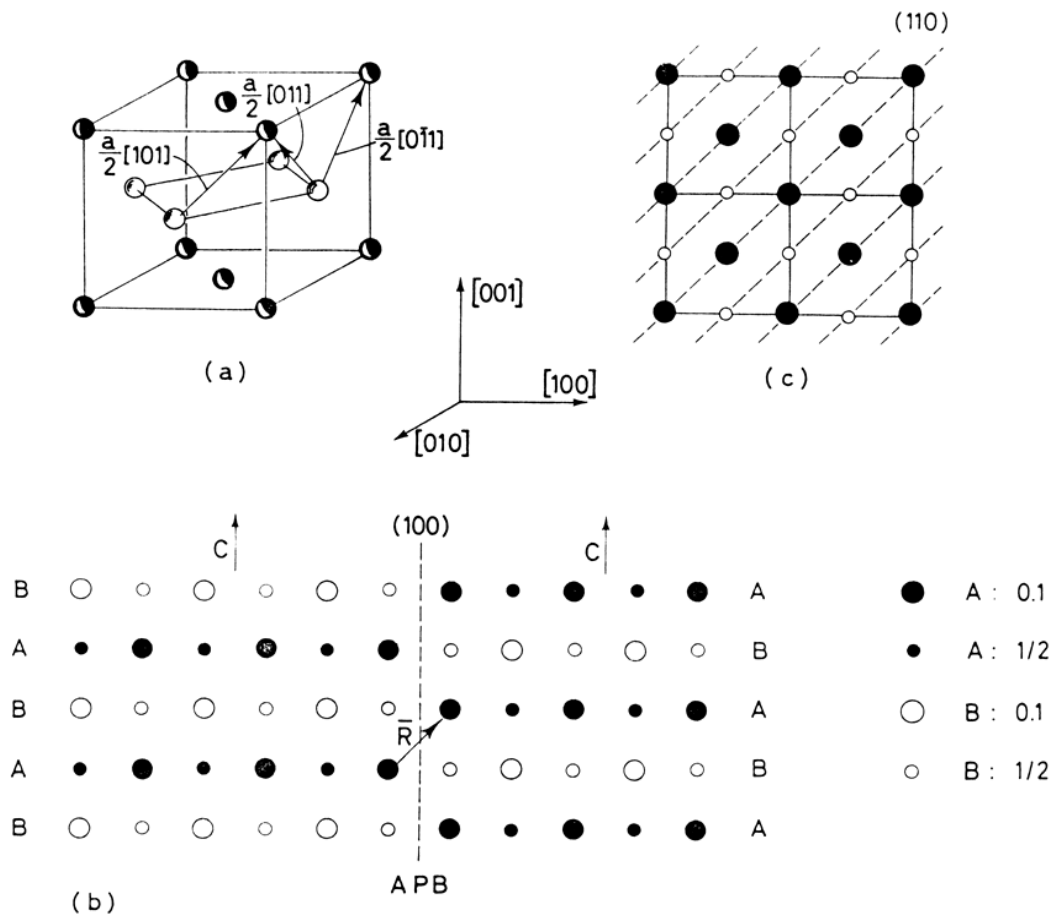


Fig.2.5. Antiphase boundaries in AuCuI structure: (a) structure and vectors of possible displacements, (b) conservative boundaries: however $R.n \neq 0$, Where the layer in insertion (in extraction) has the same stoichiometric composition. (c) non conservative antiphase boundaries [36, 53].

2.1.7.2. The structure AuCu₃

The antiphase boundaries in this structure are formed by sliding of the partial dislocations in the superlattice [54]. They must be planar to be stable; normally a planar antiphase boundary can take any orientation in the crystal [55], but energy considerations suggest that some orientations can be favored [51]. So the antiphase boundaries of this structure are conservative in the direction $\langle 001 \rangle$ and not conservative in other two directions $\langle 100 \rangle$ and $\langle 010 \rangle$ as shown in Figure.2.6 [51].

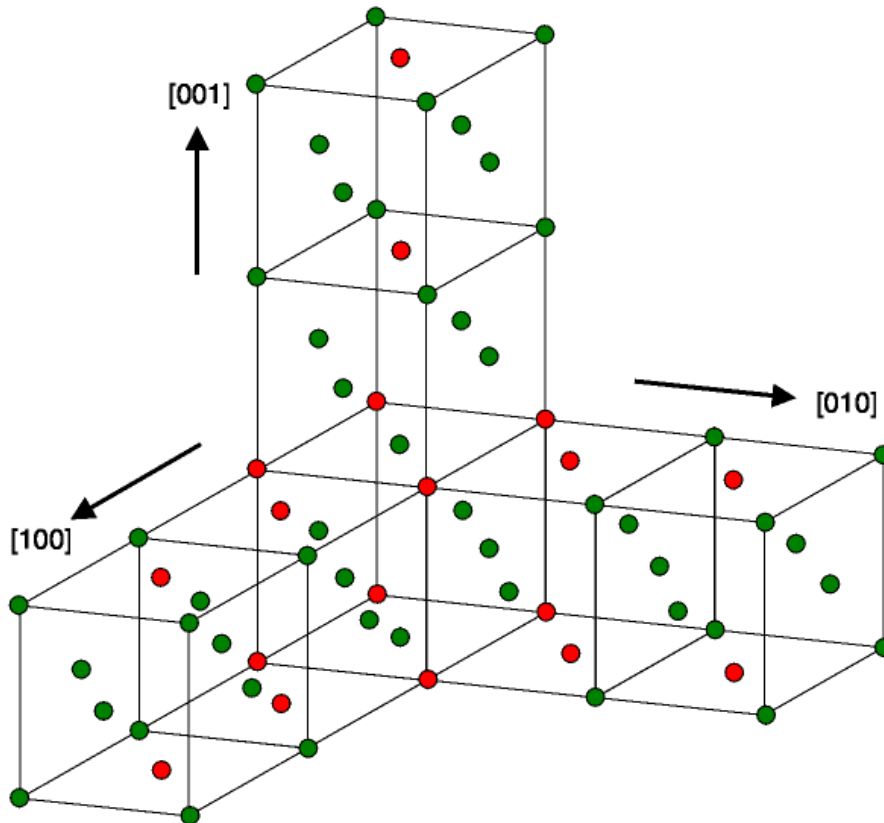


Fig.2.6. Antiphase boundaries in the ordered Au Cu₃ phase: conservative along $\langle 001 \rangle$, non-conservative along $\langle 100 \rangle$ and $\langle 010 \rangle$ [51].

2.1.8. Vacancies effect on the order processes

2.1.8.1. Punctual defects "vacancies"

A Punctual defect is a perturbation of the crystal which can be entirely included in a small sphere of diameter at most equal to some interatomic distances. The most classic example is the vacancy which is the default that corresponds to the absence of an atom at a normally occupied site (Fig.2.7), and the auto-interstitial, i.e. the presence with excess of an atom of the same nature in the crystal [1]. Schematically, a vacancy can be produced either by ejecting an atom (or an ion) from its normal site in the lattice and bringing it to the surface of the crystal, or by a Frenkel defect, which is a type of defect in crystalline solids wherein an atom is displaced from its lattice position to an interstitial site, creating a vacancy at the original site and an interstitial

defect at the new location within the same element without any changes in chemical properties [56] as Figure.2.8 shows.

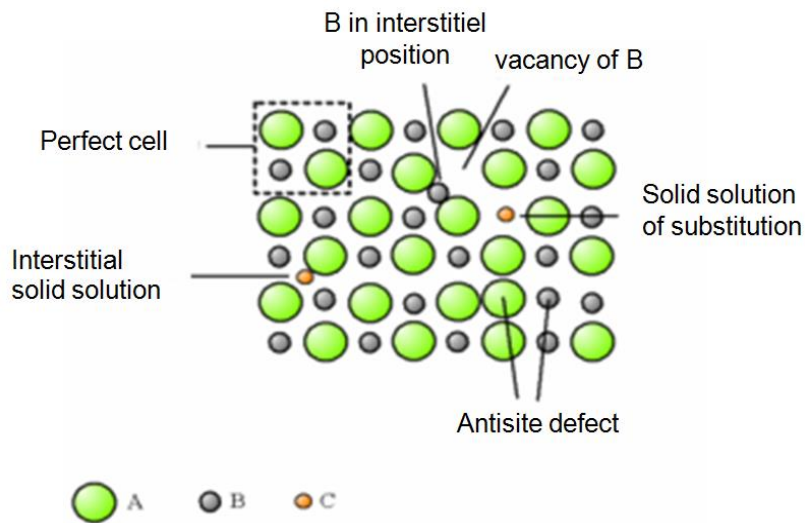


Fig.2.7. Example of punctual defects in an ordered crystal AB [1].

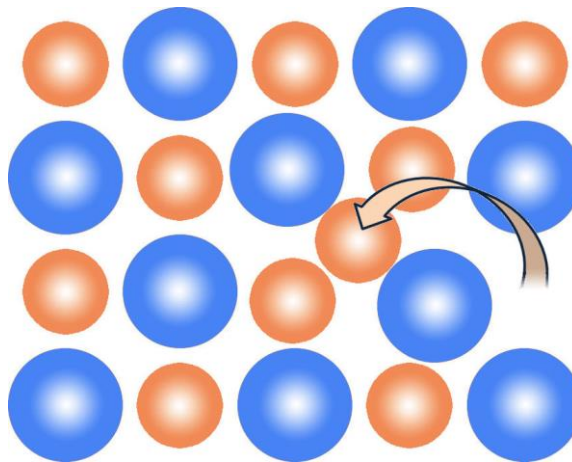


Fig.2.8. The Frenkel defect within binary ordered structure.

2.1.8.2. Identification of vacancies

When a metal is heated in the vicinity of its melting point, small anomalies of various physical properties are actually observed. For example, specific heat, which varies linearly with temperature. On the other hand, if from a high temperature close to the melting point the solid is cooled very rapidly to a temperature sufficiently low,

so that there is no evolution after cooling, it can be seen that The characteristics of the physical quantities which we have just mentioned are different from those which would have been obtained as a result of slow cooling. The anomalies mentioned above are therefore likely to be retained by quenching [1].The quenching in general is done in a liquid (water, gallium, ...) or a gas (He,...).

The main objective of this work is to obtain an excess in the vacancies concentration after holding at very high temperatures, followed by a rapid quenching in water so that the vacancies do not have time to migrate to wells where they would be eliminated [1].

2.1.8.3. Trapping of vacancies during quenching

If the quenching speed is not very great, the vacancies migrate during cooling. There is still a sufficiently high range of temperatures for the vacancies to diffuse rapidly (and consequently to encounter impurities), but already quite low, so that they can practically no longer leave the trap where they fell. This process leads, at low temperature, to a proportion C_0 of abnormally high trapped vacancies [54].

2.1.8.4. Accelerated diffusion by quenching

If it is true after quenching, that many vacancies are trapped on solute atoms, we must expect that the elimination of the vacancies supersaturation is accompanied by a diffusion of these atoms. This is what happens in the quenching experiences of some disordered alloys, which are ordered at low temperature, the higher the quenching temperature, the higher the concentration of vacancies, as well as during the structural hardening phenomenon [54].

2.1.8.5. Ordering of quenched alloys

Every migration of quenching vacancies is accompanied by a movement of atoms. If it takes place in a pure metal, this diffusion is not easy to be brought out. It is not the same when it happens in an alloy [1].

If this alloy presents an order-disorder transformation at the temperature T_C , it is very natural, to attribute to vacancy movements, the disordering above T_C and the

ordering below it. Therefore, in such alloys, it must exist trajectories for vacancies creative of the order and trajectories for the destructive of the order [1].

This problem has been studied, among others, by Beeler and Delaney [55]. These authors have treated this problem by electronic calculation using a Monte Carlo method. One places at the nodes of a lattice, planar square or cubic centered, atoms of two elements A and B in equal numbers. One introduces one or more vacancies whose migration is to be studied. This assuming that the probability of jumping from the initial position (0) to the position (i) of close neighbor is:

$$P_{0i} = \exp (\Delta n_{0i} \varphi) / [1 + \exp \Delta n_{0i} \varphi] \dots \dots \dots (2.1).$$

Δn_{0i} is the variation of the number of dissimilar binds A-B during the jump $0 \rightarrow i$ and φ is the quantity ξ_{AB} / KT , ξ_{AB} being the energy of the link A-B. The energy of the bonds A-A and B-B is assumed to be zero. In each position, the vacancy then makes the most probable jump.

This calculation method was applied to an initially disordered crystal placed at a low temperature or an initially ordered crystal and placed at an elevated temperature. After migration of vacancies, partial ordering is observed with the formation of the antiphase domains in the first case, a disorder in the second. These calculations thus confirm the well-accepted idea that the establishment of order or that of disorder is due to the migration of the gaps [1].

An examination of diffusion paths followed by the vacancies, reveals the exact role played by these defects. For example, when a vacancy migrates at a relatively low temperature in an ordered crystal, we find the six jump cycles proposed by Elcock, which correspond to a transport of matter without modification of the order, but also cycles of ten jumps (Fig. 24).

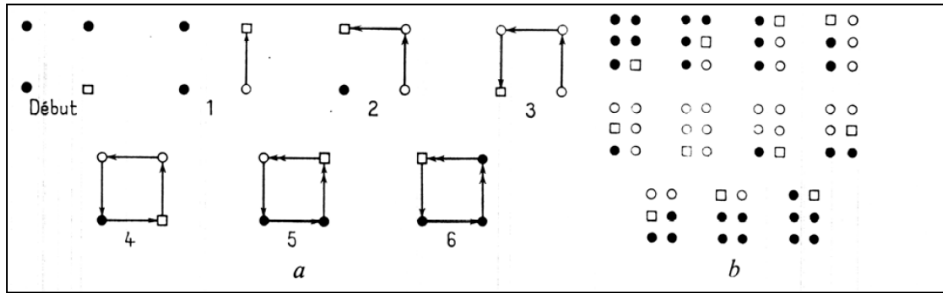


Fig.2.9. Circuits for a vacancy, in an ordered alloy, restoring order after migration.

□ Vacancy position

● Atomic position corresponds to the order

○ Atomic position corresponds to the disorder

a- Simple cycle of Elcock [56], in six jumps, the vacancy has migrated with $a\sqrt{2}$ without destruction of the order (a: the side of the square).

b- Double cycle of Beeler et Delaney [55], in ten jumps, the vacancy has migrated with $2a$ without destruction of the order.

Experimentally, it is well known that the diffusion coefficients are weaker in the ordered than in the disordered state. But especially these calculations predict that if an alloy is quenched from the disordered state, at low temperature where the order is the stable state, then the appearance of the order can be accelerated with the migration of the quenching vacancies.

This effect has been observed by several others [57, 58]. They found that when AuCu_3 alloys are quenched from temperatures above T_C , the temperature of the order-disorder transition, and we anneal them at temperatures below T_C , they have observed a strong decrease of the resistivity. They interpreted this by the establishment of the order by the vacancies migration formed in the disordered quenched alloys. Admitting that the decrease of the resistivity is proportional to the vacancies concentration [58].

Part II: Order-disorder transitions in the AuCuAg ternary system.

The AuCuAg alloy is the basis of the most common gold jewellery and dental alloys used today [59]. As it is acting as the basic phase diagram for an understanding of gold dental alloys, it has been studied for the past 94 years [60, 61]. The ternary 12-carat and 18-carat systems exhibit several phase compositions upon heating and cooling that depend on the weight participation of the added elements to gold as reported in ref [60-62]. And it displays a variety of diffusional phase transformations including compositional demixing and ordering [60, 61]. It is well known that order-disorder transitions produces significant effect on the properties of alloys [63, 64]. The debate on features, characteristic of constituent atoms, which drive ordering in different systems, has been going on for well over half a century [65]. Big ambiguities still persist concerning the phase transition mechanisms in AuCu system [66-69] as well as in the ternary AuCuAg alloy.

The ternary phase diagram is characterized by ordering superstructures on the AuCu side, and it inherits the solid state miscibility gap from the AgCu system [70], i.e. the high temperature disordered solid solution (α) decomposes into the Ag-rich (α_1) and Cu-rich (α_2) phase.

Some cuts of the ternary phase diagram are showed in figure2.10.

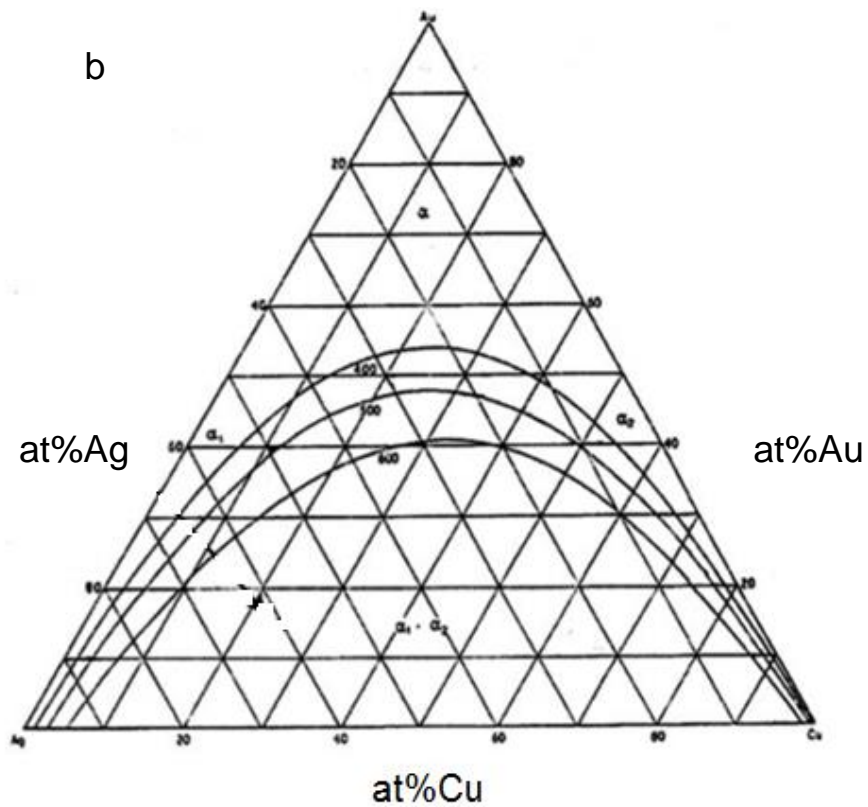
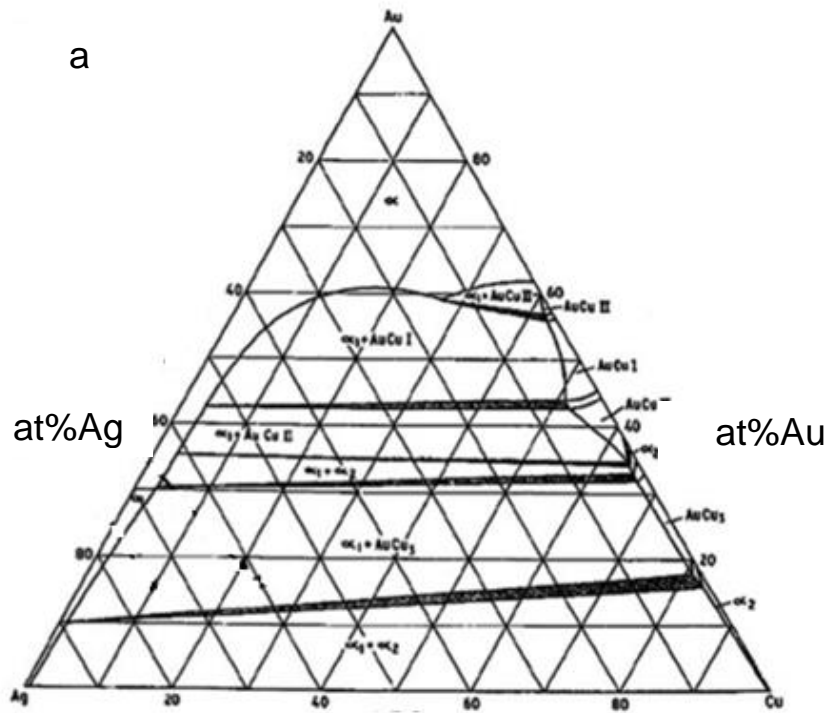


Fig.2.10. Isothermal sections of the Ag–Au–Cu ternary phase diagram: (a) at 300 °C (b) through the solvus surface at 400, 500 and 600 °C.

Part III: Mechanical behavior of gold alloys

2.III.1. Some previous mechanical results for AuCu and AuCuAg systems:

Gold alloys are very ductile materials. They can be cut or laminated easily at room temperature without breaking or fissuring. This is an advantage for shaping fine pieces. It is a soft material and it is therefore very easily scratched. Since plastic deformation in metals is mainly due to dislocation movement through the crystal, alloying elements slightly increase the hardness with respect to pure gold because of solution hardening. Therefore, the gliding of dislocations becomes more difficult if more than one element is present in the material and the hardness is increased with respect to a pure metal [71].

Recently, quite scientific works have been devoted to well investigate the mechanical properties of AuCu and AuCuAg systems due to their main application as dental prosthesis and jewellery industry. Therefore, we find in the literature some focus on these systems especially by D.Mari et al [71]. Where for example they worked on grain boundary relaxation and grain growth in 18-carat yellow gold alloy, they have used the Zener's model of the mechanical loss caused by the grain boundary sliding in metals to explain the experimental data of internal friction tests and microstructures obtained by the optical microscope.

As another study, done by the same research group D.Mari et al [72], but this time as comparison between 18-carat and 14-carat yellow gold alloys. Where the relaxation peak has been observed in the internal friction spectrum of 18-carat AuAgCu (Au60%at. Ag30%at. Cu10%at.) yellow gold alloys it is related to the presence of grain boundaries, since it is absent in the spectrum of single crystals. For the 14-carat yellow gold alloys, (Au38%at. Ag32%at. Cu30%at.) a phase decomposition between silver rich and copper rich solid solution occurs in the same temperature range. Where in this work they studied the phase decomposition effect using the internal friction and isochronal and isothermal measurements and correlated with the microstructure evolution. Several works have been done on gold

alloys using mechanical spectroscopy and always by the same researched group D. Mari *et al* [74-80]. Where, the Zener relaxation is always present in gold alloys [81].

Commercial gold alloys can be obtained easily, especially in the case of 18-carat yellow gold alloys. Their composition is well monitored and the samples have a uniform microstructure. It has been shown by John Hennig [5] that the mechanical loss spectrum of the yellow gold alloy containing 30.5% Ag atoms is particularly simple. The spectrum contains 2 stable and reproducible relaxation peaks superimposed on a high temperature background.

2.III.2. Zener Relaxation near Order-Disorder Transitions

The stress-induced ordering has been described by several theories either as a reorientation of elastic dipoles formed by solute pairs, or by a lattice gas model.

The reorientation of elastic dipoles as directional order of (nearest-neighbor) bonds, as variations in short-range order beyond nearest neighbors. In the experieal point of view, the primary interest manifests in the fact that the Zener relaxation time that is of the same magnitude as the time between atomic jumps, but can be measured at temperatures far below those accessible to radio-tracer diffusion experiments [5].

The mismatch of the size between the elements of the alloy causes lattice distortions in the solid solution, such as those observed in Au–Cu by XAFS. Hens, it gives rise to a relaxation mechanism: stress-induced directional ordering of bonds. Clarence Zener , is the first who has put onward such reasoning in order to explain a mechanical loss peak he observed in an α -brass single crystal in 1942 [5]. After five years, Zener proposed the theoretical model, associating the effect to the atomic pairs reorientation. Since then, the phenomenon is known as Zener relaxation.

The theory of Zener's pair reorientation is proper for small concentrations of one of the two alloying elements. When it is a solid solution, a pair of solute atoms locally deforms the lattice of the surrounding solvent matrix. Therefore, it can be considered as a structural defect. Figure.2.11 illustrates the case of an undersized atomic pair in a (100) plane of an f.c.c. lattice[5].

The pair orientation is random, at zero stress. But as soon as an external stress field manifests this symmetry is broken. It will lower the free energy level of those orientations $\lambda^{(p)}$ that would relax the elastic strain, i.e. further increase it while the stress remains constant [5]. The diffusion of one of the atoms constituting the pair to a neighboring lattice site leads to modify the orientation. By consequence, the relaxation time T will be of the order of a^2/D , where a is the lattice parameter and D the diffusion coefficient [5].

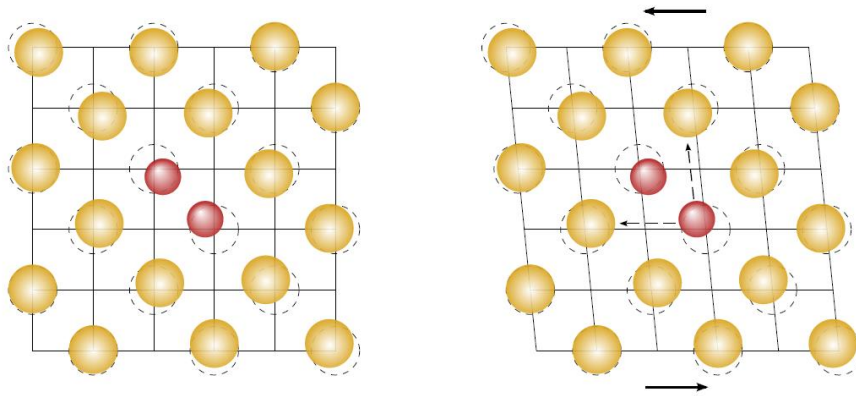


Fig.2.11. Schematic illustration of the Zener relaxation in dilute alloys: when a pair of undersized atoms in a (100) plane locally distorts the f.c.c. lattice (left), an external stress will favor some sites over others (right) [5].

The alloys that present long range order, are not "or are much less" susceptible to stress-induced diffusion. If the order is perfect, they are not only free of static lattice distortions but any bond reorientation would then incur the same energy penalty that stabilized the ordered structure in the first place.

Only as long as some disorder is present, the stress-induced bond relaxation can occur as substitutional or thermal. Thus, the Zener relaxation strength in a stoichiometric alloy should tend to zero as the long-range order parameter reaches unity. Compared to the solid solution, at the off-stoichiometric compositions the peak height may remain finite, but should drop off markedly [5].

III: Materials and Experimental Techniques

3 Materials and Experimental Techniques

3.1. Studied alloys and applied heat treatments

Since our work aims for the study of the order-disorder transitions in the gold based alloys, we especially focused on two kind of systems: AuCu and AuCuAg.

Two different weight compositions for every system are used in our work as following: Au-25wt.%Cu, Au-50wt.%Cu, Au-7wt.%Cu-18wt.%Ag and Au-15wt.%Cu-35wt.%Ag. The electronic microscopy analyzes of the weight composition of the prepared ingots have been done to confirm the compositions as detailed in table3.1.

The used ingots are prepared by means of fusion by torch, using very pure elements: 99.999% Au, 99.999% Ag and 99.999%Cu.

For the applied heat treatment, we basically homogenized all used samples for two hours at 973 K (700°C) followed by water quenching. After homogenization treatment, the heat treatment depends on the analyzes wanted as detailed after. The measurements have been carried out under primary vacuum (for DSC and Dilatometry) and under secondary vacuum (for in-situ XRD, SEM and the mechanical analyzes).

Codes used in this study	Weight compositions %			Atomic compositions %		
	Au	Cu	Ag	Au	Cu	Ag
25	75	25	0	50	50	0
50	50	50	0	25	75	0
7-18	75	7	18	57	17	26
15-35	50	15	35	32	28	40

Tab.3.1. Nominal composition of the yellow gold alloys studied in this work.

3.2. The used characterization techniques

3.2.1. Electron probe microanalysis (EPMA)

The EPMA configuration varies according to the user's requirements, but is always centered on an electron gun that fires beams of electrons at the specimen. The electron gun is fitted to a vacuum chamber equipped with a stage that can move the specimen in steps as small as one tenth of a micrometer, allowing the beam to explore the entire specimen surface.

An optical microscope coaxial to the electron beam, and with continuously variable magnification, identifies the exact points of interest on the specimen surface. A charge-coupled device (CCD) camera allows samples to be viewed in reflected light and thin sections to be imaged in transmitted polarized light. Meanwhile, CL detectors attached to the optical microscope port collect the visible light generated when the electron beam hits the specimen (Fig.3.1).

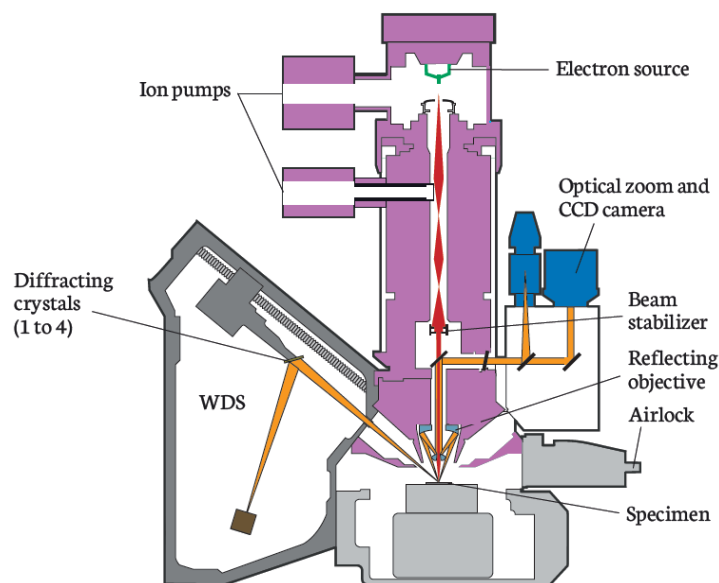


Fig.3.1. Schematic of EPMA.



Fig.3.2. The model of commercial EPMA used (UNIOVI).

The EDS collects the entire energy spectrum of the emitted X-rays simultaneously from all elements present in a sample. This qualitative information can be combined with information collected by the SE and BSE detectors. The EDS is used to identify the major elements in a specimen, but can struggle to identify peaks from minor and trace elements.

The EPMA have been used in our study in order to determine the exact weight composition of the prepared ingots and of the pieces used in the different tests. In this work the corresponding measurements have been taken at "University of Oviedo".

3.2.2. Differential Scanning Calorimetry (DSC)

The differential scanning calorimetric (DSC) study allows the study of the physical and chemical transitions involving thermal effects in a material.

A linear rise in the temperature of the sample and the reference is ensured, and then the heating power of the sample is adjusted at each instant, so that the temperature of the sample is the same as the reference, by compensation of the exothermic or endothermic effects. The compensation of the calorific power is measured as a function of the temperature $dQ / dT = f(T)$.

DSC is a method of scanning temperature, heating and cooling. It can be used to perform isothermal measurements to study the kinetics of transitions. During a reaction recorded by DSC, two kinds of peaks can be distinguished:

- An exothermic peak (phase formation) above the baseline,
- An endothermic peak (phase dissolution) below the baseline.

Cylindrical samples of almost 5 mm in diameter and 2 mm in thickness were used for this analysis. The DSC measurements were carried out under an argon atmosphere with a DSC Setaram 131 (Fig.3.3). The thermal cycle applied consists in heating from room temperature up to 973 K (700 °C). using the velocity of 10K/min. In this work the corresponding measurements have been taken at "University of Constantine1".

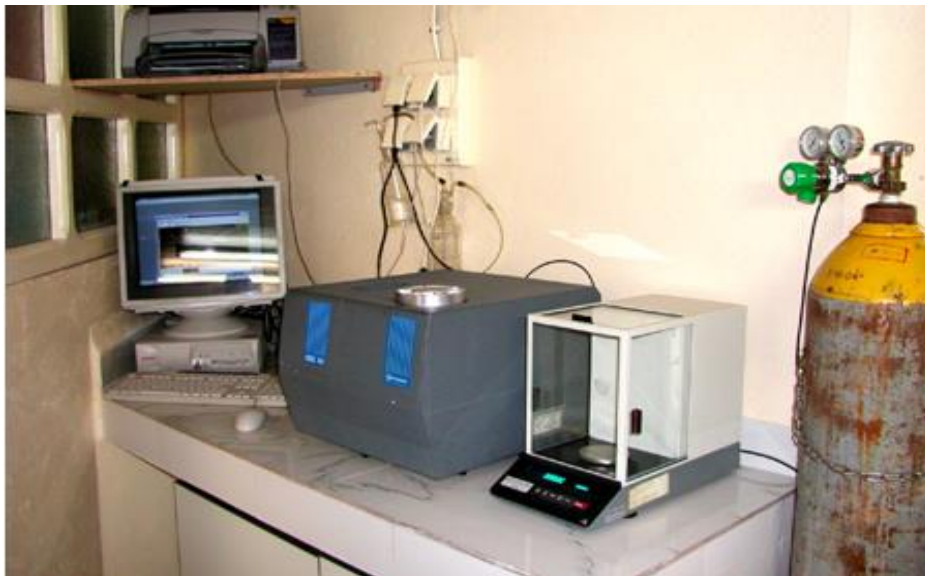


Fig.3.3. The used DSC analyzer SETARAM DSC 131 connected to a computer(UC1).

3.2.3. Dilatometric analysis

The technique of dilatometric analysis is reserved for the structural transformations is accompanied by a change of volume. With the aid of a quenching dilatometer of

type DT1000 it is possible to measure the dimensional variations of a test piece subjected to heating or cooling cycles at different speeds.

In this work, the dilatometric analysis was carried out using an Adamel Lhomargy DT1000 dilatometer connected to a microcomputer (Fig.3.4). The use of the recorded dilatometric curves is carried out using a special software (LOGIDIL) which allows the processing of the expansion curves as a function of time or temperature for each segment of the thermal cycle imposed, with the corresponding derivative curve . Cylindrical samples of almost 2 mm in diameter and 10 mm in length were used. The thermal cycle applied consists in heating from room temperature up to 973 k (700 °C). using the velocity of 10k/min. In this work the corresponding measurements have been taken at "University of Constantine1".



Fig.3.4. The used dilatometer ADAMEL LHOMERGY of DT1000 type, connected to a computer (UC1).

3.2.4. Scanning Electron Microscopy (SEM)

SEM has been used in our study for the imaging of certain phase transition in gold alloys. The scanning electron microscope (SEM) uses a focused beam of high-energy electrons to generate a variety of signals at the surface of solid specimens. The signals that derive from electron-sample interactions reveal information about the sample including external morphology (texture), chemical composition, and

crystalline structure and orientation of materials making up the sample. In most applications, data are collected over a selected area of the surface of the sample, and a 2-dimensional image is generated that displays spatial variations in these properties.

Accelerated electrons in an SEM carry significant amounts of kinetic energy, and this energy is dissipated as a variety of signals produced by electron-sample interactions when the incident electrons are decelerated in the solid sample. These signals include secondary electrons (that produce SEM images), backscattered electrons (BSE), diffracted backscattered electrons (EBSD that are used to determine crystal structures and orientations of minerals), photons (characteristic X-rays that are used for elemental analysis and continuum X-rays), visible light (cathodoluminescence–CL), and heat. Secondary electrons and backscattered electrons are commonly used for imaging samples: secondary electrons are most valuable for showing morphology and topography on samples and backscattered electrons are most valuable for illustrating contrasts in composition in multiphase samples (i.e. for rapid phase discrimination). X-ray generation is produced by inelastic collisions of the incident electrons with electrons in discrete orbitals (shells) of atoms in the sample. As the excited electrons return to lower energy states, they yield X-rays that are of a fixed wavelength (that is related to the difference in energy levels of electrons in different shells for a given element). Thus, characteristic X-rays are produced for each element in a mineral that is "excited" by the electron beam. SEM analysis is considered to be "non-destructive"; that is, x-rays generated by electron interactions do not lead to volume loss of the sample, so it is possible to analyze the same materials repeatedly.

In our work we needed only 2-Dimensional imaging of the samples to have an idea about what happens to the surface during some phase transition. by means of FEG-SEM-FEI instrument, using secondary electron mode with accelerating voltage of 10 kV. Furthermore, JSM-7100F instrument has been used for the EDS tests. In this work the corresponding measurements have been taken at "University of Constantine1".



Fig.3.5. The used "JSM-7100F" SEM (UC1).

3.2.5. Scanning Tunneling Microscopy (STM)

For more precision and magnification of the surface aspect during some phase transition, SEM technique has been used. VT AFM XA, ST-Microscope was in use.

The scanning tunneling microscope [82] (STM) allows the topography of surfaces to be visualized up to the atomic scale. The circulation of a tunnel current restricts the field of observation to metals and semiconductors. This technique can operate in air, in a vacuum, in liquid medium and at high or low temperature.

A very fine metal point is approached at a distance of about one nanometer from a surface. When a potential difference (of the order of a volt) is applied between these two electrodes, a current is observed, authorized by quantum mechanics and not by classical mechanics. This current, called tunnel, decreases exponentially with the point-surface distance. A current control is therefore equivalent, for a given material, to a remote control that can be adjusted by means of a piezoelectric ceramic. Two

other piezoelectric ceramics allow scanning parallel to the surface of the sample. The iso-current layer thus traveled is a constant distance sheet. In other words, a 3D image of the surface of the sample is obtained. The fineness of measurement of the collected current makes it possible to reach the atomic resolution.

The tunneling microscope is also a local probe of the electronic structure. The electrons that contribute to the current change from a solid state density to an empty state density. By varying the voltage difference between the two electrodes, the offset between the Fermi levels is changed.

The study of surfaces constitutes the major part of the applications of this technique. Huge progress has been made in the understanding and preparation of surfaces. More than crystallography, it is undoubtedly in the gaps in crystallography (defects, markets, local reactivity) that the technique is the most fruitful. More marginally, the probe tip can be used as a tool to create artificial nanometric structures.

The images obtained make it possible, in addition to the observation of the surface topography, the resolution of the surface crystalline structure. As well as the observation of the atomic steps, defects (gaps, adatoms ...) and possibly supported nano-objects.

It is also possible to access the electronic surface structure using elastic or inelastic spectroscopy techniques [83].

In this work the corresponding measurements have been taken at "University of Oviedo".

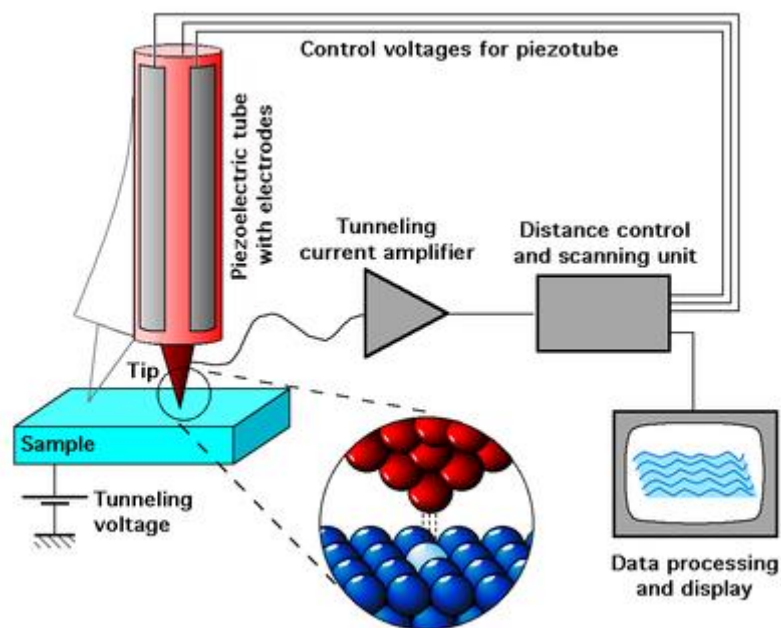


Fig.3.6. Schematic view of an STM [84].

3.2.6. X-Ray Photoelectron Spectroscopy (XPS)

We counted on this technique to identify the chemical composition of some clusters on the top of the samples. Therefore, an Omicron ESCA spectrometer has been used, equipped with a monochromatic Al K_{α} X-ray source ($h\nu=1486.7$ eV) operating at 300 W, with an Argus Cu analyzer, to analyze the energy of the emitted photoelectron from the surface. A multi-channel plate and delay line detector under vacuum of 2×10^{-8} Pa, and an electron take off angle of 45° were employed. The spectra of non-conducting samples were referenced to the C1s peak at 285.0 eV BE.

XPS (also referred to as Electron Spectroscopy for Chemical Analysis or ESCA) is an analytical technique where x-rays are used to bombard a specimen and the energies of emitted electrons are analyzed.

X-rays penetrate the specimen surface to a depth of a few micrometers but only the electrons near the surface can be emitted without losing energy due to collisions

with other atoms. The kinetic energy (KE) of the electrons is measured and the binding energy (BE) of the electrons can be determined with a simple relationship:

$$h\nu = KE + BE + \phi \dots \dots \dots (3.1)$$

where $h\nu$ is the x-ray energy and ϕ is the spectrometer work function (usually only a few eV). An energy spectrum is obtained with a scan over the kinetic energy range from 0 eV to the incident x-ray energy. The energy spectrum is different for each element and permits elemental identification of the species present in the top 1-2 nm. The detection limit is approximately 0.1% atomic. XPS is more sensitive for higher atomic number elements.

The energy resolution of the spectrometer is sufficient to resolve differences in binding energy for different chemical bonds. For example, it is possible to separate C-C from C-O and O-C=O. The area under the peak for each bond represents the percentage of that bond that is present. Since the XPS electrons originate mostly from the first few monolayers, sample cleanliness and handling are crucial to obtain useful results. This technique has been used to analyze a very wide range of materials. The limitations are that it must be a solid and vacuum compatible. Powders can be mounted with sticky tape and liquids can be dried on a substrate such as silicon.

. In this work the corresponding measurements have been taken at "University of Oviedo".

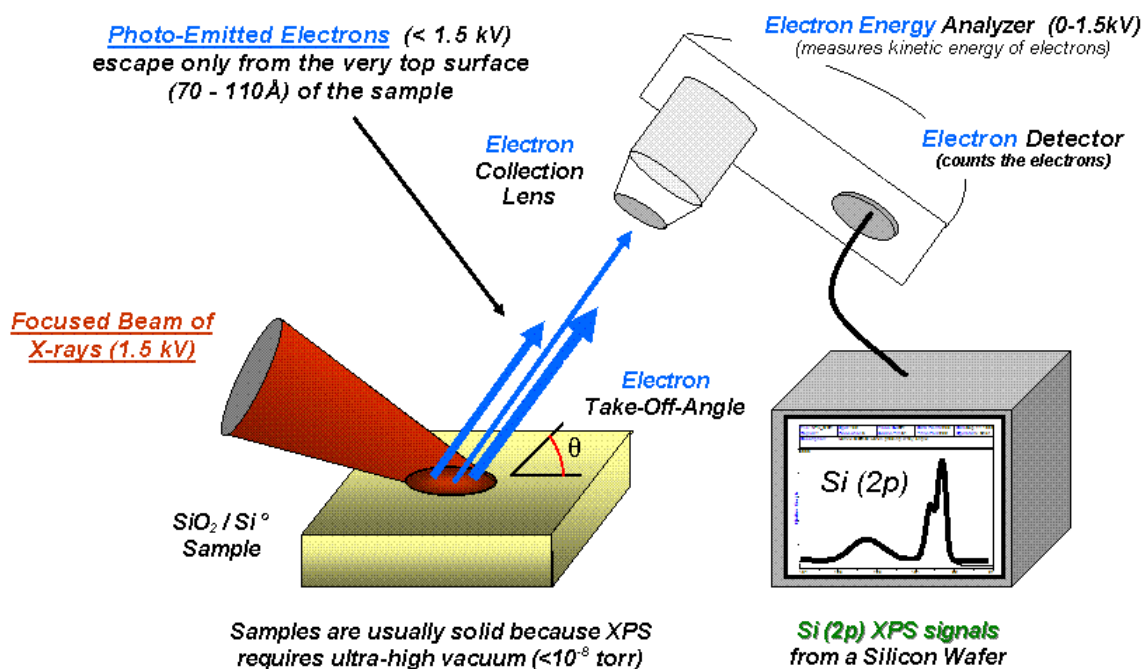


Fig.3.7. Basic components of a monochromatic XPS system [85].

3.2.7. X-Ray Diffraction (XRD)

X-ray diffraction is based on constructive interference of monochromatic X-rays and a crystalline sample. These X-rays are generated by a cathode ray tube, filtered to produce monochromatic radiation, collimated to concentrate, and directed toward the sample. The interaction of the incident rays with the sample produces constructive interference (and a diffracted ray) when conditions satisfy Bragg's Law ($n\lambda=2d \sin \theta$). This law relates the wavelength of electromagnetic radiation to the diffraction angle and the lattice spacing in a crystalline sample. These diffracted X-rays are then detected, processed and counted. By scanning the sample through a range of 2θ angles, all possible diffraction directions of the lattice should be attained. Conversion of the diffraction peaks to d-spacings allows identification of the mineral because each mineral has a set of unique d-spacings. Typically, this is achieved by comparison of d-spacings with standard reference patterns. All diffraction methods are based on generation of X-rays in an X-ray tube. These X-rays are directed at the sample, and the diffracted rays are collected. A key component of all diffraction is the angle between the incident and diffracted rays.

X-ray diffractometers consist of three basic elements: an X-ray tube, a sample holder, and an X-ray detector. X-rays are generated in a cathode ray tube by heating a filament to produce electrons, accelerating the electrons toward a target by applying a voltage, and bombarding the target material with electrons. When electrons have sufficient energy to dislodge inner shell electrons of the target material, characteristic X-ray spectra are produced. These spectra consist of several components, the most common being K_{α} and K_{β} . K_{α} consists, in part, of $K_{\alpha 1}$ and $K_{\alpha 2}$. $K_{\alpha 1}$ has a slightly shorter wavelength and twice the intensity as $K_{\alpha 2}$. The specific wavelengths are characteristic of the target material (Cu, Fe, Mo, Cr). Filtering, by foils or crystal monochrometers, is required to produce monochromatic X-rays needed for diffraction. $K_{\alpha 1}$ and $K_{\alpha 2}$ are sufficiently close in wavelength such that a weighted average of the two is used. Copper is the most common target material for single-crystal diffraction, with $\text{Cu}K_{\alpha}$ radiation = 1.5418\AA . These X-rays are collimated and directed onto the sample. As the sample and detector are rotated, the intensity of the reflected X-rays is recorded. When the geometry of the incident X-rays impinging the sample satisfies the Bragg Equation, constructive interference occurs and a peak in intensity occurs. A detector records and processes this X-ray signal and converts the signal to a count rate which is then output to a device such as a printer or computer monitor.

In situ X-ray thermo diffraction was performed inside an Anton Paar HTK 1200N chamber between 298 and 973 K at rates of 1 K/min under secondary vacuum ($\sim 1 \times 10^{-5}$ mbar). This platform is mounted at the goniometer of a Panalytical XPERT-PRO diffractometer which use copper K_{α} radiation (1.5418\AA) and a PIXcel detector for record each diffraction pattern measured at sweeping mode. The disk is fixed on the top of an alumina rod with a diameter of 15 mm and suitable fixed slits and mask are selected to illuminate only the surface of the sample. NIST standard reference material SRM 660a was used to determine precisely angle and/or height errors on the equipment and sample position. Besides, two equivalent experiments have been carried out over large range (from 20 to 90° on 2θ) and short range (from 29 to 42° on 2θ) in order to establish the type and temperatures of each phase transformations respectively. Finally, X-ray diffraction patterns have been analyzed by Le-Bail method [25] implemented in the Fullprof Suite package [26], allowing us to

settle the parameters of every peak according to our structural models. . In this work the corresponding measurements have been taken at "University of Oviedo".



Fig.3.8. The used XPERT PRO Diffractometer (UNIOVI).

3.2.8. Forced torsion pendulum

A forced torsion pendulum has been used in order to study the mechanical behavior (elastic "internal friction and anelastic "shear modulus") upon the whole thermal cycle and the phase transitions that appear during it.

A forced torsion pendulum is an experimental set-up to measure the mechanical loss spectrum and the dynamic modulus of a specimen. The measurement can be carried out at different temperatures and at different excitation frequencies. A schematic drawing is shown in Figure.3.9(a). A harmonically varying torque T is applied to the sample via a magnetic excitation system. Two magnetic coils driven by a harmonic current I attract or repel a pair of permanent magnets, which are attached to the rod. The sample is twisted such that the top end rotates whereas the bottom part remains fixed. The torsion angle is measured by a laser spot that is reflected on an mirror attached to the rod. The position of the laser spot is detected by a photocell. In order to compensate for slight plastic deformation of the sample during the experiment, the photocell is mounted on a centring stage. A furnace surrounds

the sample and the control of the heating coils allows one to vary the temperature between 290 K (17°C) and 1200 K (927°C). A balance system with a counterweight attached to it compensates the weight of the rod and the permanent magnets such that no compression or tension acts on the sample. The upper end of the rod is attached to the balance by a three-wire suspension (upper part of Figure.3.9 (b), which permits the rod to turn freely around its vertical axis. During the measurement, the installation is set under vacuum with the exception of the laser and the photocell. A pallet pump creates a primary vacuum, a secondary vacuum of 10^{-5} mbar is maintained with a oil-diffusion pump. The output signal from the photocell is analyzed by a Solartron 1250 frequency analyzer. By comparing the output signal with the excitation, the relation between input and output amplitudes gives access to the dynamic modulus of the specimen. The phase lag of the output signal with respect to the excitation signal provides directly a measurement of the mechanical loss [71].

. In this work the corresponding measurements have been taken at "EPFL".

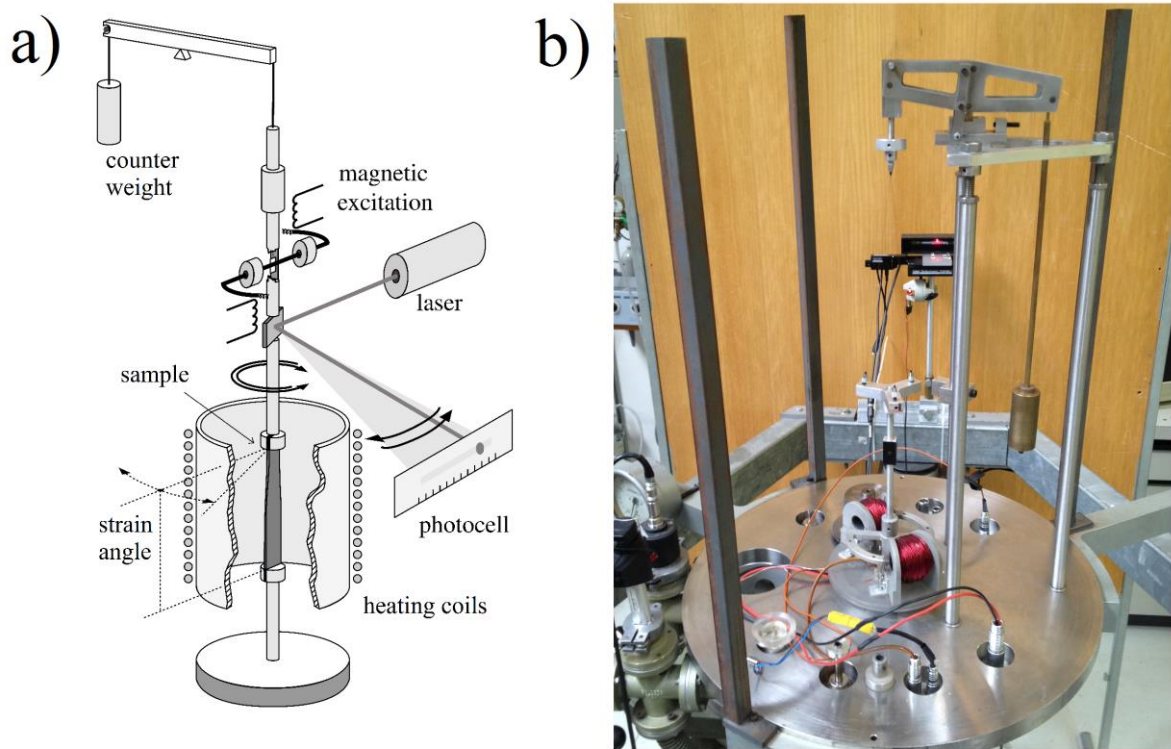


Fig.3.9. (a)Sketch of an inverted forced torsion pendulum. (b) Photo of the upper part of the mechanical spectroscopy experimental installation. The balance with the counter weight is visible in the upper part. The mirror (black) in the middle reflects the laser spot to a photocell in the background. The electromagnets (red) excite the rod in torsion. The sample is situated below the metallic disc and cannot be seen on the photo [71] (EPFL).

3.2.9. Quantitative elemental depth profile analysis

Using HORIBA Pulsed Radio Frequency Glow Discharge Optical Emission Spectroscopy (RF GD-OES). This profiler combines a glow discharge source powered by pulsed radio frequency to sputter "layer by layer" a representative area of the investigated material, with a high resolution and high sensitivity emission spectrometer that will measure in real time all elements of interest as a function of depth.

IV: Results and discussions

4 Results and discussions

Introduction

12-carat gold alloys (Au-50wt.%Cu and Au-15 wt.% Cu-35 wt.% Ag) present important systems with poor knowledge of their physical properties. The binary 18-carat yellow alloy (Au-25 wt.% Cu) appears to be a testing ground for different order-disorder phase transitions. This last system is known to pass by three phases as following: AuCuI, AuCuII, A1. The ternary 18-carat system Au-7 wt.% Cu-18 wt.% Ag represents an important system for the jewelry industry.

Basing on these compositions, our experimental study has been built on four principal parts.

Part I: Kinetic study of the metastable phase in 12-carat compositions

A new pre-ordering reaction that precedes the formation of the ordered phase in the equiatomic Au-Cu system occurs at low temperature, and it has been observed for the first time by Hamana *et al* [86]. Therefore, this part is interested with the checking of the presence of such reaction in 12-carat binary and ternary gold alloys. Thus, one binary (Au-50wt.%Cu) and one ternary (Au-15wt.%-Cu-35wt.%Ag) compositions have been included in this part. The thermal results were unexpected. The study is completed with a trial to identify the nature and the origin of the new meta-stable phase that appears in very specific conditions of temperature. That can lead to new properties then new exploit of these systems at low temperature.

4.1.1. Results of previous experiments on AuCu equiatomic system

In previous study of Hamana *et al* [86], a new reaction has been detected at low temperature using DSC in the equiatomic Au-Cu system, where they have used several heating velocities for the same homogenization temperature to check if this

phase appear independently to the heating rate and they found that more the velocity gets higher more the peak gets sharper but it exists anyway. On the other hand they have studied the effect of the temperature of homogenization on this peak and they found that arriving to 1023 K (750°C) and more, there is diffusion of this peak with the one corresponding to the ordering reaction. Where, bellow 1023 K (750°C) there is separation between the two peaks.

Since this kind of phase transitions affects crucially the physical properties of the material especially the mechanical part [88-92], and basing on these previous results, this first part of our work is concerned with using another compositions of 12-carat gold alloys instead of 18 carat (Au-25wt.%Cu) used by Hamana *et al* [86] and using different experimental conditions and characterization techniques.

4.1.2. DSC and Dilatometric studies

The used samples in this part have been homogenized for two hours at 973 K (700°C) followed by water quenching. Therefore, and according to the used thermal treatment, the starting state for the DSC and the dilatometric tests is the disorder for both compositions (i.e. A1 for the binary and the solid solution α for the ternary composition) (As confirmed with the XRD spectra in figure 4.1). The corresponding curves have been focalized at the area bellow 573 K (300°C), the region where the anomaly have been found in previous work on 12-carat binary composition ref. [86].

The obtained DSC heating curves are presented in figure 4.2. On the basis of the binary and ternary phase diagrams [43,60,61] and on the starting state for the thermal analyses which is the disorder in both compositions, the analyze of the first heating curve which corresponds to the binary composition Au-50wt.%Cu (Fig.4.2 (a)) shows two discerned exothermic peaks **P1** and **P2** with two maximums situated at 438K (165°C) and 481K (208°C). The appearance of the first peak (**P1**) confirms that the reaction discussed by Hamana *et al* [86] at low temperature is also present in the binary 12-carat alloy. The second peak (**P2**) corresponds to the ordering reaction presented in A1- AuCu₃ phase transition.

Concerning the ternary composition, Au-15wt.%Cu-35wt.%Ag, the DSC heating curve (Fig.4. 2(b)) shows the presence of three exothermic peaks (P1) located at 393K (120 °C) which is likely to be a sign of the pre-ordering reaction at low temperature in the ternary composition.

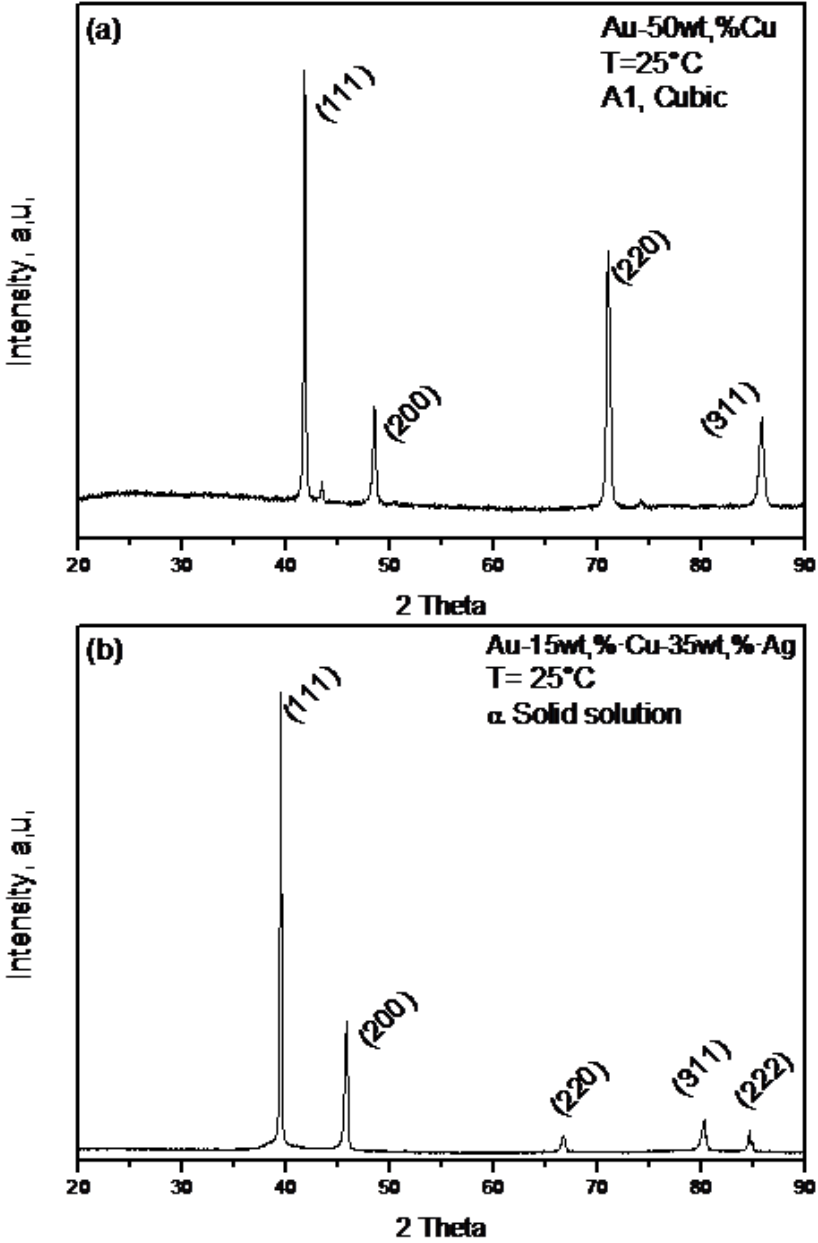


Fig.4.1. X-ray diffraction spectra in the initial state after the homogenization and water quenching (before heating up) of the Au-50wt.%Cu (a) and Au-15wt.%Cu-35wt.%Ag (b).

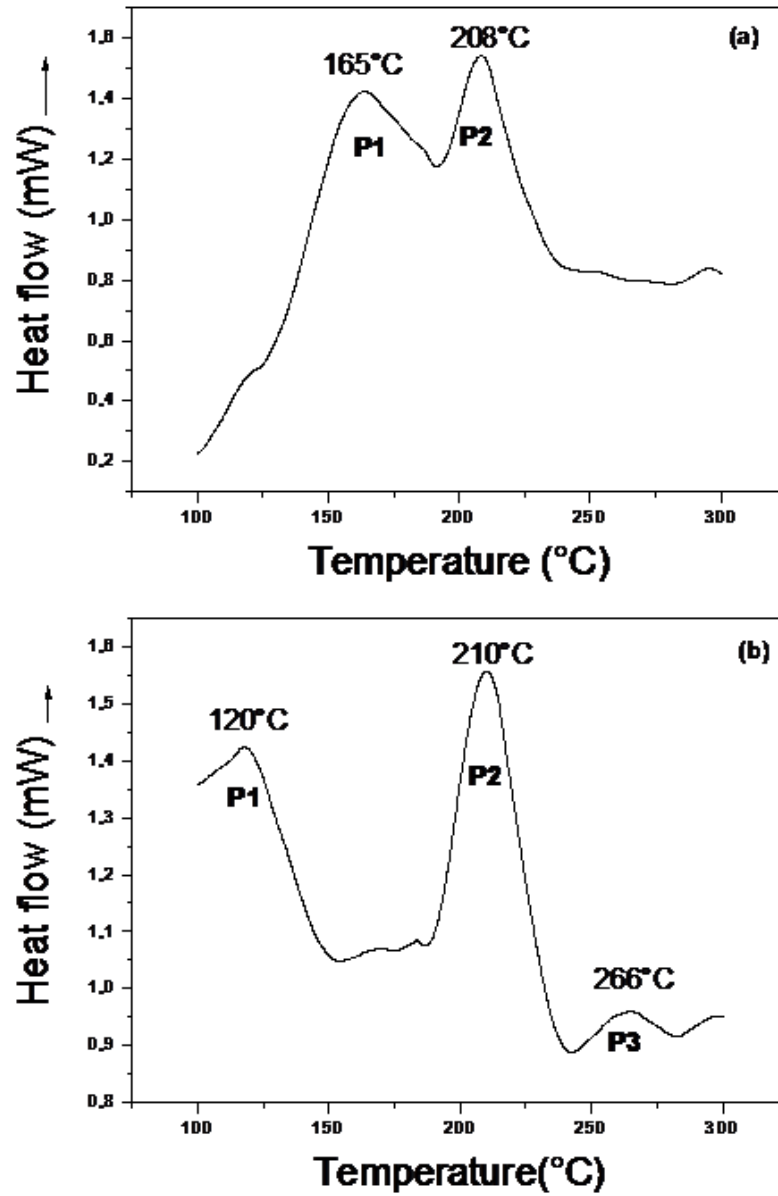


Fig.4.2. DSC curves of Au-50wt.%Cu (a) and Au-15wt.%Cu-35wt.%Ag (b) homogenized 2 h at 973 K(700 °C), and water quenched.

The silver presence in Au-Cu system leads to the acceleration of the ordering reaction, this pre-ordering reaction should also be accelerated as figure 4.2 (b) shows. The second and the third peaks in the ternary composition (**P2**) and (**P3**), located at 483K (210°C) and 539K (266°C) respectively, correspond to the phase separation embodied in the fact of the precipitation of α_1 reach in silver then α_2 reach in copper phases [60,61].

The dilatometric study has been done to confirm the results already observed by the DSC with the same experimental conditions. The obtained curves are presented in figure 4.3. The derivative curve of the heating segment, corresponding to the binary Au-50wt.%Cu sample (Fig.4.3(a)), shows a large contraction situated between 393K (120°C) and 553K (280°C) which results from an overlap of two peaks corresponding to the first reaction at low temperature (pre-ordering) and the formation of the ordered phase AuCu₃ represented in (**P1**) and (**P2**).

The derivative dilatometric heating curve corresponding to the Au-15wt.%Cu-35wt.%Ag ternary composition (Fig. 4.3(b)) exhibits a large contraction situated between 333K (50°C) and 542K (269°C) represents an overlap of two peaks **P1** and **P2** and a second clear peak **P3** between 542K (269°C) and 573K (300°C) with a minimum situated at 561K (288°C). **P1** should corresponds to the pre-phase transition at low temperature. **P2** and **P3** should correspond to the precipitation of α_1 reach in silver and α_2 reach in copper phases respectively [60,61].

The above results indicate that the DSC and the dilatometric curves are in a good agreement. To investigate the origin of the unknown first peak which appears at low temperature, further techniques are required.

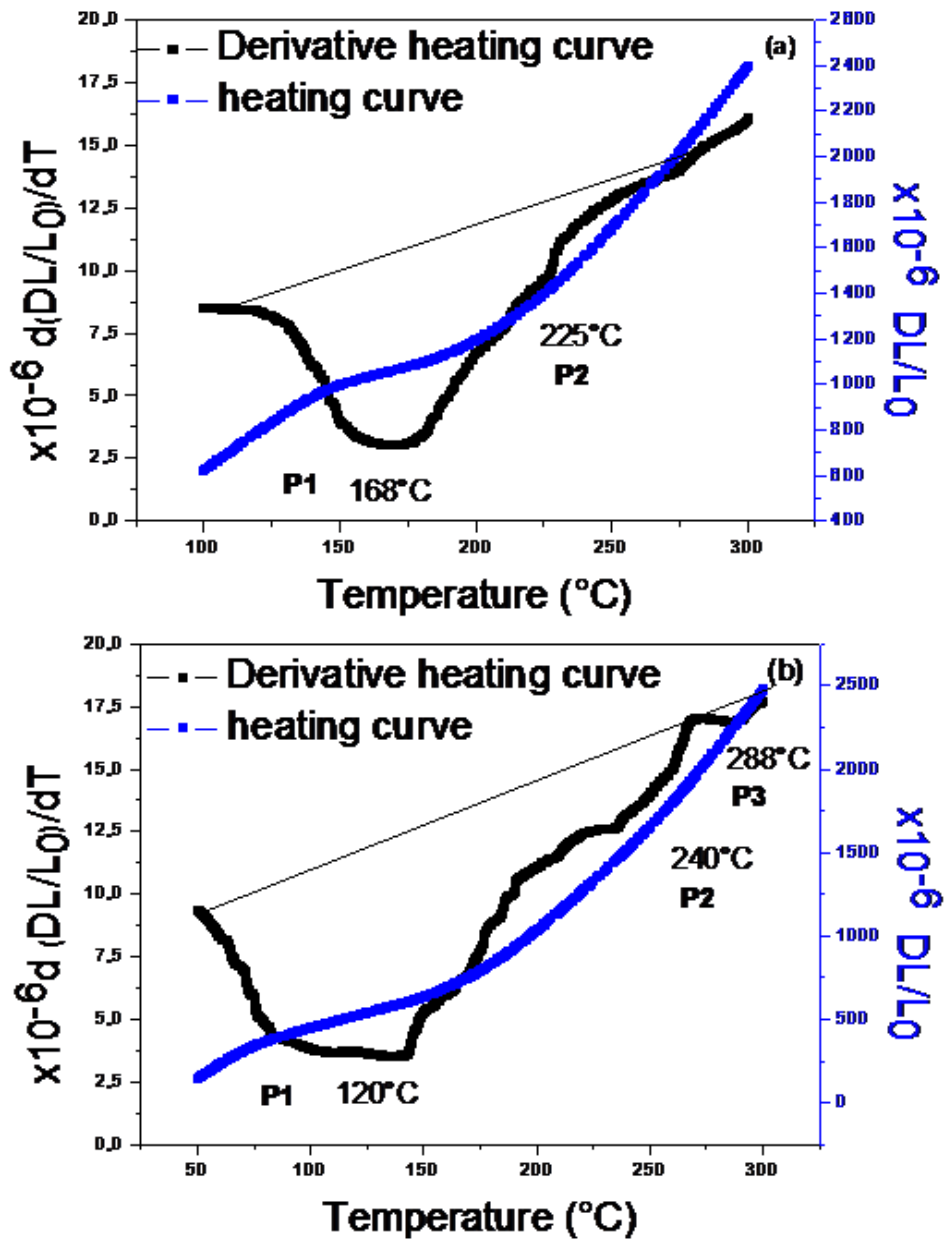


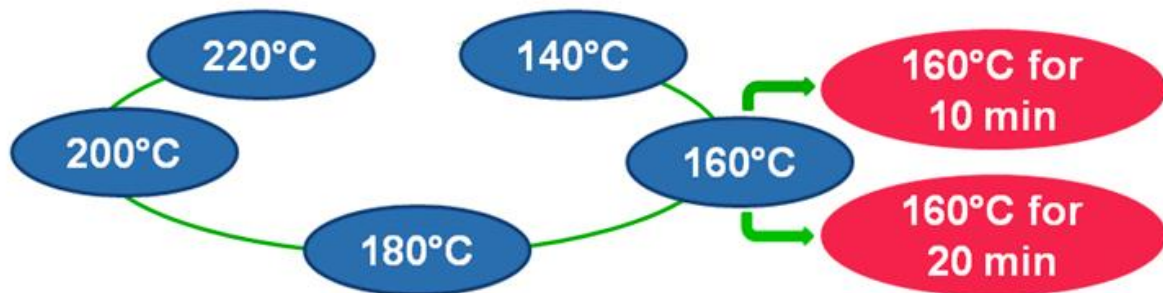
Fig.4.3. Dilatometric curves and derivative heating curves of Au-50wt.%Cu (a) and Au-15wt.%Cu-35wt.%Ag (b) samples homogenized 2 h at 973K (700°C), and water quenched.

4.1.2. Morphological study (SEM and STM)

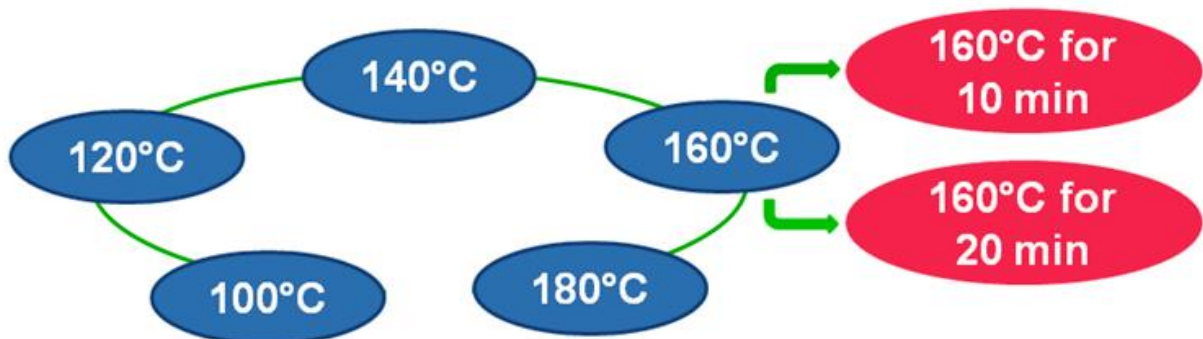
As the imaging study is important for the phase transitions, we used two techniques SEM and STM. The SEM images have been taken on two series of samples, from the disorder and from the order. Knowing that at 973K (700°C) we did not notice any anomaly or special appearance neither in SEM nor in STM images for the both compositions.

4.1.2.1. SEM study from the disordered state

The used samples in this part were in the disordered phase A1 for the binary and the solid solution α for the ternary compositions, obtained after annealing for two hours at 973K (700°C) followed by water quenching. As first step, the annealed samples have been heated from room temperature up to 433K (160°C) with different holding times (0, 10, and 20min) for both compositions. The second step was concerned with SEM imaging of samples heating from room temperature up to 140, 180, 200, and 220°C for the binary composition and up to 100, 120, 140, 180°C for the ternary composition as clarified in Scheme 4.1.



Heating cycle scheme of the Au-(50)Cu composition



Heating cycle scheme of the Au-(15)Cu-(35)Ag composition

Scheme 4.1. Heating cycle schemes of the SEM study from the disordered state.

- Au-(50)Cu corresponds to the composition Au-50wt.%Cu.

- Au-(15)Cu-(35)Ag corresponds to the composition Au-15wt.%Cu-35wt.%Ag.

4.1.2.1.1. The binary composition Au-50wt.%Cu

Figure 4.4 presents SEM images of the binary composition taken at 433K (160°C). The simple heating up to 433K (160°C) without holding (Fig.4.4(a,b)) leads to the

appearance of cubic precipitates scattered on the sample surface. The holding at 433K (160°C) for 20 min (Fig.4.4(c,d)) leads to remarkable increase in precipitates density with dendrite shape.

The noticeable effect of the pre-ordering reaction on sample surface aspect proved by figure 4.4 after heating up to 433K (160°C), and to follow the formation kinetic of these precipitates, heating up to lower and upper temperatures than 433K (160°C) have been carried out.

Figure 4.5 presents the corresponding SEM images. For upper temperatures, figure 4.5(a,b) correspond to the heating up to 453K (180°C). The precipitates are homogeneously scattered on the whole surface with dendrites shape instead of cubes at 433K (160°C) (Fig.4.4(a,b)). Figure 4.5(c,d) correspond to the heating up to 473K (200°C). The precipitates are much bigger by comparison to figure.4.5(a,b). Figure 4. 5(e) corresponds to the heating up to 493K (220°C). It shows the total absence of any precipitates on the whole surface. For temperature lower than 433K (160°C), SEM image after heating up to 413K (140°C) presented in figure 4.5(f), there is no precipitates.

The SEM images for the binary composition prove that the precipitation on the sample surface starts at 433K (160°C), by the appearance of scattered cubes on the whole sample surface. By increasing the holding time, the precipitates get more dense and take a dendrite shape (Fig.4.4).The cubes that present the onset of the precipitates at 433K (160°C), become dendrites at 453K (180°C) and 473K (200°C) then the precipitates disappear beyond 473K (200°C) (Fig.4.5).

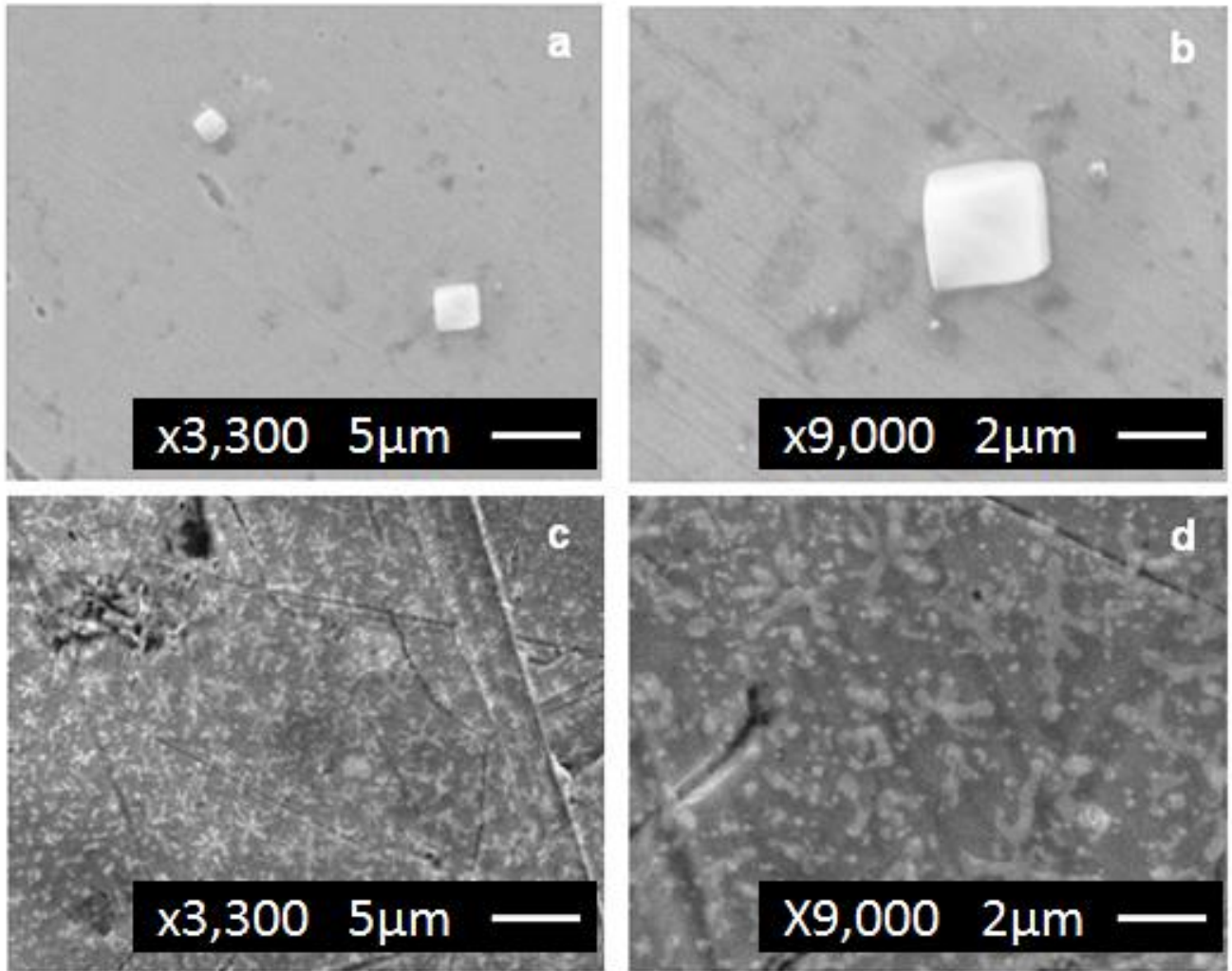


Fig.4.4. SEM surface morphology of Au-50wt.%Cu sample, heated from the disorder up to 433K (160°C) without holding then water quenched (a,b), with holding 20min at 433K (160°C) followed by water quenching (c,d).

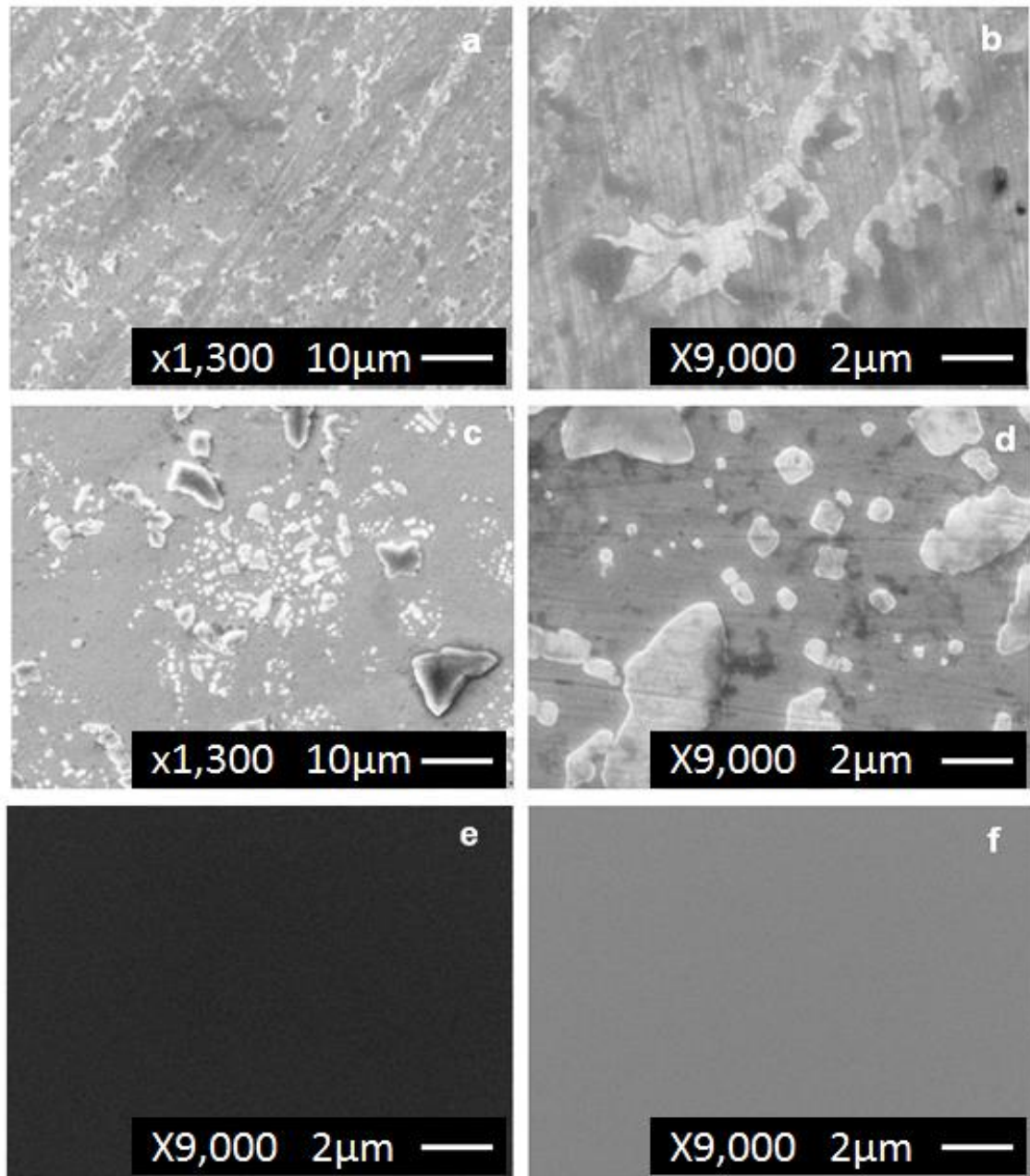


Fig.4.5. SEM surface morphology of Au-50wt.%Cu sample heated from the disorder up to 453K (180°C) (a,b), to 473K (200°C) (c,d), to 493K (220°C) (e) and to 413K (140°C) (f), without holding. Where in the (a) image the whole sample surface were covered homogeneously with the dendrites. For the (c) image only some few spots on the surface presented the presence of the precipitates.

4.1.2.1.2. The ternary composition Au-15wt.%Cu-35wt.%Ag

Figure 4.6 presents SEM images of the ternary composition taken at 433K (160°C). Figure 4.6 (a,b) correspond to simple heating up to 433K (160°C), and it exhibits large precipitates with dendrite shape. Figure 4.6 (c, d, e) are taken after heating up with holding for 10min at 433K (160°C), and it exhibits that the dendrites get thinner and longer with a filamentary extension by comparison to the case without holding at 433K (160°C) (Fig.4.6 (a, b)) after holding for 20min at 433K (160°C) the precipitates disappear completely from the whole surface (Fig.4.6(f)).

After the noticeable effect of the pre-ordering reaction on sample surface aspect proved by figure 6 after heating up to 433K (160°C), and to follow the formation kinetic of these precipitates for the ternary composition, heating up to lower and upper temperatures than 433K (160°C) have been carried out. Figure 4.7 presents the corresponding SEM images.

For temperature upper than 433K (160°C), figure 4.7(a) corresponds to the heating up to 453K (180°C), the image shows the total disappearance of the precipitates.

For lower temperatures, SEM image after heating up to 413K (140°C) presented in figure 4.7(b), shows the presence of scattered cubes on the sample surface as precipitates. More lower, 393K (120°C) (Fig.4.7(c)) also cubes scattered on samples surface. However, going more down to 373K (100°C) (Fig.4.7(d)), no trace of precipitates is noticeable.

The SEM images for the ternary composition prove that the precipitation on the sample surface starts at 393K (120°C), by the appearance of scattered cubes on the whole sample surface. The cubes persist on the surface with the increase of the temperature where they become large dendrites from 413K (140°C) to 433K (160°C). By increasing the holding time at 433K (160°C) these dendrites get longer and thinner in order to disappear completely after 20min of holding at 433K (160°C).

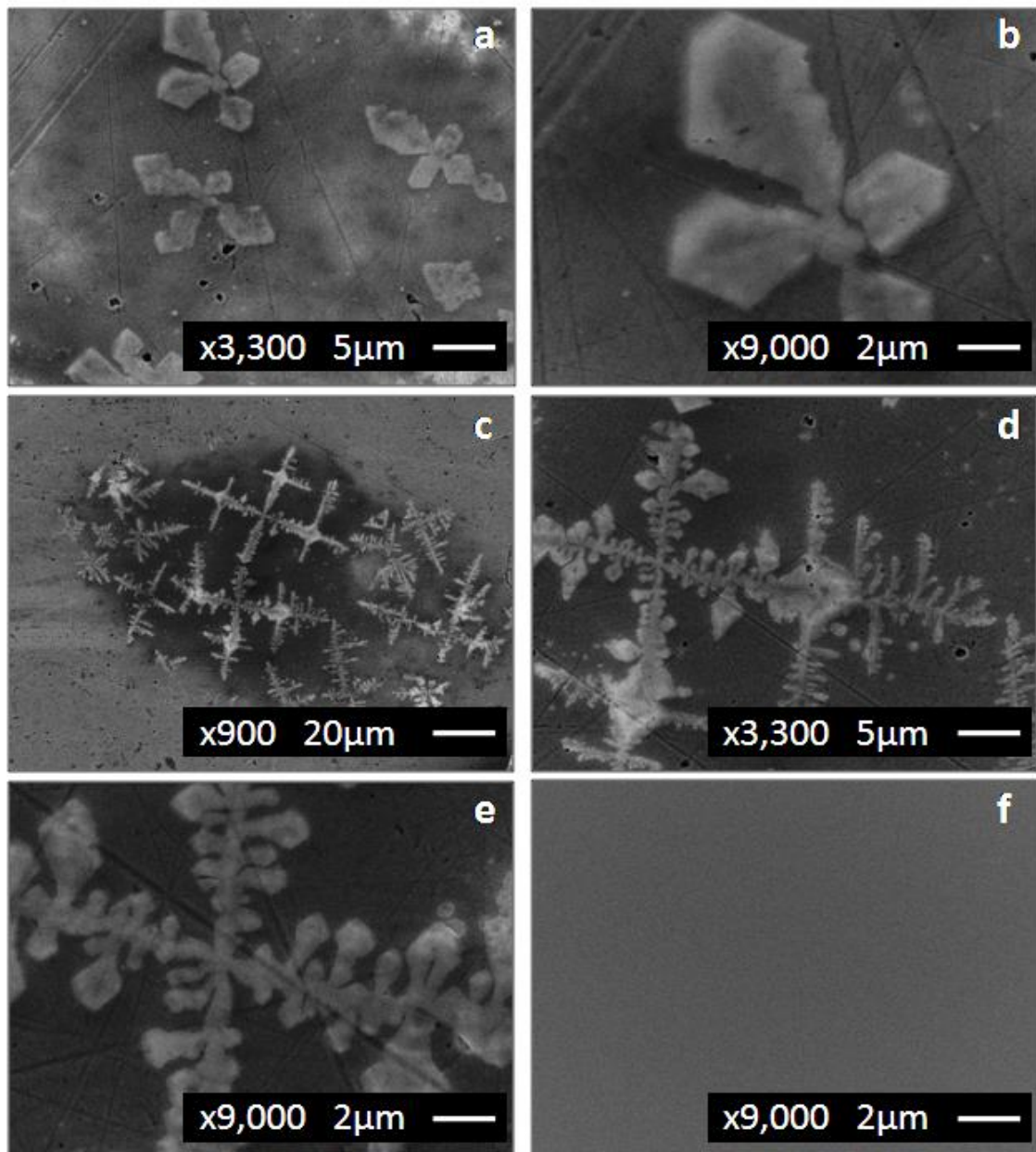


Fig.4.6. SEM surface morphology of Au-15wt.%Cu-35wt.%Ag composition, heated from the disorder up to 433K (160°C) water quenched without holding (a,b), with holding 10min at 433K (160°C) (c,d,e) and with holding at 433K (160°C) for 20 min (f).

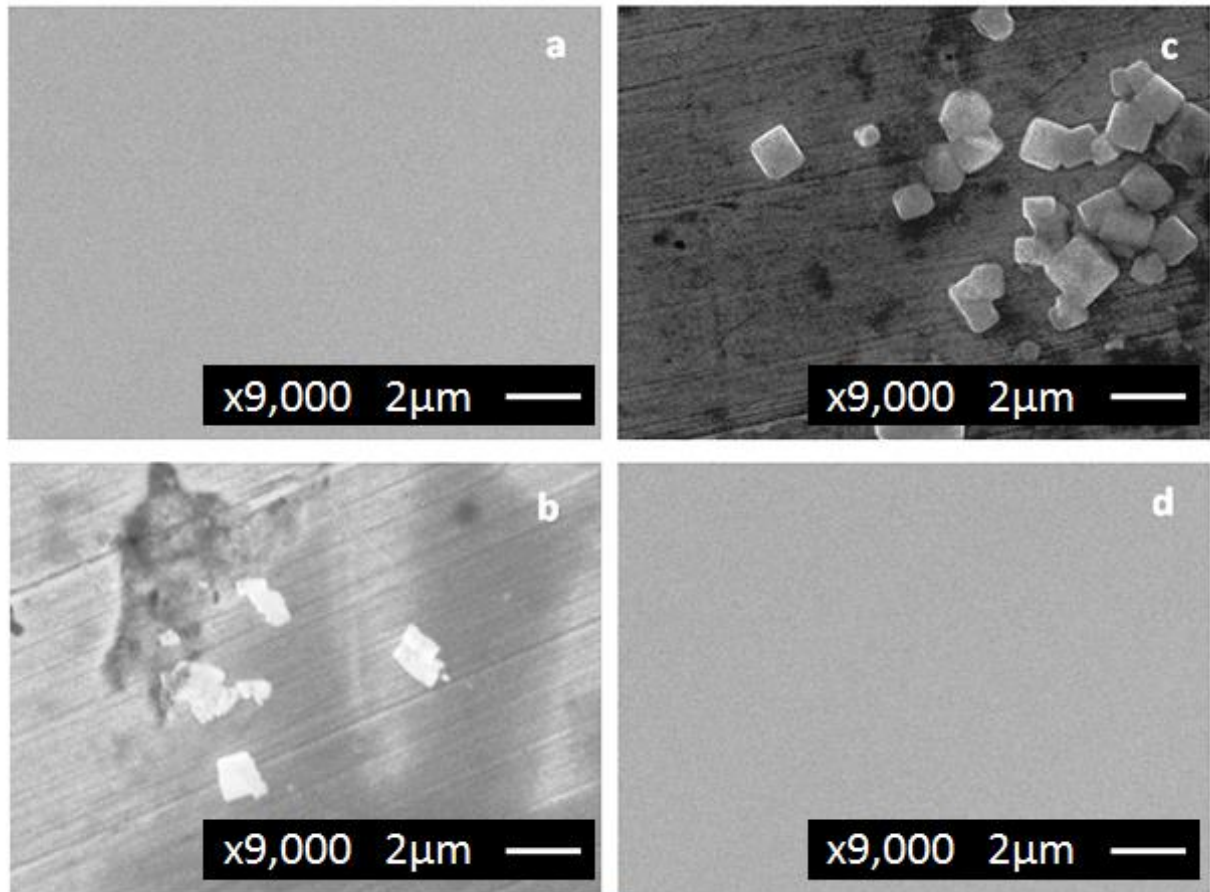


Fig.4.7. SEM surface morphology of Au-15wt.%Cu-35wt.%Ag sample, heated without holding from the disorder up to 453K (180°C) (a), 413K (140°C) (b), 393K (120°C) (c) and to 373K (100°C) (d).

The SEM images and the kinetic study are in very good agreement and explain very well the positions of the first peaks that correspond to the pre-ordering reaction in the DSC and the dilatometric studies as shown in figure.4.2 and figure.4.3 for both compositions. Where, the thermal study using DSC and dilatometry shows that the pre-ordering reaction in the binary composition have a maximum at 433K (160°C) which is the same temperature of the precipitates onset. For the ternary composition, 393K (120°C) is the pre-ordering reaction peak maximum in DSC and dilatometry and as well it presents the onset temperature of the precipitates. The SEM kinetic study, prove the direct relationship of these peaks to the precipitations on sample surfaces.

4.1.2.2. SEM study from the ordered state

The used samples in this part were in the ordered state i.e. AuCu₃ for the binary composition and $\alpha_1 + \alpha_2$ for the ternary composition after slow cooling down from 973K (700°C) to room temperature. Figure 4.8 shows the corresponding SEM images. In both compositions there is existence of dendrites where the ternary composition shows dense presences of them.

Moreover, figure 4.8 demonstrates that the anomaly at low temperature is present upon heating as upon cooling for both binary and ternary compositions of 12-carat gold alloy. These precipitates are denser for the ternary alloy comparing to the binary composition.

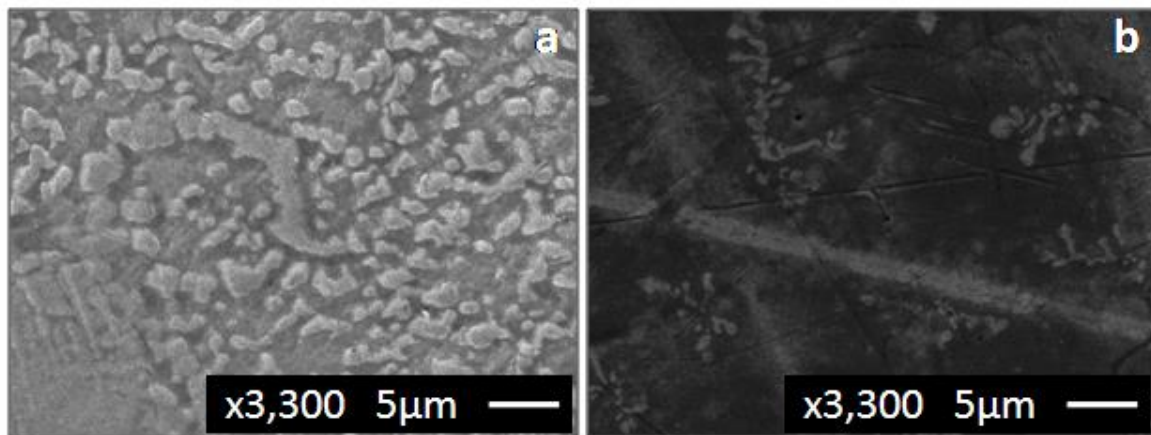


Fig.4.8. SEM surface morphology of Au-50wt.%Cu (a) and Au-15wt.%Cu-35wt.%Ag (b) samples after cooling down from 973K (700°C) to room temperature using velocity of 1K/min.

4.1.3. STM study

For more details STM images have been taken for both used compositions. Where, we have chosen 433K (160°C) as heating up temperature for both alloys because it represents a common temperature where there are precipitations for both alloys.

Figure 4.9 shows the 2D micrograph and the typical line scans of both studied compositions. Both compositions show a homogeneous distribution of nanoparticles.

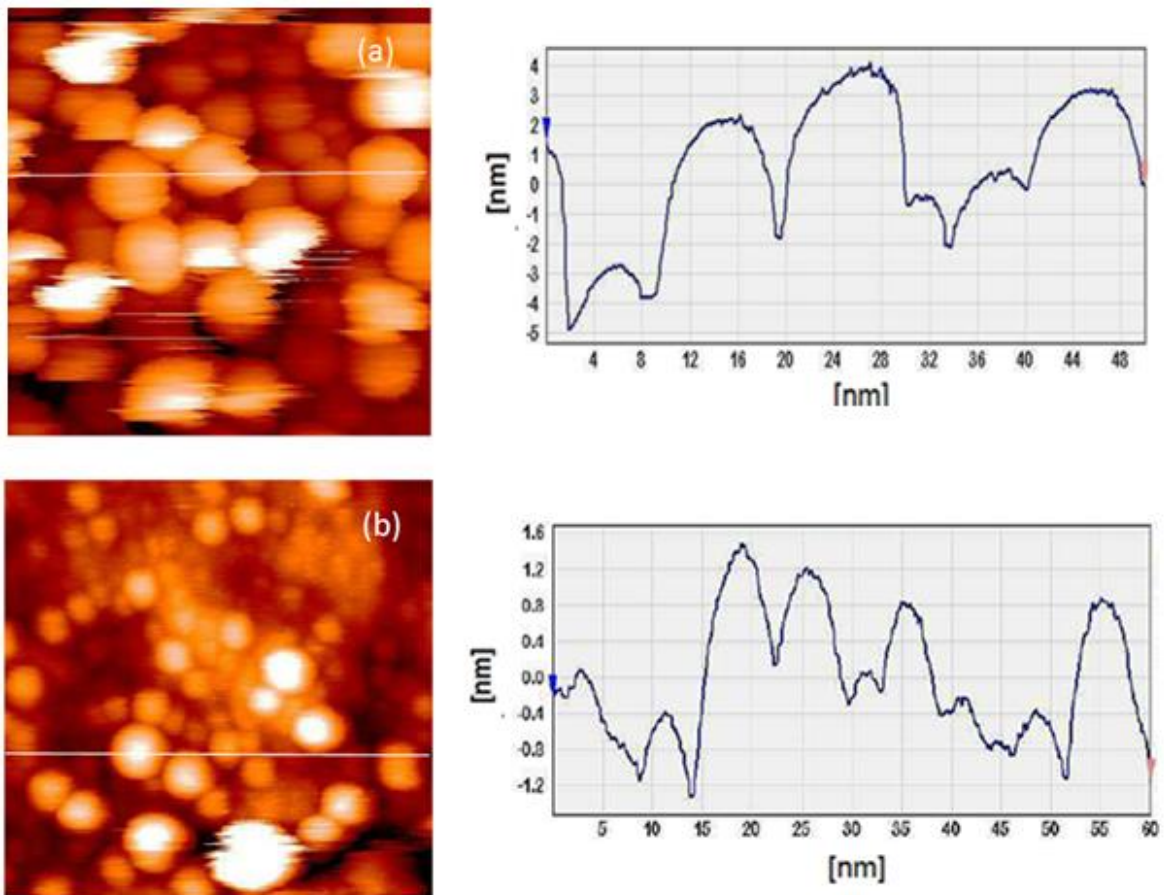


Fig. 4.9. Two dimensions STM micrograph (a,c) and a typical line scan (b,d) of spherical nanoparticles appeared on Au-50wt.%Cu sample surfaces (a) and Au-15wt.%Cu-35wt.%Ag (b) homogenized and heated from room temperature up to 433K (160°C), followed by water quenching.

4.1.4. Further techniques

XPS and grazing incidence X-ray diffraction data have been carried out on heated samples up to 433K (160°C) only for the ternary composition (Fig.4.10 and 11) in order to determine the nature of the precipitates that appear at low temperature on the surface of gold alloys. Where it is more likely to be a new phase with new properties that precedes the ordering phase transition as pre-ordering reaction.

The XPS spectra (Fig.4.10) show a positions of binding energies. For O1s spectrum the detected value for two different samples for the same composition is about 532 eV which does not fit to Cu_2O , Ag_2O nor Au_2O_3 according to NIST database [88]. This may come from the fact that the sample is an alloy instead of the neat material. Furthermore, it could be also adsorbed oxygen on the surface. However, the second spectrum that corresponds to Cu2p 3/2 shows two overlapped peaks. According to NIST database [88] the first maximum at 932 eV corresponds to the copper Cu and the second at 934.5 eV corresponds to copper oxide CuO.

The extra peaks on the grazing incidence X-ray diffraction pattern (Fig.4.11) correspond clearly to the copper oxide CuO. Both techniques confirm the copper oxide.

Conclusion of the part I

A new anomaly at low temperature has been investigated in ref [86] for 18-carat binary composition. This part has proven the appearance of such new reaction in binary and ternary 12-carat gold alloys. The new phase transition at low temperature has been assessed as pre-ordering reaction using thermal analyzes DSC and dilatometry. SEM technique has a big virtue to attribute this unknown phase transition to the precipitation of some new phase on sample surface with dendrite shapes from 433K (160°C) to 473K (200°C) for the binary composition and from 393K (120°C) to 433K (160°C) for the ternary composition. STM technique showed that these precipitates are accompanied with nanoparticles that are neither stable nor strongly attached on sample surfaces. The grazing incidence XRD and the XPS confirm the copper oxide on the surface.

The obtained results provide an important background for the study of the fundamental mechanisms underlying phase transitions from thermodynamic metastable phase to thermodynamic stable one.

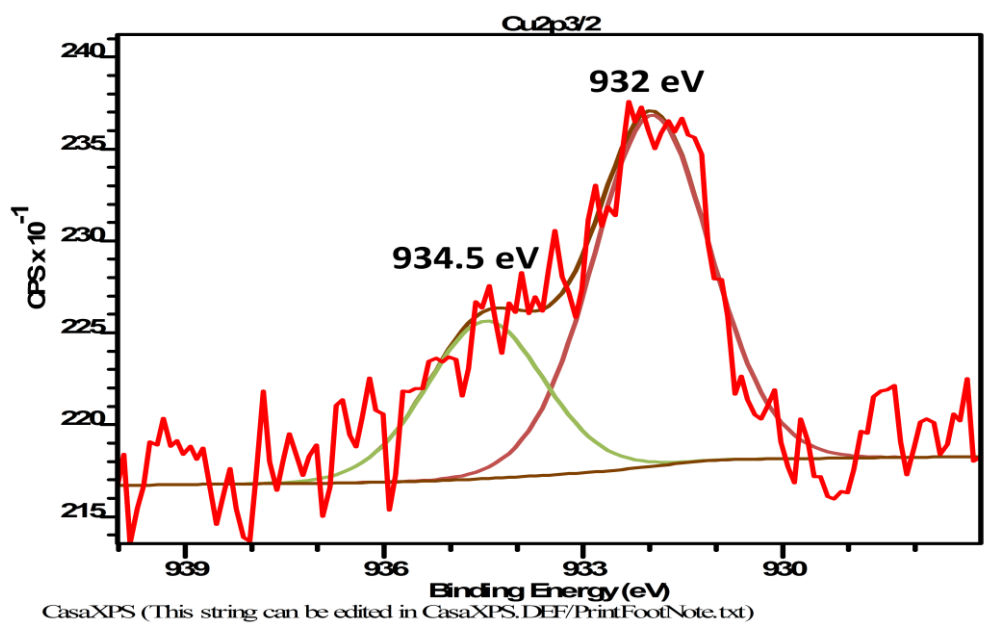
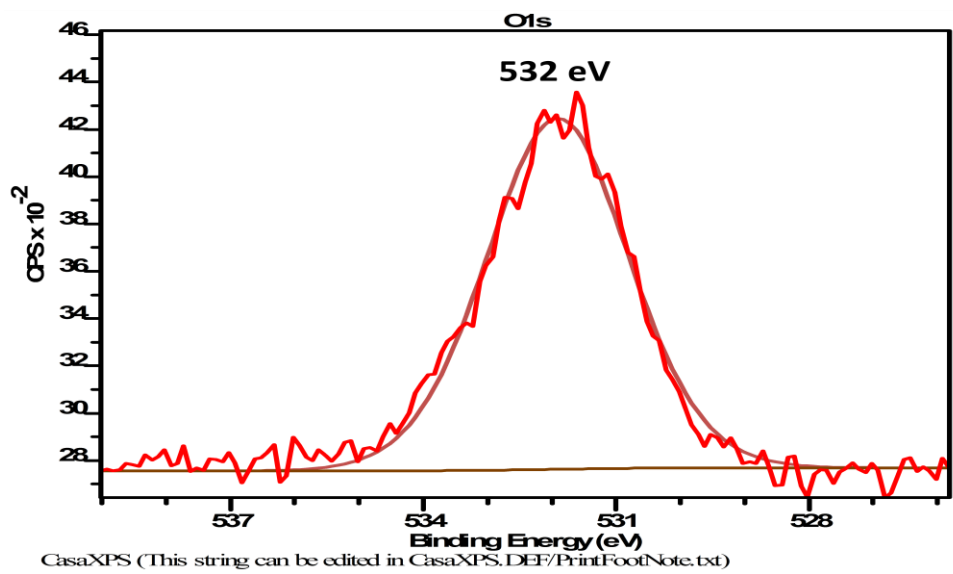


Fig.4.10. XPS spectra of Cu 2p and O 1s of Au-15wt.%Cu-35wt.%Ag composition after heating up to 433K (160°C).

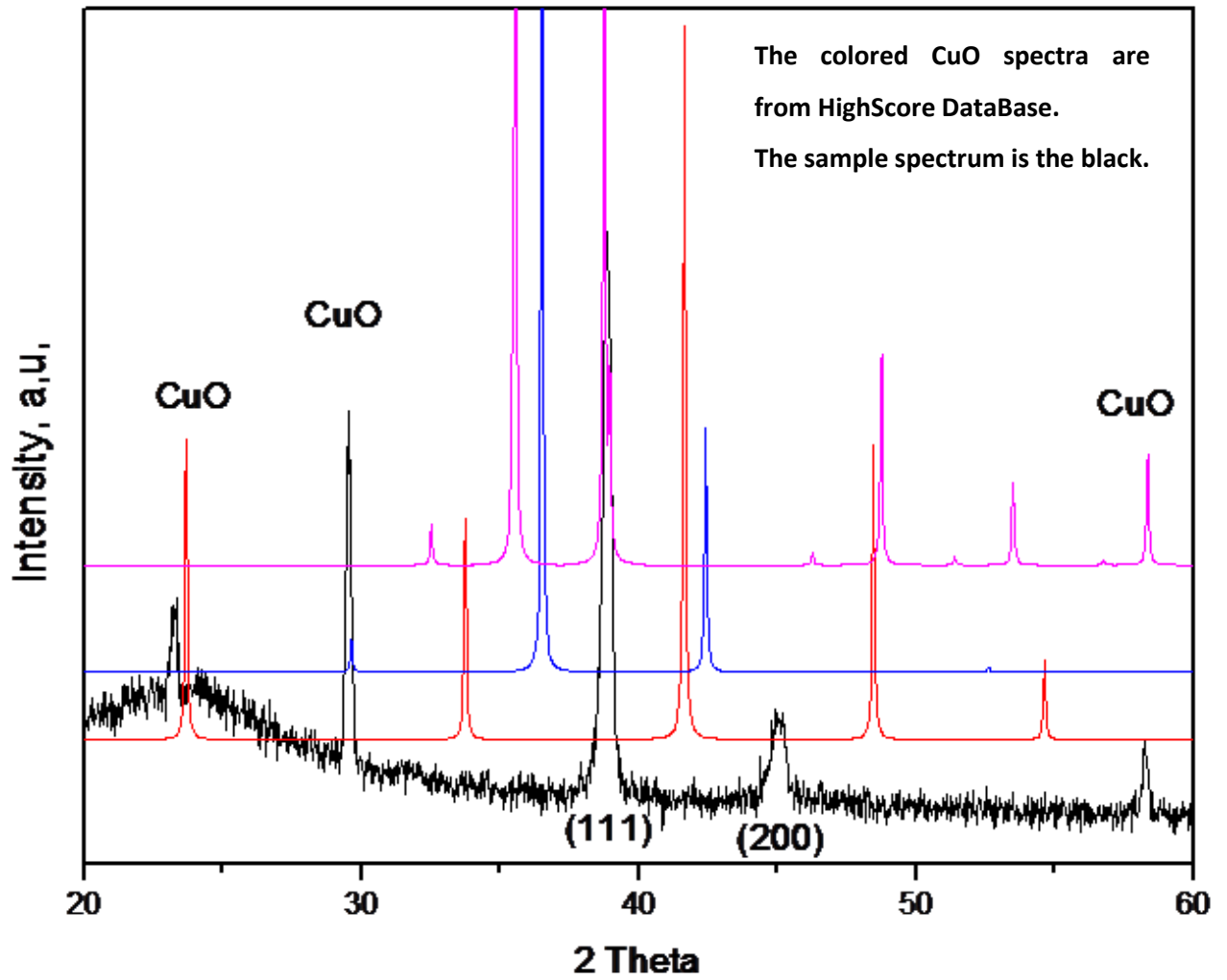


Fig.4.11. Grazing incidence X-ray diffraction spectra of Au-15wt.%Cu-35wt.%Ag composition after heating up to 433K (160°C).

***Part II: Trial for characterization of the pre-ordering phase
at low temperature in 18 carat binary gold alloys Au-
25wt.%Cu.***

The first part which was concerned with 12-carat gold alloys, has shown the kinetic of the evolution of certain new pre-ordering phase in 12-carat alloys. Therefore, this second part aims for the use of different characterization techniques in order to characterize the behavior of such pre-ordering reaction in the 18-carat binary gold alloy (Au-25wt.%Cu).

4.II.1. DSC and dilatometric results

The DSC and the Dilatometric tests were carried out on homogenized (2h at 973K (700°C)) and water quenched Au–25wt.%Cu alloy. The interpretations hereafter of the thermal anomalies are based on the binary phase diagram [43].

The DSC curve (Fig.4.12) recorded during heating from 298K (25 °C) up to 773K (500 °C) with 10 °C/min shows four peaks; an exothermic peak (**P1**) at low temperature with a maximum at around 413K (140°C) which is related more likely to the pre-ordering reaction. This first reaction has been already observed by Hamana *et. al* [86] without identifying its origin which will be discussed below, a second peak (**P2**) with a maximum around 593K (320°C) corresponds to the formation of AuCu₁ (L1₀) ordered phase in the Au–25wt.% Cu composition [43] and two endothermic overlapped peaks noted between 673K (400 °C) and 743K (470 °C) are related to the transformation from AuCu₁ to AuCu₁₁ followed with the disordering presented in the appearance of the solid solution A1.

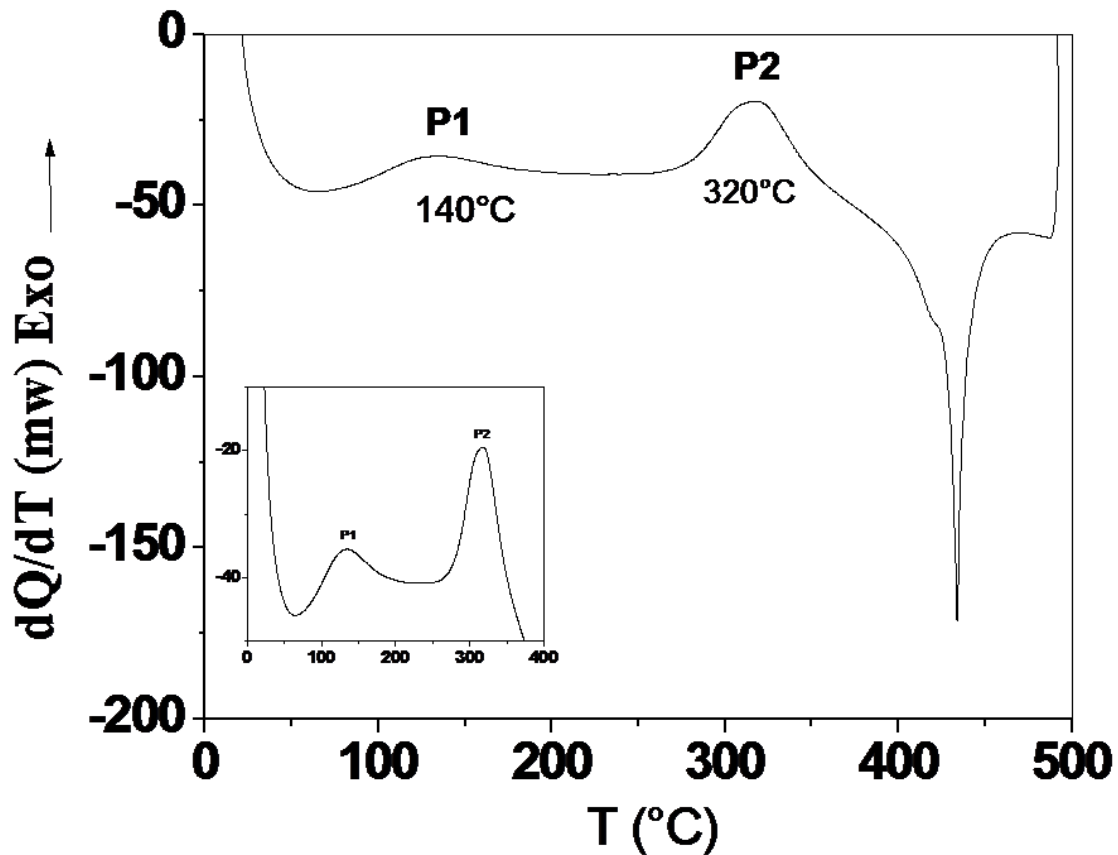


Fig.4.12. DSC curve of Au-25wt.% Cu alloy homogenized for 2 h at 973K (700 °C), and water quenched.

A dilatometric study has been done to confirm the presence of the pre-ordering reaction peak observed by DSC at low temperature. The obtained curve is presented in figure 4.13. The derivative curve of the heating segment shows some effects namely; a small contraction situated between 398K (125°C) and 453K (180°C) corresponding to the first reaction at low temperature, considered as pre-ordering reaction in ref [93]. However, the effect related to the ordered phase does not appear, a first expansion with a maximum of the derivative curve situated at 573K (300°C), should be attributed to the decrease of the order degree and the formation of the semi ordered phase AuCu₁₁ which is in agreement with the binary phase

diagram [43], a second expansion with a maximum of the derivative curve situated at 669K (396°C) corresponds to the formation of the disordered phase A1.

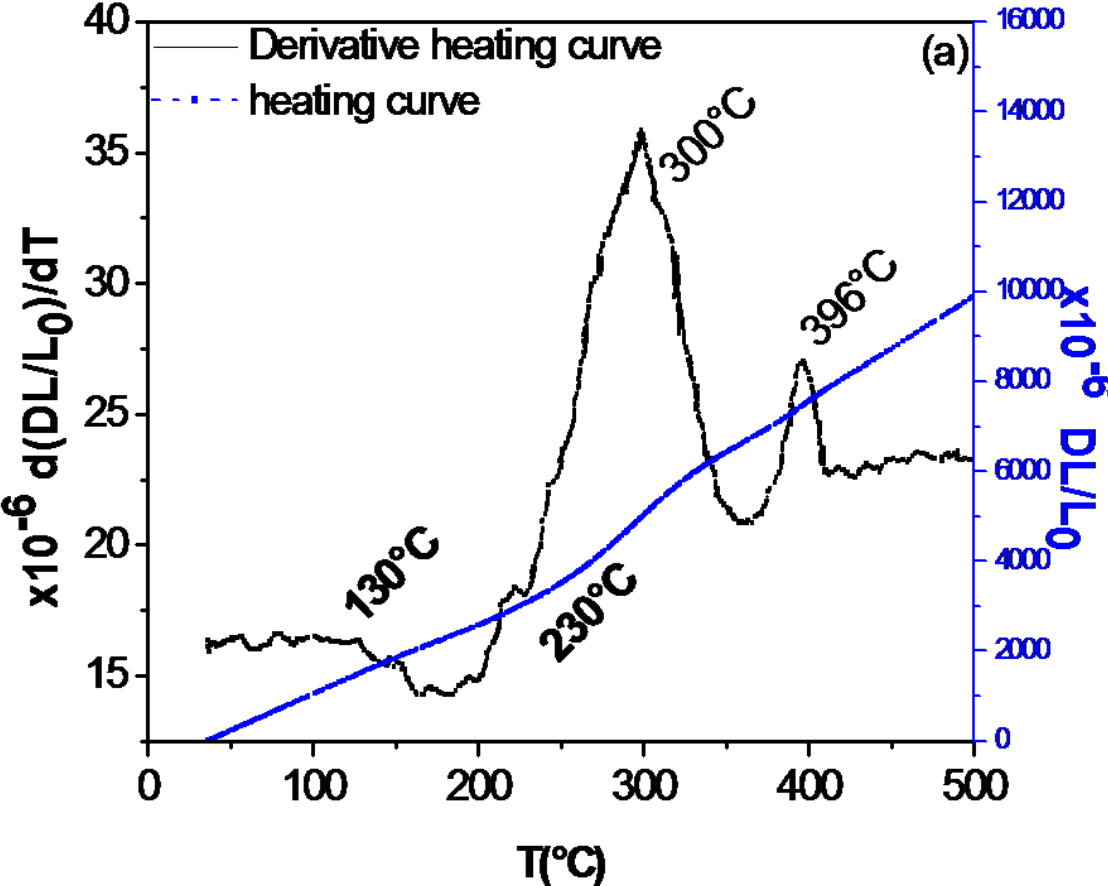


Fig.4.13. Dilatometric curve and derivative heating curve of Au–25wt.% Cu alloy homogenized for 2 h at 973K (700 °C),and water quenched.

To investigate the origin of this unknown pre-ordering reaction at this temperature 433K (160°C), further analyses will be used as following.

4.II.2.Morphological study

Figure.4.14 shows SEM observation of the Au–25wt.% Cu surface morphology after heating of the homogenized samples from room temperature up to 433K (160°C). This micrograph reveals a very clear nanostructured surface homogeneously covered by spherical nanoparticles.

Two different elemental analyses are used to identify the chemical composition of the formed nanoparticles on the AuCu surface after heating up to 433K (160 °C).

Elemental mapping analysis of a selected area is shown in figure.4.15 (a), where the concentration is indicated by the color bar. In figure.4.15 (b) the distributed spherical particles are clearly enriched with oxygen which indicates that the observed reaction at low temperature is basic copper oxide phase (Cu_2O , CuO , and CuO_2), the oxidized state will be discussed below using XPS analyses. Since copper is a bulk element we cannot observe the same distribution as oxygen on the surface figure.4.15 (c). Therefore, energy dispersive spectroscopy (EDS) has been performed to check the difference of composition between bulk (clear surface) and spherical nanoparticles.

EDS spectrum (figure.4.16) of the spherical nanoparticles (spot 2) shows the presence of oxygen comparing to bulk one (spot 3), which is mainly made of copper and gold elements.

To provide more information about the surface morphology, AFM and STM analyses have been performed. AFM image is shown in figure.4.17 and it reveals monodispersed nanograins with 100-150 nm in size. This is in good agreement with SEM observations.

High resolutions STM images are presented in figure.4.18. This technique can provide more information at the nanoscale using very sharp tip. It shows a very clear nanostructured surface homogeneously covered by nanoparticles with a typical diameter of 7 nm - 10 nm.

In this used composition Au–25wt.%Cu, the nanoprecipitates are scattered homogeneously on the sample surface, as shown in figure.4.14 the detail that was not present in the part 1 for 12-carat alloys.

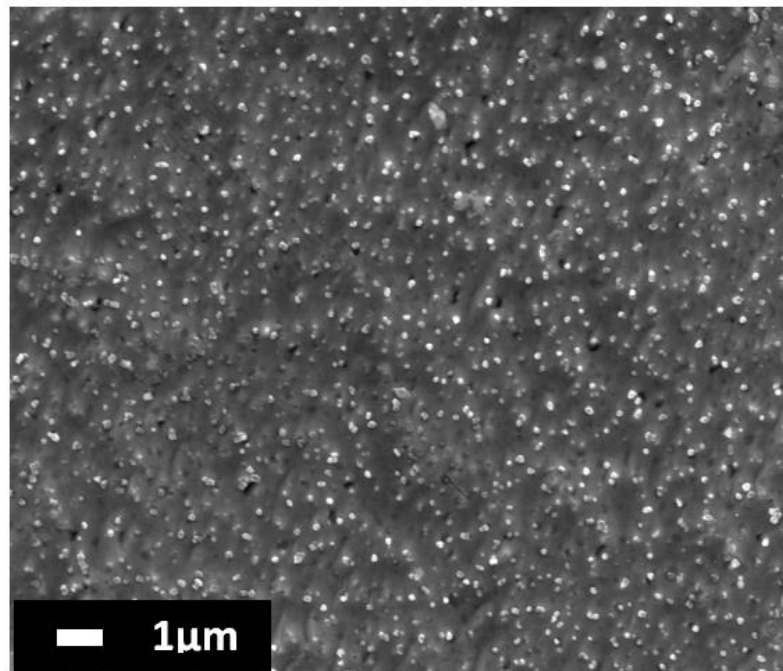


Fig. 4.14. SEM surface morphology (a, b) of Au–25wt.% Cu composition heated up to 433K (160°C) after the homogenization (2 h at 973K (700 °C)).

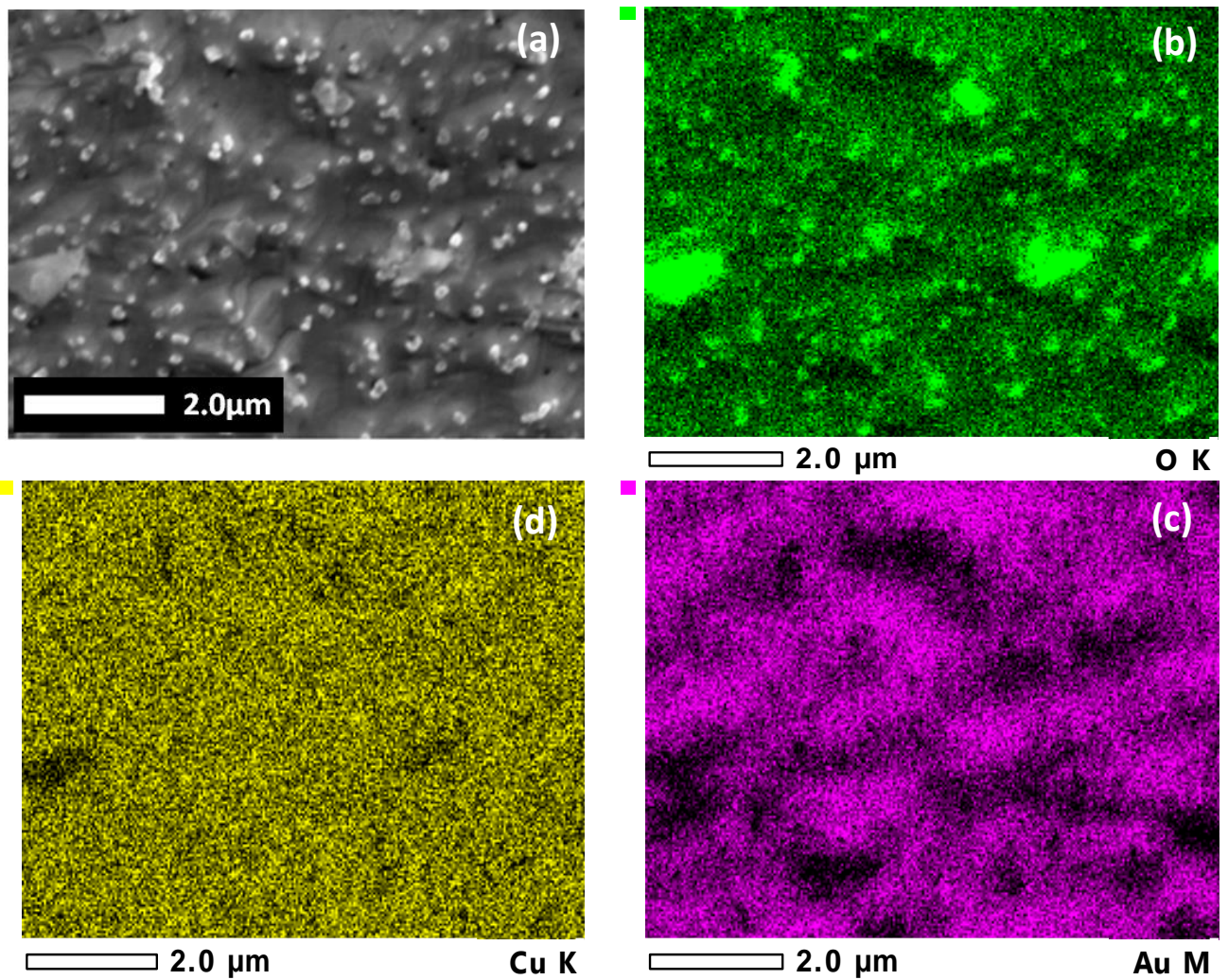


Fig. 4.15. Elemental mapping analysis of a selected area from Au–25wt.% Cu sample heated up to 433K (160°C) after the homogenization (2 h at 973K (700 °C)). The micrograph (a), elemental mapping of the oxygen (b), the gold (c) and the copper (d).

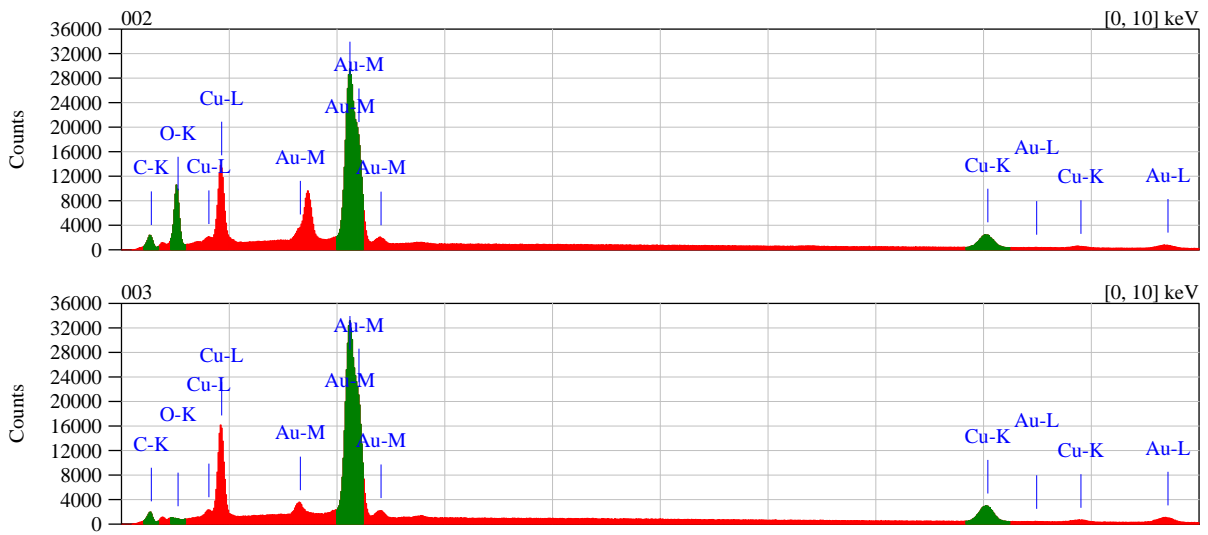
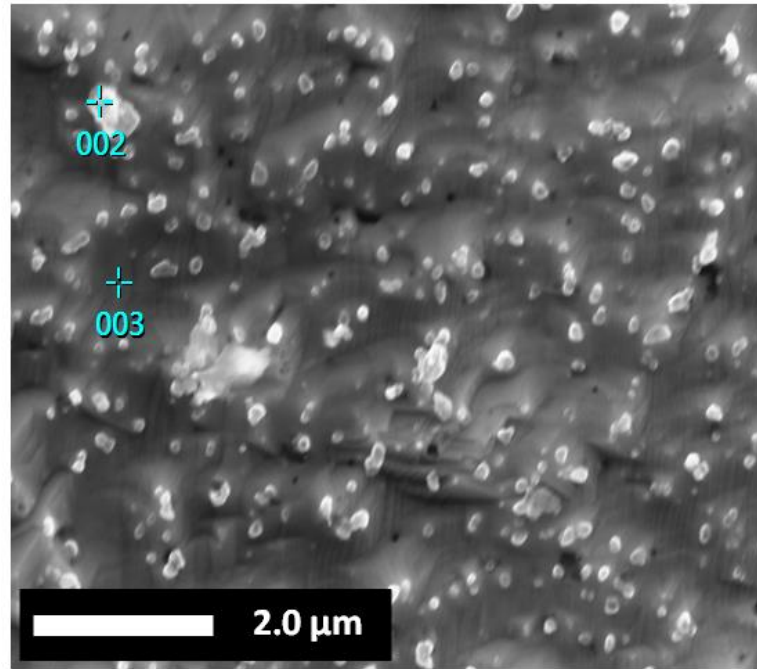


Fig.4. 16. EDS analysis of the observed spherical nanoparticles on Au–25wt.% Cu sample heated up to 433K (160°C).

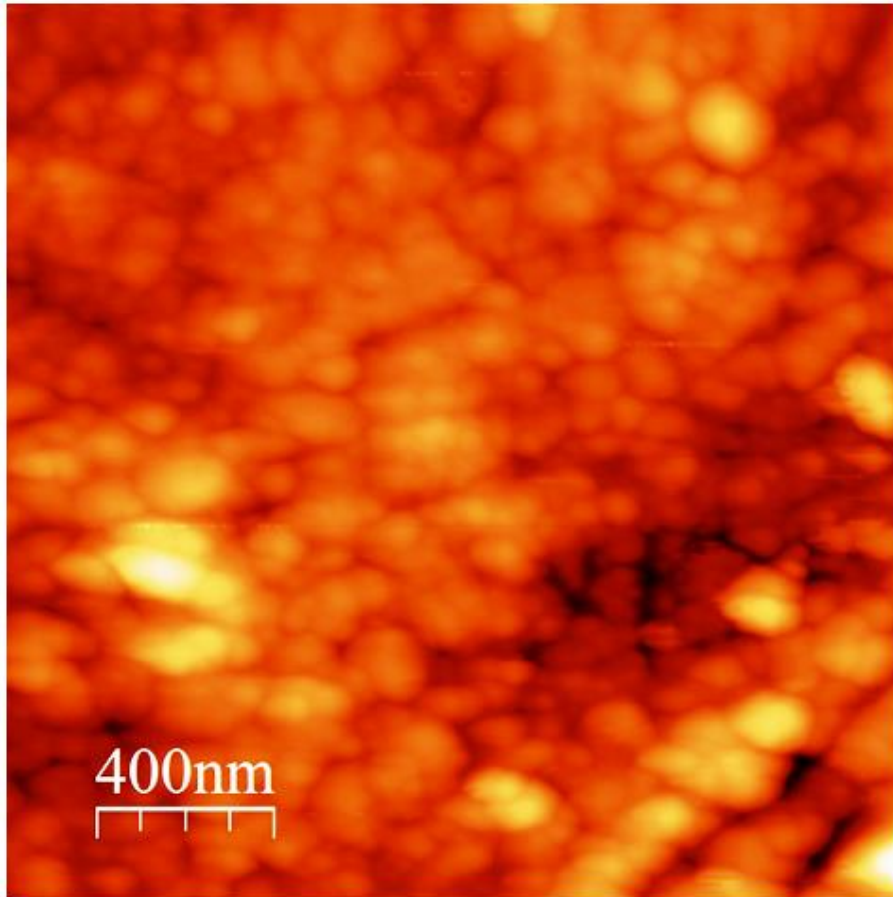


Fig.4.17. Two dimensions AFM micrograph of Au-25wt.%Cu sample surface homogenized and heated from room temperature up to 433K (160°C), followed by water quenching.

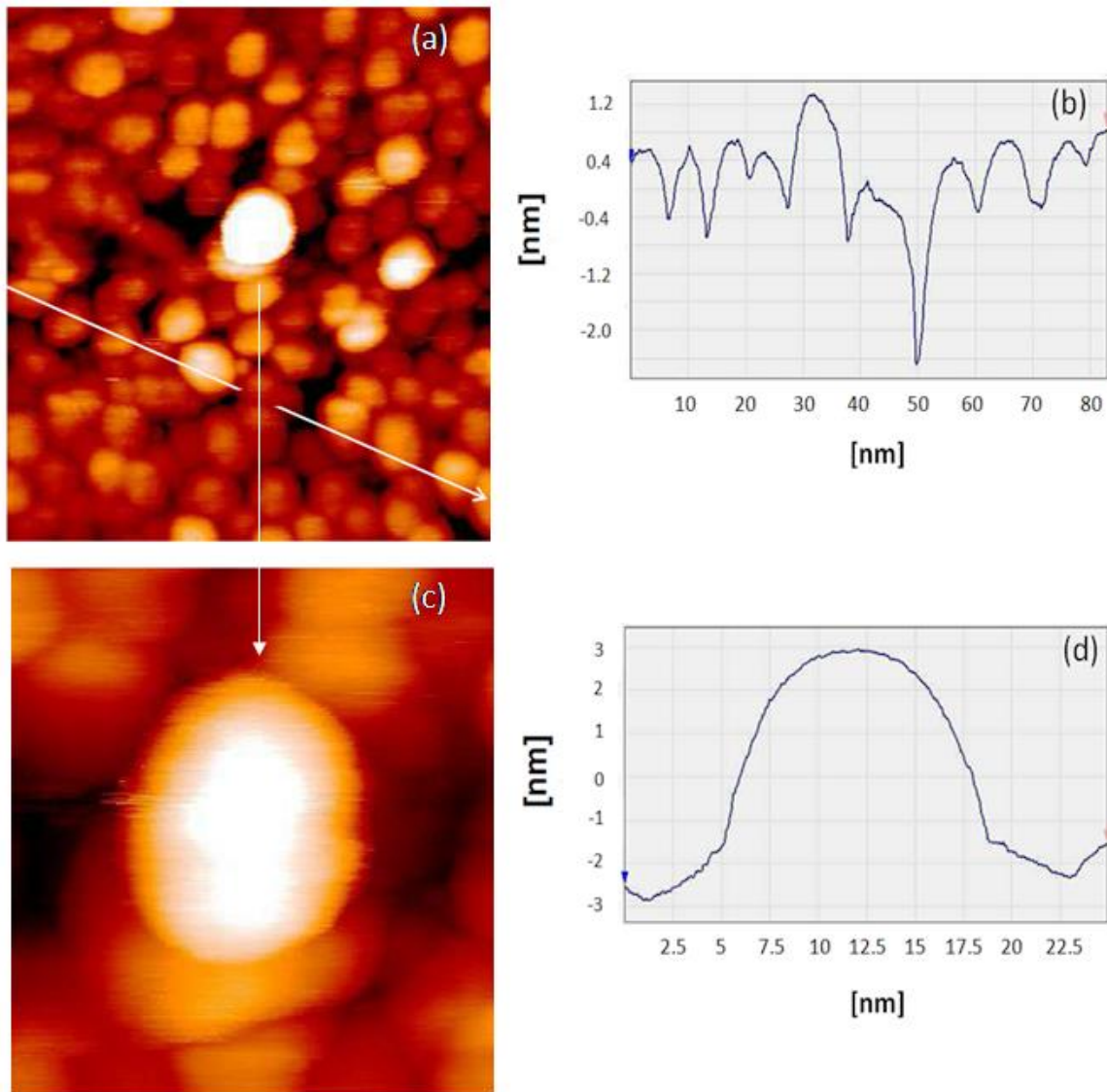


Fig.4.18. Two dimensions STM micrograph (a, c) and a typical line scan (b, d) of spherical nanoparticles appeared on Au–25wt.%Cu surface after heating up to 433K (160°C).

4.II.3. X-Ray Photoelectron Spectroscopy (XPS)

XPS analyzes were conducted to study the chemical state of the observed nanostructured surface by SEM, AFM and STM in Au–25wt.%Cu alloy. The surveys of the quenched and heated up to 433K (160°C) samples show that the surface is mainly composed of Au, Cu, O and C. The XPS data from Cu and O core levels of the quenched and heated up to 433K (160°C) samples surface are shown in figures.4.19 and 20 respectively. Binding energy (BE) values of the quenched samples (Fig.4.19) are: BE (Cu 2p_{1/2}) = 952, 2 eV and BE (Cu 2p_{3/2}) = 932, 4 eV, according to XPS handbook and database [87, 88], the BE of Cu 2p in this case (quenched state) correspond to metallic copper state.

After heating up to 433K (160°C), the XPS spectra (Fig. 4.20) show a shift of the binding energy Cu 2p peaks to higher binding energies to BE (Cu 2p_{1/2}) = 952, 8 eV and BE (Cu 2p_{3/2}) = 933, 0 eV. This shift is due to the formation of Cu₂O [87,88]. On the other hand, the O 1s binding energy is shifted toward low energies, which confirm the formation of copper oxide layer on the surface. From this result we can conclude that the composition of the observed nanospheres by STM can be assigned to copper oxide Cu₂O.

Consequently, we can say that for the Au–25wt.%Cu composition the formation of such nanospheres at low temperature is due to the diffusion of copper from the bulk to the surface, which is confirmed also by the dilatometric curves that show a contraction at low temperature due to the migration of copper from the crystal lattice to the surface and combine with oxygen to form copper oxide (Cu₂O).

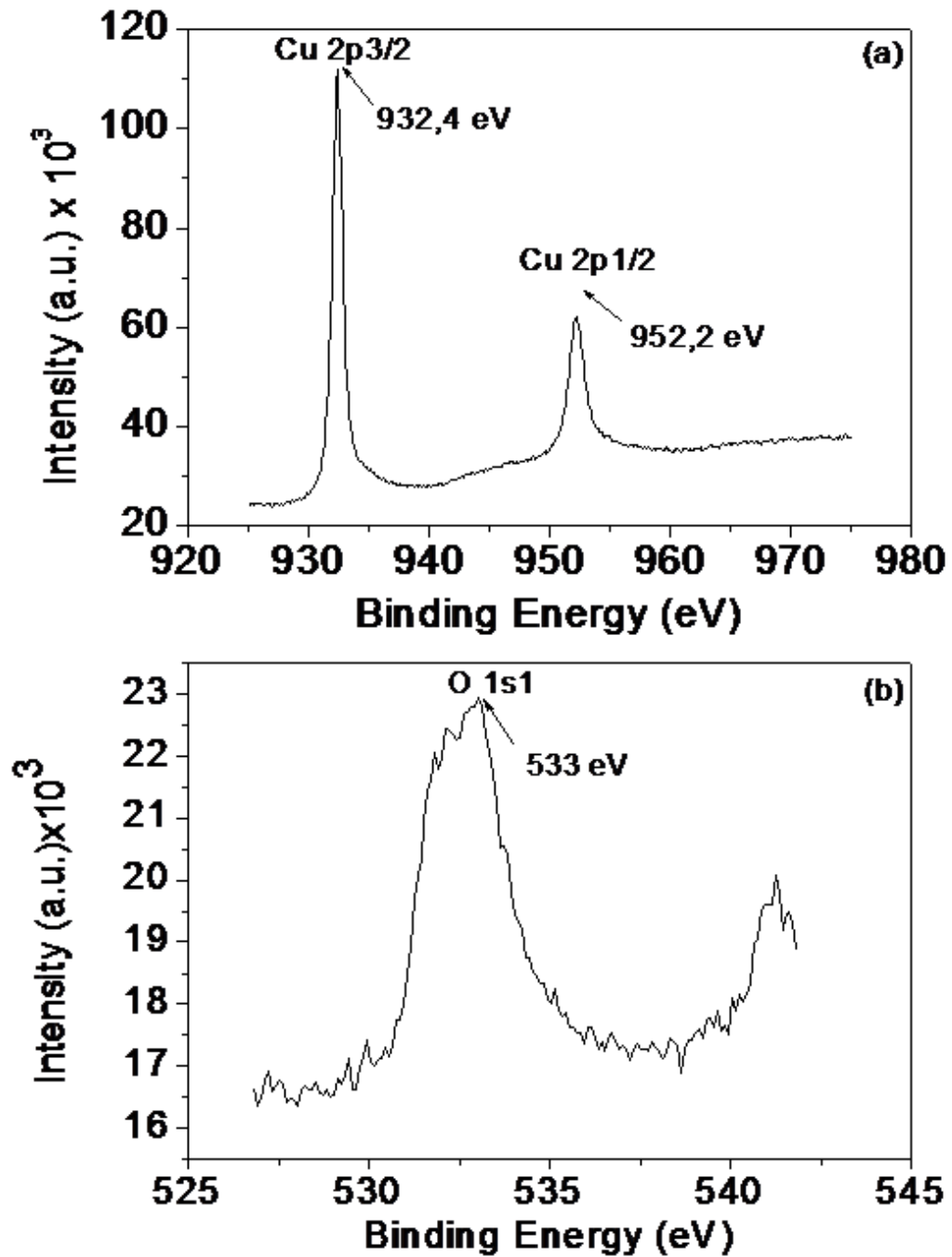


Fig.4.19. XPS spectra of Cu 2p and O 1s of Au–25wt.%Cu sample after homogenization (2 h at 973K (700 °C)).

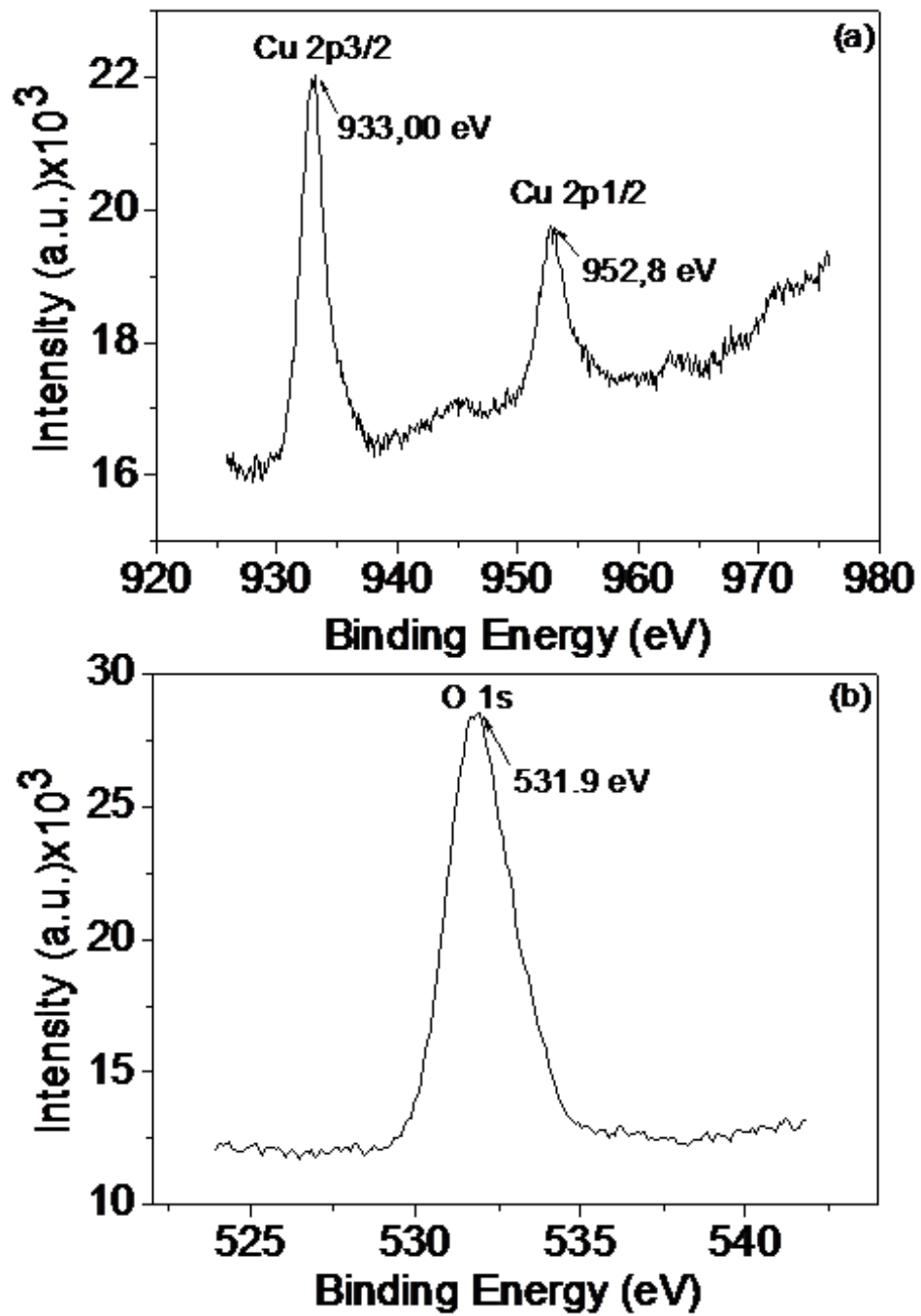


Fig.4.20. XPS spectra of Cu 2p and O 1s of Au–25wt.%Cu alloy after heating up to 433K (160°C).

4.II.4. Quantitative elemental depth profile analysis

GDOES depth profiles of copper, gold, oxygen and carbon in the Au–25wt.%Cu composition after heating up to 433K (160°C) are presented in figure.4.21. The depth profiles of copper and oxygen reveal high levels at the surface that decrease at the interface and stabilize over the bulk. Where, gold profile appears stable over time. The GD-OES analysis therefore proves the diffusion of copper from the bulk to the surface forming Cu₂O nanospheres as observed by STM, SEM and XPS. The very thin carbon layer detected in this GDOES profile is due to the surface contamination.

4.II.5. Electrical Resistance study

The electrical resistance of the studied samples (surface and volume resistance) was characterized by means of two-probes method in order to investigate the copper oxide (Cu₂O) nanoparticles effect on the electrical properties. The used samples thickness is 1mm.

Table.4.1 reports the electrical resistance values associated with the sample composition studied in this part. Two electrical resistance configurations have been carried out; volume and surface resistance measurement using Sandwich and coplanar structures, respectively. The electrical resistance measurements give different electrical behaviors as follows:

Quenched and heated up to 433K (160°C) states have been measured. The surface electrical resistance measurement in the heating up state, shows significant increase to five times comparing to the homogenized state, while a small decrease in the volume resistance value has been noted. The small decrease of the volume resistance values is probably due to the decrease of copper content in the bulk after its segregation to the surface to form copper oxide nanoparticles. The thing that has to be associated with the decrease of the crystallographic defects after the ordering reaction that grants an ease to the electron motion.

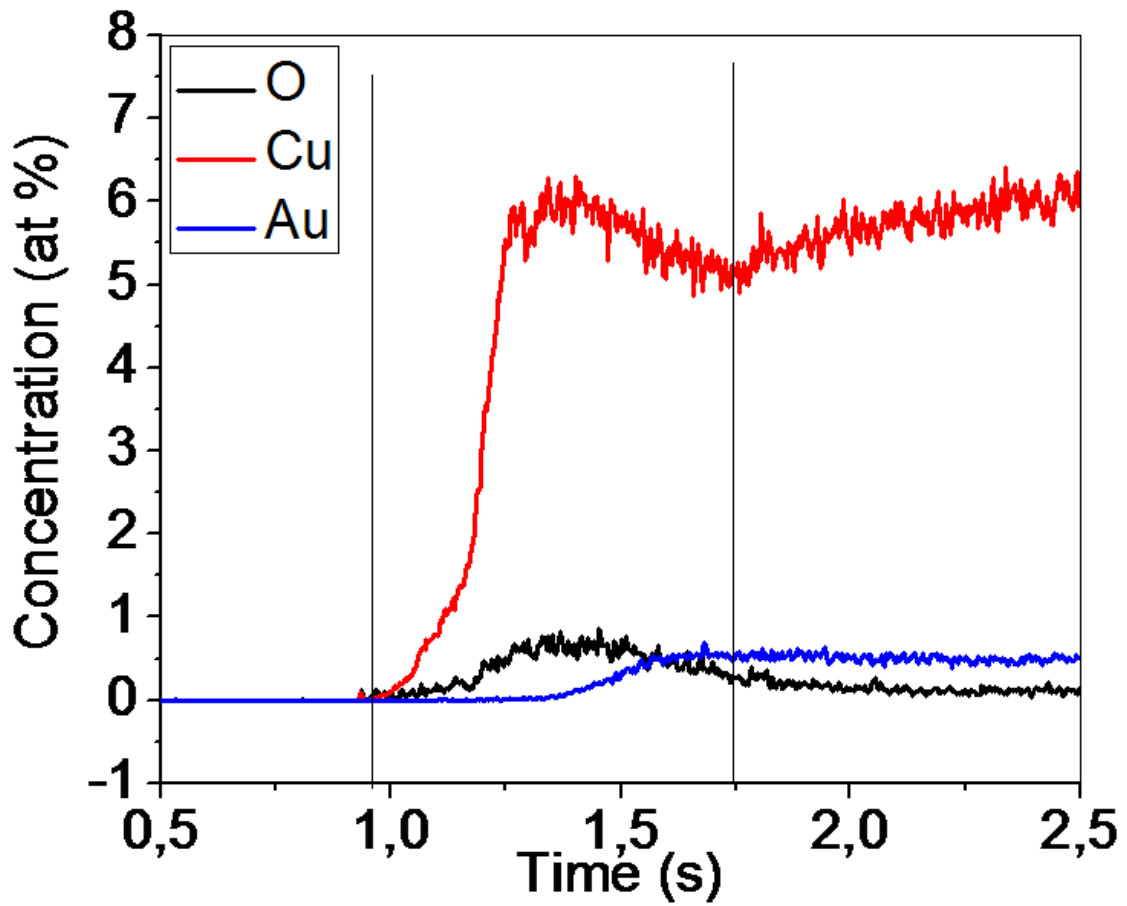


Fig.4.21. Depth profile curves of Au–25wt.%Cu sample after heating up to 433K (160°C) by pulsed RF GD-OES.

	Homogenized sample		Homogenized sample and heated up to 433K (160 °C)	
	volume Ω	surface Ω	volume Ω	surface Ω
Au-25wt.% Cu	52.9	48.9	47.8	257.7

Table.4. 1. The Electrical Resistance measurement values.

Finally, this pre-ordering reaction in the binary 18-carat gold alloy that happens at around 433K (160°C), corresponds to the segregation of the copper from the superficial layers of the lattice to the surface then with the coalescence of the oxygen of the air it forms nanograins of copper oxide. The fact that happens only at 433K (160°C).

Therefore, this 18-carat gold alloy characteristic presented in the fact of the pre-ordering reaction at 433K (160°C) accompanied with copper segregation to the surface and the formation of the copper oxide nanograins, be useful for the determination of the now reaction from metastable to stable phase.

Conclusion of the part II

In this part a pre-ordering phase that accompanies the reaction between the diffused copper from the bulk to the surface with the oxygen, has been investigated. This part presents an important contribution to determine the nature of such new and interesting low temperature reaction. SEM, AFM and STM exhibit a specific topography, showing homogeneously nanostructured surface. The precipitates in the binary 18-carat alloy are quite homogeneously scattered on the sample surface. Elemental mapping and EDS analysis present clear information of the chemical nature of such phase, that is basically a copper oxide. XPS analysis is used to identify the type of the formed oxide which is Cu_2O . Quantitative Elemental Depth Profile Analysis proves the segregation of copper from the bulk to the surface.

Part III: Investigation of the order -disorder phase transition series in 18 carat binary gold alloys Au-25wt.%Cu by in-situ temperature XRD and mechanical spectroscopy.

In this third part we used in-situ temperature X rays diffraction to monitor the sequence and kinetics of phase transitions in annealed (homogenized) and quenched Au-25wt.%Cu system, during the complete thermal cycle upon heating and cooling. This part of the study mainly focuses on phase transformation in bulk sample from the disordered state A1. Furthermore, we show how these transitions affect the mechanical properties by measuring the internal friction and mechanical shear modulus in temperature scanning tests performed in the same conditions as the x-ray diffraction.

4.III.1. In-situ XRD structural study

Upon continuous heating, an optimum heating rate was chosen in order to evidence ordering from the quenched state. A heating rate of 1K/min has been chosen. Long diffraction scans, with frequency of one pattern every 10K (1pattern/10min), have been performed to well distinguish the characteristic peaks of every phase since the highest peak of the disordered cubic A1 overlap with the related peaks of the tetragonal AuCuI and the orthorhombic AuCuII. On the other hand, scans performed in the short diffraction angle range (2θ from 29 to 42 °), with frequency of one pattern per 1 K (precisely 1 pattern /1.1 min), have been used to determine the precise temperatures of the phase transitions.

Figure.4.22 shows the RTX-Ray patterns (Room Temperature X-Ray) measured in the initial state (homogenized and water quenched) (a) and in the final state after heating-cooling cycle (b). All Bragg peaks observed in the initial state belongs to reflections of the disordered cubic A1 structure although small tetragonal AuCuI ordered phase peaks are present. They appear as humps in figure.4.20(a) at low diffraction angles, which shows that AuCuI phase is present as nanograins. At the

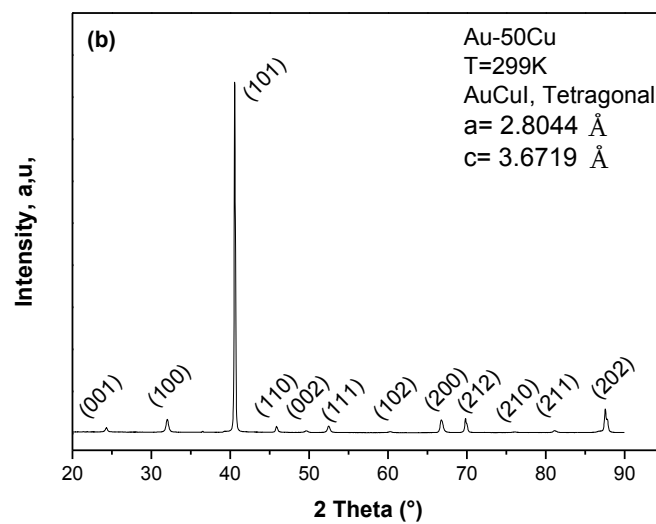
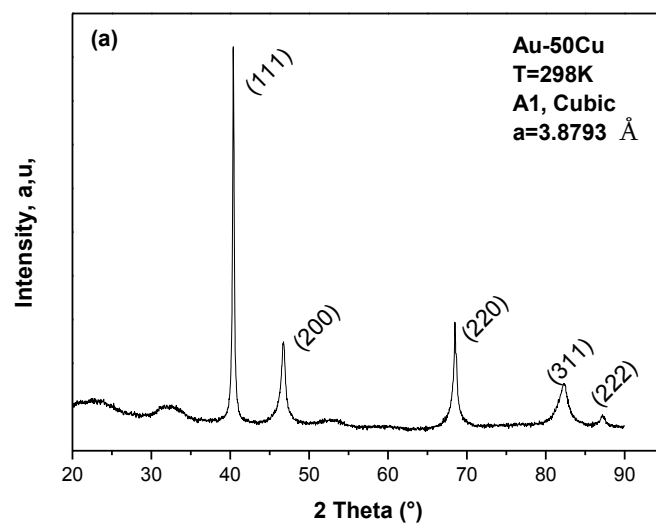


Fig.4.22. X-ray diffraction spectra of the Au-51Cu compound in (a) the initial state and (b) after heating and cooling. Diffraction indexes of every Bragg peak are presented in brackets.

end of heating/cooling cycle pure microcrystalline ordered tetragonal AuCuI is obtained.

Figure.4.23 and figure.4.24 present the 3D plots of the XRD measurements upon heating and cooling for the large diffraction angle scans and for the short diffraction scans, respectively. Three phase transitions can be discerned upon heating as follow: A1 - AuCuI - AuCuII - A1, and two upon cooling: A1- AuCuI+AuCuII–AuCuI. Moreover, in every transition there is an interval of temperature where two phases coexist. The exact temperatures of every phase transition are presented in Table.4.2 mainly obtained by analyzing the short diffraction scans data. However, the phase transition temperature upon heating that correspond to the onset of the tetragonal AuCuI and the total disappearance of the cubic A1 (i.e. the presence of the pure tetragonal AuCuI) where extracted not only from short diffraction angles spectra, but also basing on the long diffraction angles spectra shown in figure.4.25.

Figure.4.26 and figure.4.27 show the intensity behaviors of selected peaks of every phase during heating/cooling cycle, where data have been extracted from the fitting of the short and large diffraction angle range scans respectively. The intensity of (111) A1 upon heating increases abruptly (up to 50%) in two scans before decreasing continuously from 408K (135°C) with the onset of (101) AuCuI peak and the increase of (100) AuCuI peak. The (101) AuCuI peak decreases before stabilization with the pure presence of AuCuI phase. For the figure.4.27 The data have been extracted from the large diffraction angle range scans. The intensity of (220) A1 upon heating (Fig.4.27 (a)) decreases remarkably at around 368K (95°C) followed by a second decrease with the onset of (200) AuCuI peak. Figure.4.26 and figure.4.27 emphasize the sequences of the phase transitions and the transition temperatures upon heating and cooling. The phase transition temperatures are referred with dotted lines. After that, the temperature dependence of peak intensities are correlated with different phase transitions.

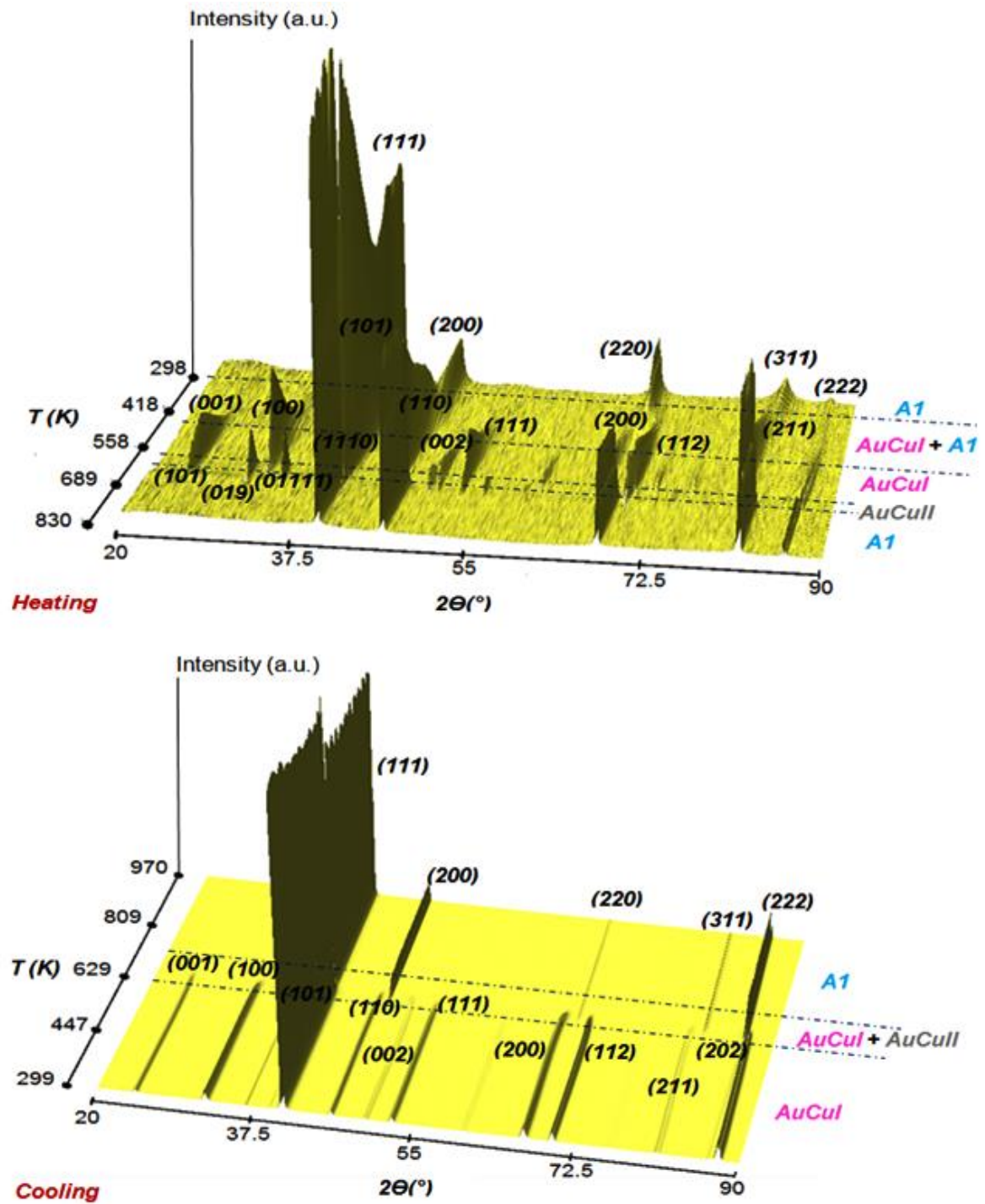


Fig.4.23. Large angle 3Dschemes of the diffraction peaks evolution of the AuCu system upon heating and cooling from $2\theta=20^\circ$ to $2\theta=90^\circ$. The blue lines depict the phase transition temperatures. The diffraction indexes of the observed peaks of the phases are presented in brackets.

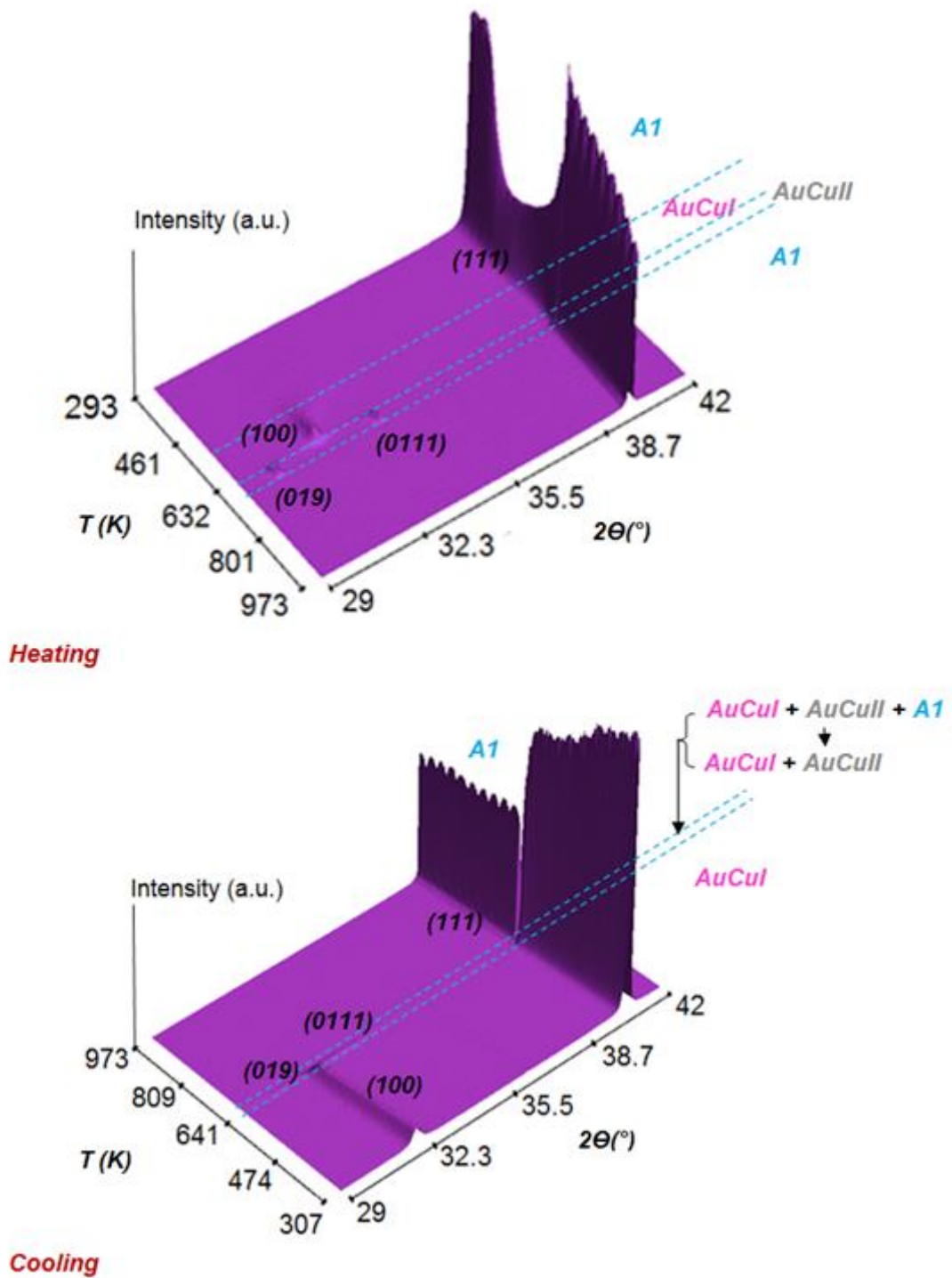


Fig.4.24. Short angle diffractions 3D schemes of the diffraction peaks evolution of the Au-25wt.%Cu system upon heating and cooling from $2\theta=29^{\circ}$ to $2\theta=42^{\circ}$. The blue lines depict the phase transition temperatures. The diffraction indexes of the observed peaks of the phases are presented in brackets.

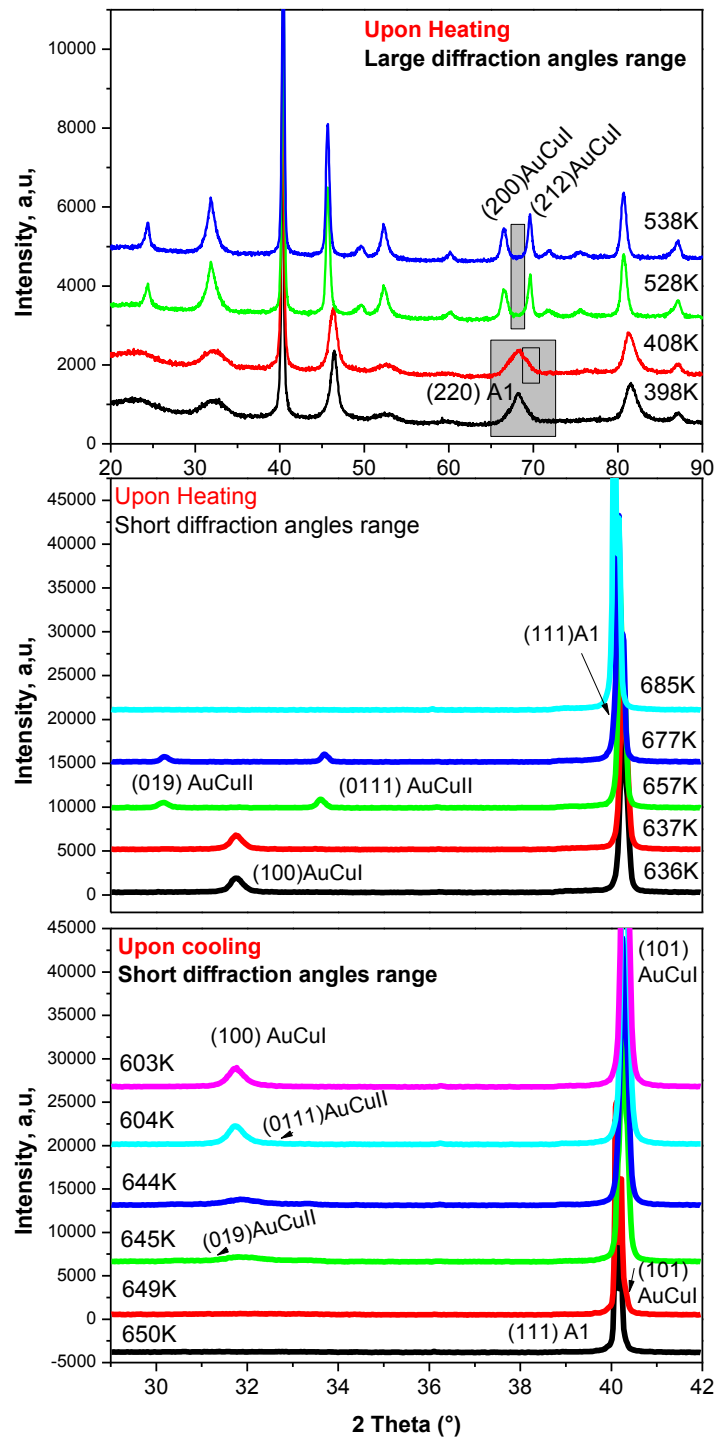


Fig.4.25. Superimpositions of diffraction patterns, which limit the intervals where phase transitions take place. Upon heating, the large diffraction scans were used to determine the onset of AuCuI and the total disappearance of A1. Short diffraction scans were used to determine all the rest of the phase transitions (upon heating and cooling) as shown in Table.4.2.

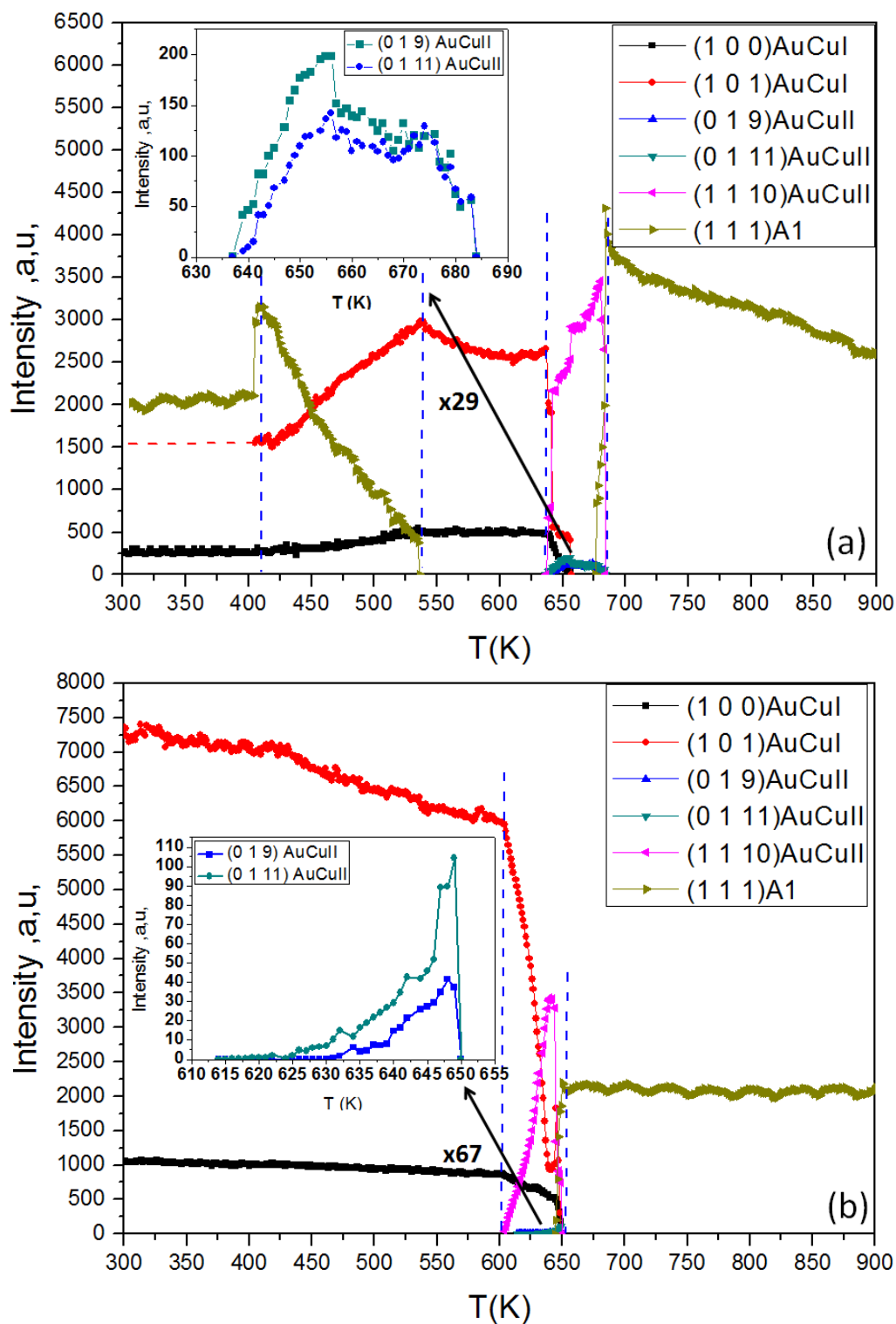


Fig.4.26. Temperature dependence of the intensities of selected peaks, labeled with their diffraction indexes, for the three phases A1, AuCuI and AuCuII upon heating (a) and cooling (b). The dotted vertical blue lines show the transition temperatures.

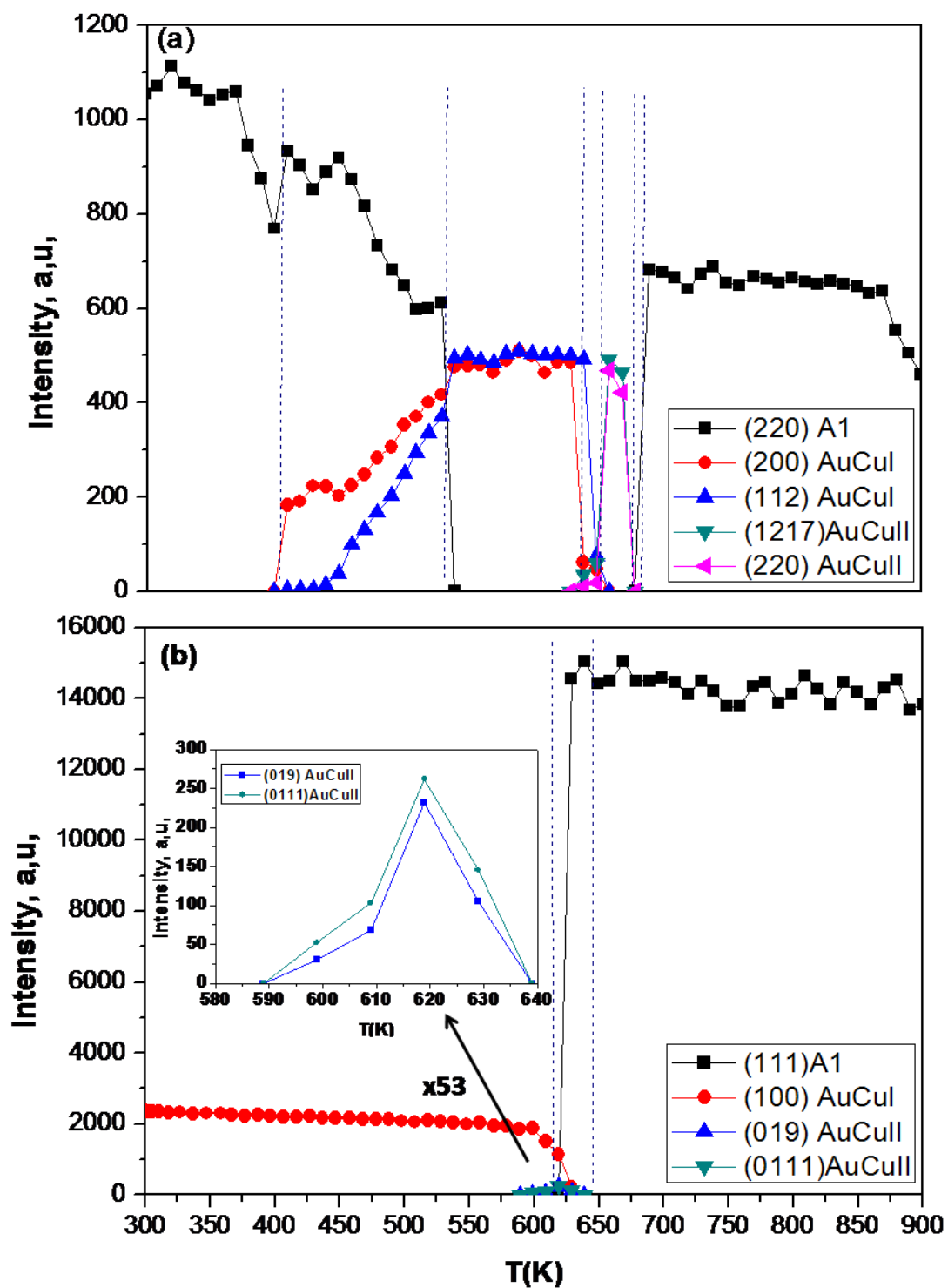


Fig.4.27. Temperature dependence of the intensities of typical peaks for the three phases A1, AuCuI and AuCuII upon heating (a) and cooling (b). The dotted lines show the transition temperatures.

	Phase transition	Phase transition
Heating	(A1)- (A1+ AuCul)	(A1+ AuCul)- (AuCul)
Temperature	408K (135°C) (± 2 K)	538K (265°C) (± 1 K)
Heating	(AuCul) - (AuCul+AuCull)	(AuCul+AuCull) - (AuCull)
Temperature	637K (364°C) (± 1 K)	657K (384°C) (± 1 K)
Heating	(AuCull) - (AuCull+A1)	(AuCull+A1) - (A1)
Temperature	677K (404°C) (± 1 K)	684K (411°C) (± 1 K)
Cooling	(A1)- (A1+ AuCul + AuCull)	(A1+ AuCul + AuCull) - (AuCul + AuCull)
Temperature	650K (377°C) (± 2 K)	644K (371°C) (± 2 K)
Cooling		(AuCul + AuCull) - (AuCul)
Temperature		603K (330°C) (± 2 K)

Table.4.2. Reports the phase transition temperatures where every temperature corresponds to the beginning of the final phase. The order of the transitions is: for the heating from room temperature to 973K (700°C) and for cooling from 973K (700°C) to room temperature. The error factor is mentioned beside the phase transition temperatures according to the refinement of the data.

On the other hand, the phase transition in Au-25wt.%Cu system show a noticeable difference in thermal expansion coefficients of different phases in terms of normalized volume of unit cell of the corresponding phases per atom (Fig.4.28) and in terms of total normalized volume (Fig.4.29). The normalized unit cell volumes have been calculated from fitting XRD patterns of the large diffraction angles scans, where, the obtained unit cells of every phase have been divided by the corresponding atomic cell number. To obtain the total normalized volume, V_T , we have used the relation (1).

$$V_T = V_\alpha \cdot fr_\alpha + V_\beta \cdot fr_\beta + \dots \quad (1)$$

being $V_{(\alpha, \beta, \dots)}$ and $fr_{(\alpha, \beta, \dots)}$ the normalized volume and fraction for the phases α, β, \dots

In both figures, a noticeable decrease of the normalized unit cell volume of A1 phase is manifested in two steps, firstly in the onset of the AuCuI phase and then until the total disappearance of A1. After, total normalized unit cell volume corresponding to AuCuI increase homogenously with respect to the temperature, until the temperature of the second transition (AuCuI - AuCuII) where there is a noticeable dilatation for AuCuII pure phase. A second dilatation occurs in the third transition (AuCuII - A1). Upon cooling, a noticeable contraction accompanies the ordering reaction through the passage from A1 to AuCuI+AuCuII; followed by an expansion when only the AuCuI phase remains. Figure.4.31 exhibits the evolution of phase fractions upon heating and cooling.

This dilatometry behavior of the phase transitions at the atomic level obtained for the analysis of XRD patterns is confirmed and in total agreement with the macroscopic level by means of a dilatometer (Fig.4.30)

The normalized volume fractions presented in figure.4.31 have been calculated by the simple multiplication of the normalized unit cell volume of every phase by the phase fraction.

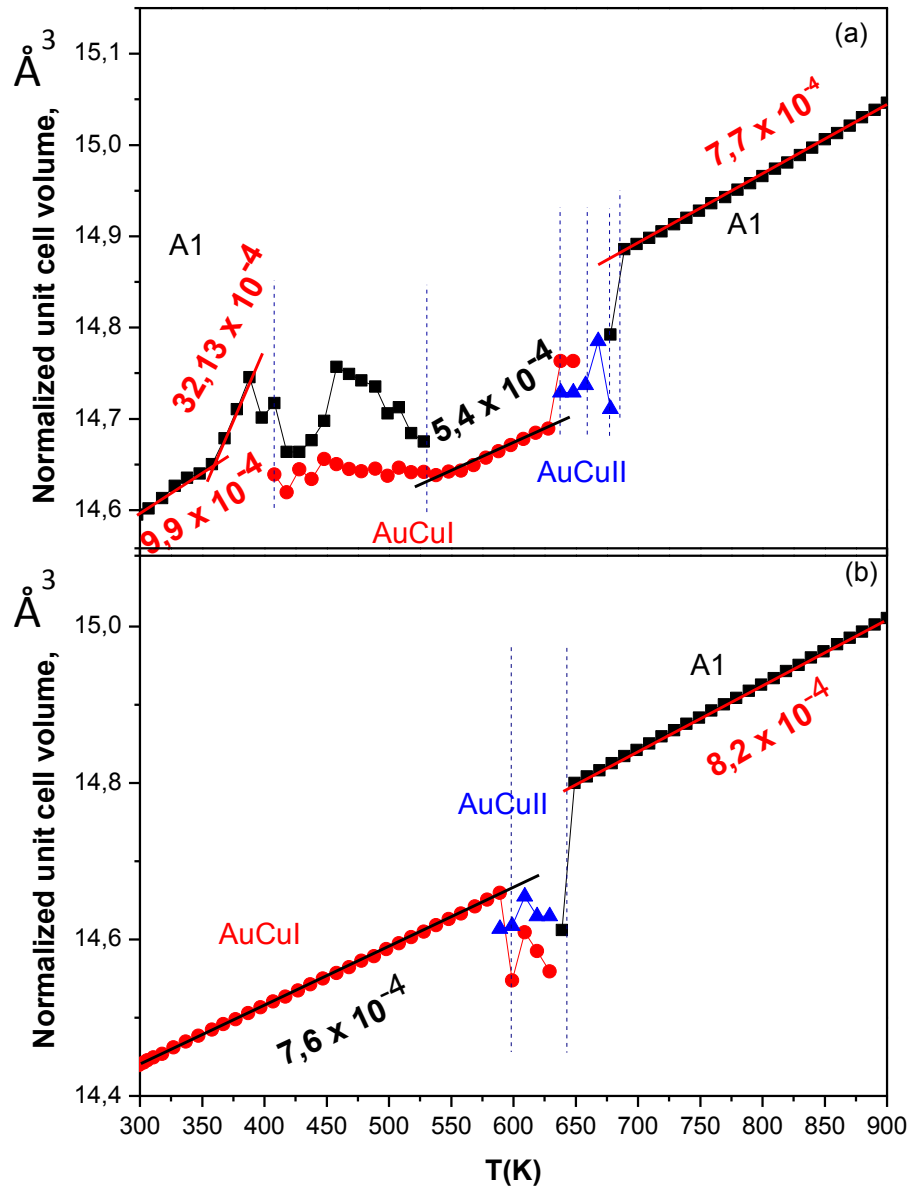


Fig.4.28. Normalized unit cell volume for A1 (black), AuCul (red) and AuCull (blue) phases upon heating (a) and cooling (b).

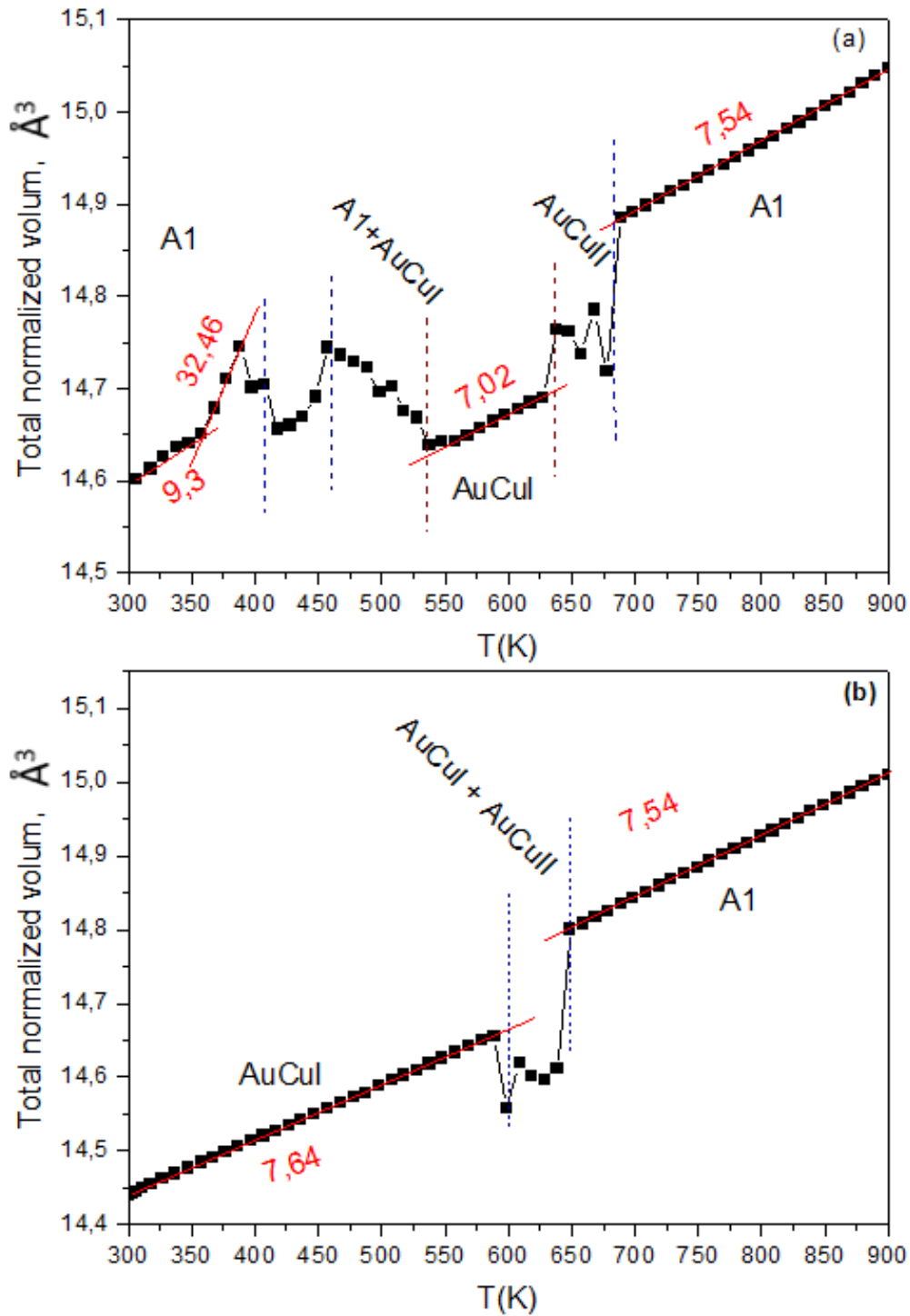


Fig.4.29. Dilatometric curves at atomic level presented in total normalized volume upon heating (a), and cooling (b). Values of thermal expansion coefficients of the pure phases (in $10^{-4}/\text{K}$) are given nearby experimental points. The most pronounced difference between them is seen upon heating of A1 phase where the expansion is outstandingly accelerated at about 360K (87°C) (from $9.3 \cdot 10^{-4}$ vs. $32.46 \cdot 10^{-4}$ 1/K).

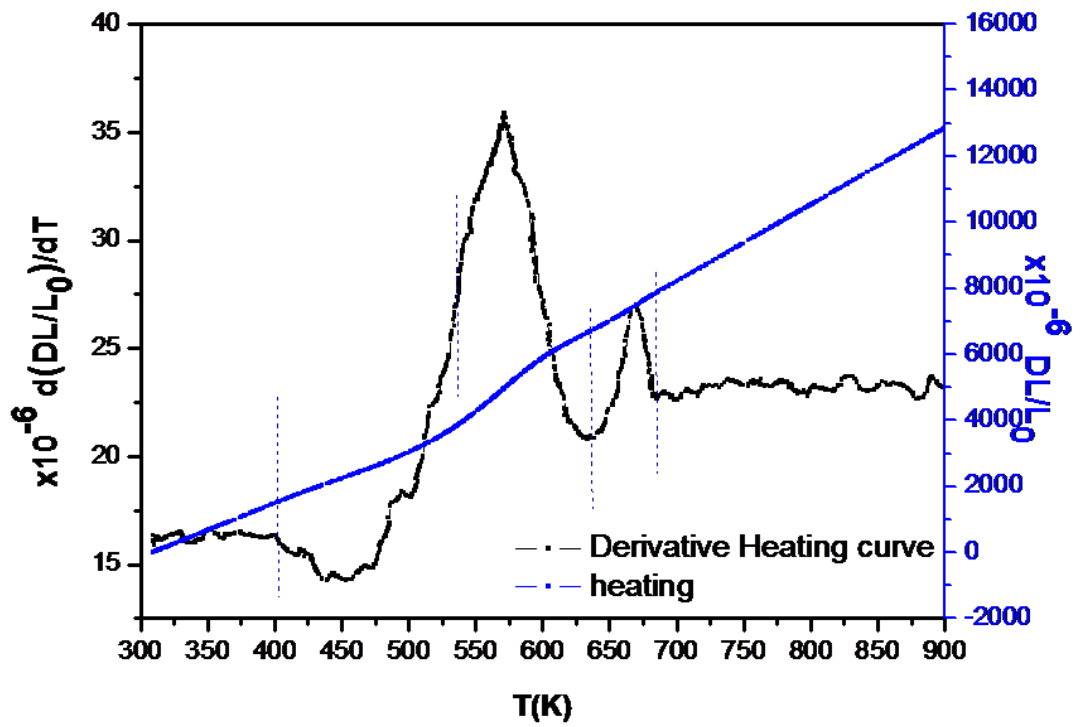


Fig.4.30. Macroscopic dilatation curve (blue) and its derivative (black) upon heating determined by means of a dilatometer with heating rate of 10K/min.

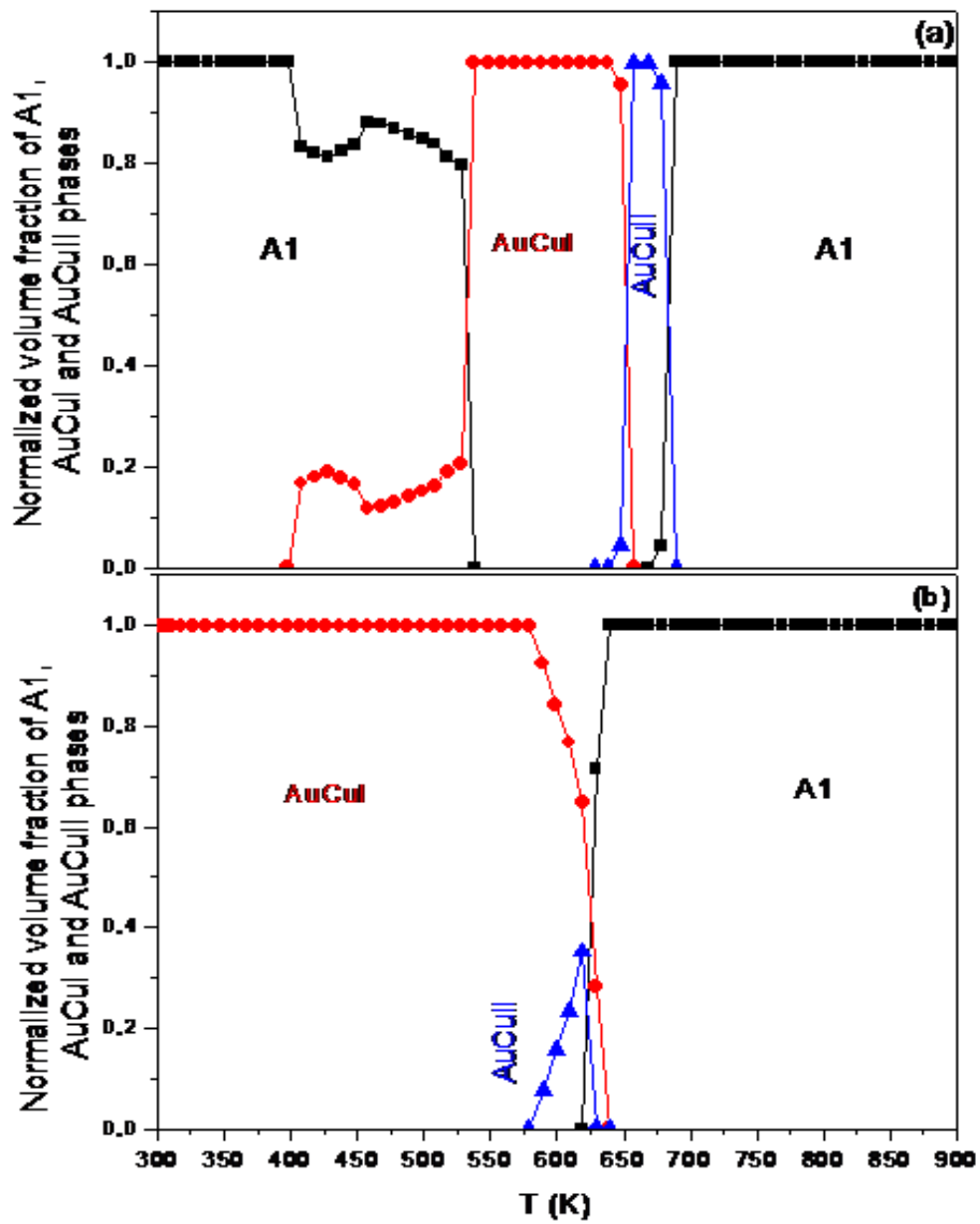


Fig.4.31. The normalized volume fractions for A1 (black), AuCuI (red) and AuCuII (blue) phases upon heating (a) and cooling (b).

4.III.2. Discussion of the structural results

4.III.2.1. Upon heating

In virtue to the slowest rate used for the thermal cycle to determine the phase transition processes and temperatures, the obtained results are of highest thoroughness possible using in-situ XRD at sweeping mode. In spite of, the very first transition from the disorder A1 to the order AuCuI presents some issues since from the beginning of the experiment there are AuCuI nanograins as result of quenching. Thus, while the intensity of (100) AuCuI peak shows a constant value from RT to 408K (135°C), corresponding to the constant quantity of the tetragonal AuCuI nanograins. we cannot determine the intensity of (101) AuCuI peak mainly by the fact that of its huge overlapping with the principle peak of the cubic A1 (111). So, assuming constant quantity of the tetragonal AuCuI nanograins, its intensity is presented in dotted red line (Fig.4.26(a)) from RT to 408K (135°C). Close to this point (exactly two degrees before), the intensity of the peak (111) of the A1 phase depicts a sudden increase in the intensity, phenomenon which can be due to the coalescence of the disordered crystalline cubic domains. In this way, the thermal induced decrease of vacancy concentration, generated in the supersaturated phase A1 after quenching, leads to some dislocation relaxation that sharpens the diffraction peaks and produces the corresponding raise of intensities too. After that, the interval from 408 K (135°C) to 538 K (265°C) shows a monotonously decrease in the intensity of (111) A1 peak which is associated with the corresponding intensity increase observed on (100) and (101) peaks of AuCuI phase (Fig.4.26(a)). Nevertheless, the assessment of the transition temperature from A1 to AuCuI upon heating is visualize along high diffraction angles measured on the large range scans, where the overlapping between (220) A1 and (200) or (212) broaden reflections is resolved better (Fig.4.25(a)). In contrast, the onset of the orthorhombic phase AuCuII upon heating that starts at 637K (364°C) and end with pure AuCuII at 657K (384°C), and the nucleation of the cubic A1 from AuCuII (begins at 677K (404°C) and finishes at 685K (412°C)) are accurately determined from the data of short diffraction angle scans (Fig. 4.25).

4.III.2.2. Upon cooling

The phase transition sequences from high temperature to RT have been proved using XRD as follow: A1 - A1+AuCull+AuCul - AuCull+AuCul - AuCul. From short range diffraction angle scans, the coexisting of the three phases A1+AuCul+AuCull goes between 649K (376°C) to 645K (372°C) (Table.4.2, Fig.4.25 and Fig.4.26). From 644K (371°C) to 604K (331°C), concomitant presence of only two phases AuCul and AuCull, is demonstrated where the small intensities of the (019) and (0111) reflections of AuCull are fitted and calculated (see Fig.4.26(b)). Cooling strictly below 604K (331°C), the phase is the pure tetragonal AuCul down to RT. The appearance of the order with cooling down engender a noticeable contraction (Fig.4.28 (b) and Fig.4.29 (b)) as the atoms rearrange to stabilize at the final sites that provide them the minimal energy.

4.III.3. Mechanical study

The experimental conditions used in this part have been united for both structural and mechanical studies; at starting the heating from the disorder A1 using heating velocity of 1K/min under secondary vacuum.

Figure.4.32 shows temperature dependent of the internal friction (TDIF) and the dynamic modulus (TDEM) of the AuCu alloy with the disordered phase A1 as starting state, where two frequencies have been used: 1 (top) and 0.5 Hz (bottom). Three peaks are visible on both heating curves (red lines), denoted by P_1 , P_Z and P_{APB} as temperature increased. Firstly, P_1 peak appears at the same temperature as the first phase transition shown in the structural study (A1 - AuCul). Then, P_Z peak arises as a broadening bump which spreads over the range where AuCul is observed and has a maximum at the temperature of the AuCul - AuCull phase transition. Finally, P_{APB} appears as a sharp spike that is cut off by the transformation into the disordered phase A1. The shear modulus presents dip and shoulders that are synchronized with every internal friction peak. Concerning the frequency, the thermally activated peak P_Z widens toward low temperatures when the frequency decreases but P_{APB} remains at the same temperature. On the other hand, the two cooling curves (blue lines) for each frequency have similar shape and both present two peaks, the peak P_Z and the

peak P_{GB} that is probably due to grain boundary sliding. The shear modulus upon cooling shows the obvious increase corresponding to the relaxation peak P_Z . However, superimposed to this appear some fluctuations that coincide with the region of co-existence of the AuCuI and AuCuII phases. Coming from high temperature, the rapid increase of the Zener peak intensity coincides with an increase of the shear modulus curve. When the Zener peak falls down a steady increase in the shear modulus is observed. Finally, it is worth to notice that the position of the P_Z relaxation peak, is not the same upon heating and cooling.

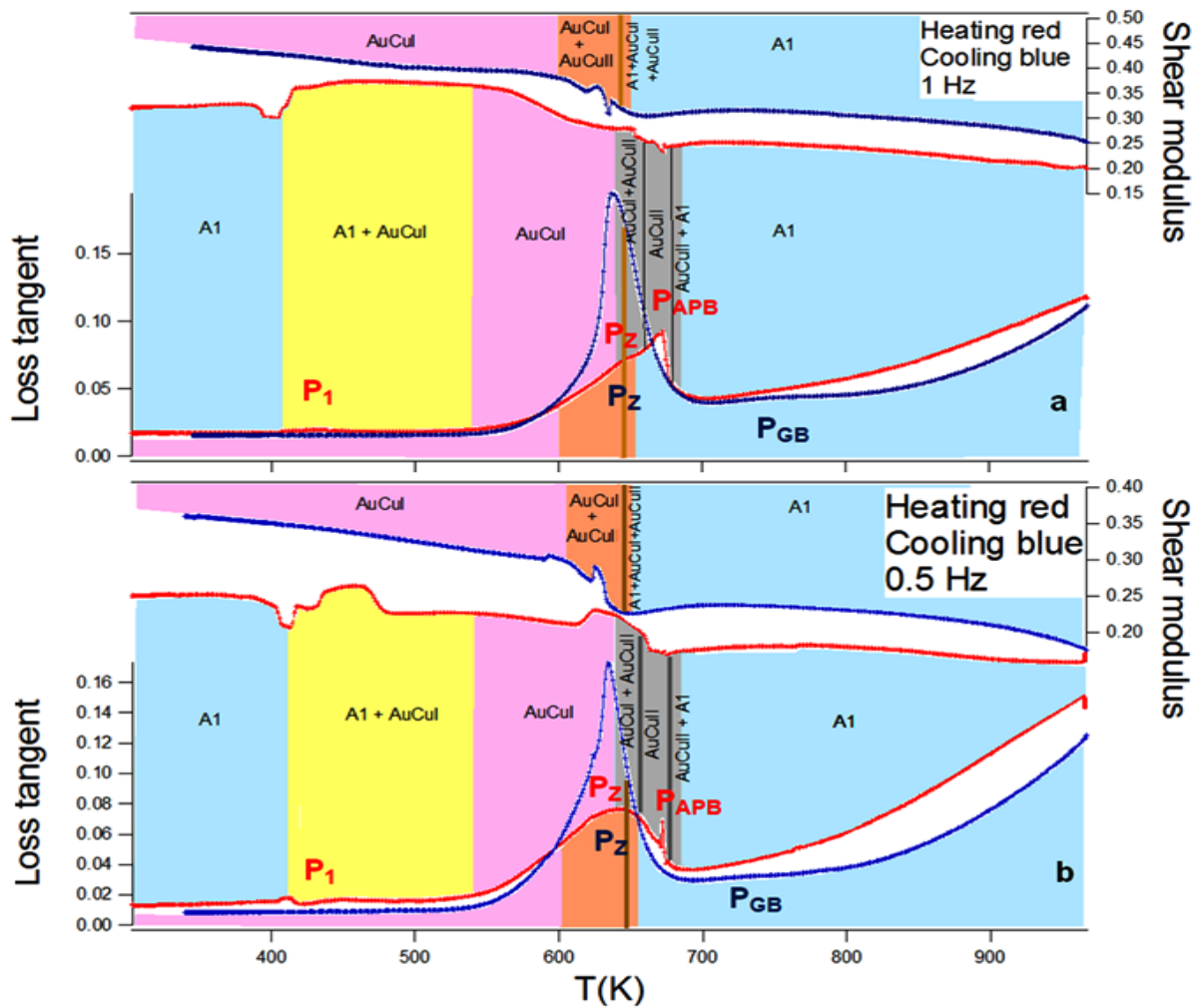


Fig.4.32. Mechanical loss and dynamic shear modulus of the Au-25wt.%Cu system as a function of temperature upon heating and cooling, using a frequency of 1 Hz (a), 0.5 Hz (b). The red lines present the mechanical behaviors upon heating and the blues upon cooling. The intervals for every phase are depicted in different colors where the limits have been established to the structural study. Upon heating, P_1 is the peak that accompanies the onset of AuCuI; P_Z presents the Zener peak and P_{APB} corresponds to antiphase boundaries relaxation. Upon cooling, P_{GB} presents the grain boundaries peak and the classic Zener peak P_Z .

4.III.4. Discussion of the mechanical results

4.III.4.1. Upon heating

The internal friction and shear modulus spectra give a better understanding of the defect diffusion or rearrangement processes that occur in the material. From figure.4.32, the first phase transition A1 - AuCuI is visible through the P_1 peak that reveals a split shape, which is more likely attributed the ordering reaction that precedes the A1 - AuCuI transition as previously studied (part II). What is more important, however, is the modulus variation. Despite the “jumpy” shape of the curve that demonstrates that the transformation probably occurs by successive bursts in different parts of the sample, we have noticed that the transformation always shows a decrease of the modulus followed by an increase. Therefore, one may suppose that the transformation needs some softening of the elastic constants to be triggered. At about 630 K (357°C), a maximum is always observed but it is clearly more visible at 0.5 Hz. According to former studies [72], this peak should be attributed to a Zener relaxation that appears in the ordered phase AuCuII and disappears abruptly when such phase transform in disordered A1. As demonstrated by Henning [80], the Zener relaxation can only occur if the Au and Cu have the possibility to exchange. The presence of the Zener peak in the AuCuII ordered phase indicates that the state of atomic order is not perfect. Indeed, due to the non-perfect stoichiometric composition of the alloy, some substitutional disorder must exist i.e. Au atoms occupy sites on the Cu sublattice [80]. The temperature range, which corresponds to the presence of the pure ordered phase AuCuII, is characterized by the P_{APB} peak that may be an antiphase boundaries relaxation peak. Such peak disappears with the onset of the cubic A1. According to ref.[66, 92], the AuCuI and AuCuII phases are characterized by the presences of twins which might produce P_{APB} . However, Tkalcec *et al.*[78] have suggested a better explanation. They show that two different peaks can appear: a twin boundaries peak that appears in AuCuI and a peak in AuCuII that they attribute to the movement of antiphase boundaries. In the present study, the peak P_{APB} appears in the AuCuII region and it more likely due to antiphaseboundaries..The spectra recorded at a frequency of 0.5Hz allows a better discrimination of the phenomena. The Zener peak, that is thermally activated appears at a lower temperature.

4.III.4.2. Upon cooling

Upon cooling the peak P_Z clearly starts when only the phase A1 is present. Therefore the right flank of the peak should be attributed to the disordered phase A1. This is the classical Zener peak already investigated in the past [81]. The maximum of the peak is close to the temperature where the A1 phase disappears. It is followed with a drop of the peak at lower temperature with the increase of the order. This drop is less abrupt with 0.5Hz, where the peak should appear at lower temperature. This observation shows that the Zener relaxation effectively fall down with the ordering when A1 disappear as. Still, the AuCul and the AuCull phases allow the presence of a lower but visible peak P_Z which manifests as a low temperature shoulder. The Zener relaxation peak maximum is accompanied with an increase of the shear modulus with the total disappearance of A1. In the area where there are two phases, the shear modulus presents fluctuations that accompany the disappearance of the small quantity of the orthorhombic phase AuCull before its stabilization with the only phase AuCul. P_{GB} represents the grain boundaries relaxation peak that appears adjacent to Zener peak at high temperature [93,94] in A1.

Conclusion of the part III

In this part of the work, we assess the phase transition sequence and temperatures in Au-25wt.%Cu composition upon heating and cooling cycle from RT to 973 K (700°C) combining in-situ thermo-diffraction experiments and mechanical spectroscopy at sweep rate of 1 K/min. The initial state after quenching is mainly a cubic A1 disordered phase but unavoidable nanograins of AuCul are present. The onset of the AuCul upon heating generates a transient peak with volume contraction. The AuCul phase shows a Zener peak, which suggests that a certain degree of disorder is present or at least non thermal vacancies. The AuCull phase is characterized by a relaxation peak that should be attributed to the movement of antiphase boundaries. The transformation from AuCul to AuCull also leads to an expansion of the lattice. Upon cooling, the presence of all three possible phases is detected at the same time from 650 to 644K. Then only AuCul and AuCull are present between 644 and 604 K, before the stabilization of the tetragonal AuCul as

final state. This time the Zener peak seems to appear before the transition $A1 \rightarrow AuCuI + AuCuII$ and partially disappear when only the AuCuI phase is present. Therefore, a consistent part of the peak should be attributed to copper relaxation in the disordered phase A1.

Part IV: Extra structural results for the ternary 18-carat composition Au-7wt.%Cu-18wt.%Ag.

This thesis ended with the last used composition the ternary 18-carat composition Au-7wt.%Cu-18wt.%Ag. As the structural study using the in-situ temperature XRD (Fig.4.33) shows that this composition do not exhibit any phase transition where there is only the pure solid solution α all along the thermal cycle. Knowing that the sample has been homogenized for two hour at 973K (700°C) followed by water quenching. And from this quenched state the structural XRD measurement began using the experimental condition of thermal velocity of about 1K/min and the time of data acquisition of 1 pattern/10min.

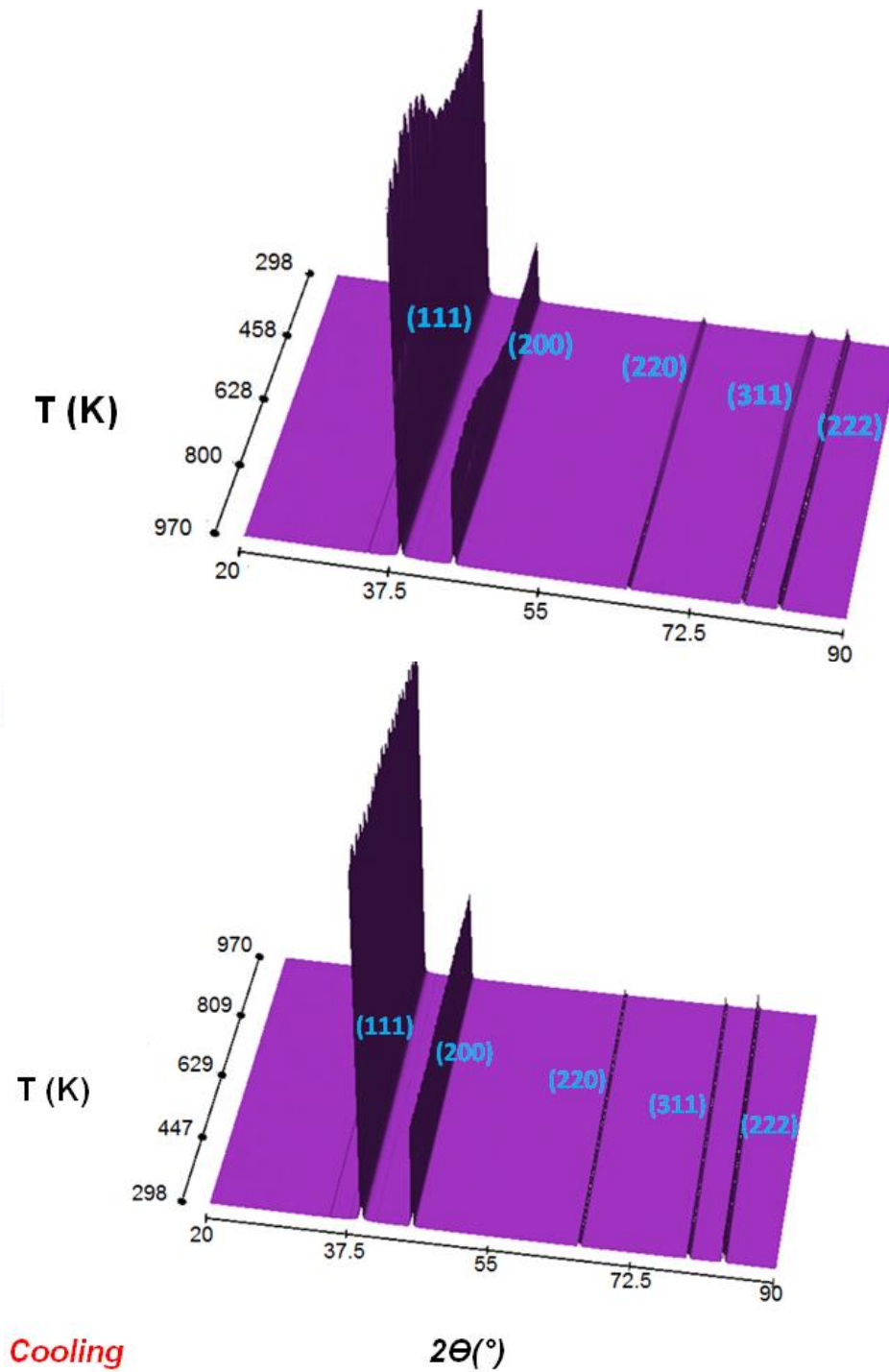


Fig.4.33. 3D schemes of the diffraction peaks evolution of the Au-7wt.%Cu-18wt.%Ag system upon heating and cooling from $2\theta=20^\circ$ to $2\theta=90^\circ$. The diffraction indexes of the observed peaks of the solid solution α are presented in brackets.

General conclusion

Gold alloys of 12 and 18-carat present several order-disorder phase transitions upon the thermal cycle from room temperature up to around the industrial used temperature and cooling down.

The thermal analyses using the DSC and the dilatometry, proved the presence of such new phase transition at low temperature. That was confirmed using imaging techniques such as the SEM, AFM and STM in dendrite shaped copper oxide on the gold alloy surfaces. These dendrites appear and grow from 433 K (160°C) to 473K (200°C) K for the binary 12 and 18 carat alloys and from 393K (120°C) to 433K (160°C) for the ternary 12 carat alloy. The XPS and grazing incidence XRD have shown that these dendrites correspond to copper oxide that has been formed on the top of the alloys. Furthermore, to well investigate this new pre-ordering phase and to determine the exact composition and structure, a trial of characterization has been performed on the binary 18-carat composition.

The use of the thermal analyzes as the DSC and the dilatometry have proven the presence of the pre-ordering phase in the binary 18-carat composition. the thing that has been enriched using surface techniques as the SEM, AFM and the STM. Where, the three of them have confirmed the nanostructured surface that accompanies the appearance of this pre-ordering phase. The micro-analysis SEM-EDS confirmed that these nanoparticles are cuprous oxide. The XPS confirmed that it is Cu_2O and quantitative elemental depth profile analysis shows that this anomaly is more likely to be attributed to the copper diffusion from the superficial atomic layers to the surface to finish with a combination with the Oxygen of the air in order to form the cuprous oxide nanograins.

The order-disorder phase transition in binary 18-carat alloy has been investigated by means of the in-situ temperature X-Ray diffraction. Where, very important results have been harvested. At first the thorough phase transition temperatures have been determined with the most precise experimental conditions possible till now. The omnipresence of the three possible phases (AuCuI , AuCuII , A1) upon cooling has

been prove as well as the formation of the obvious presence of the AuCull phase upon cooling.

The thermal mechanical internal friction and shear modulus tests on the binary 18-carat alloy, emphasize the structural in-situ XRD results. A Zener peak in the ordered phase AuCul confirms the non perfect aspect of the order in this phase. the second ordered phase AuCull presents a specific relaxation peak that should be attributed to the antiphase boundaries where this phase is characterized with the intense presence of the super lattices. At high temperature the grain boundaries relaxation peak characterize the disorder A1 and the vibration of bulk dislocations that gives rise to the high-temperature background. Upon cooling the Zener relaxation decreases drastically in magnitude when the alloy forms regions that exhibit long-range atomic order.

Bibliography

- [1] L. Chetibi, Magister report, Physics department, Faculty of science, University Constantine1, (2007).
- [2] J. Bénard, A. Michel and J. Philibert, *Métallurgie générale*. Masson, (1984).
- [3] C.S. Barrett, "MA Ph. D, TB Massalski." Ph. DD Sc.(London), C graw-Hill Book company, *structure of metals* 300, (1966).
- [4] P. Papon, J. Leblond and P.H.E. Meijer, *Physique des transition de phase*, Dunod, Paris, (1999).
- [5] J. Hennig, Ph.D. dissertation 4635, École Polytechnique Fédérale de Lausanne, Faculté des Sciences de Base, Institut de Physique de la Matière Condensée, Groupe de Spectroscopie Mécanique, (2010).
- [6] World Gold Council: *Gold Demand Trends – Full year and fourth quarter 2008*, technical report, (2009)
- A report published quarterly by the World Gold Council, a marketing organization funded by most of the largest gold mining companies, based on data provided by GFMS Limited, a precious metals consultancy specializing in gold market research.
- [7] C.W. Corti, "Strong 24 carat golds: the metallurgy of microalloying." *Gold Technol* 33, 27-36, (2001).
- [8] D. Ernst and J. Hausselt, "Uses of gold in jewellery." *Interdisciplinary Science Reviews* 17.3, 271-280, (1992).
- [9] A. Prince, *Silver–Gold–Copper*, chapter 2 in ref. LBIV11 (2006)
- [10] W.S. Rapson, "The metallurgy of the coloured carat gold alloys." *Gold Bulletin* 23.4, 125-133, (1990).
- [11] V. Šíma, "Order–disorder transformations in materials." *Journal of Alloys and compounds* 378.1, 44-51, (2004).
- [12] R. L. Krishna, *Principles of engineering metallurgy*, New Age International, (2007).
- [13] J. Rakovan, "Word to the Wise: Metasomatism." *Rocks & Minerals* 80.1, 63-64, (2005).

- [14] Y. Terada, K. Ohkubo, T. Mohri and T. Suzuki, "Thermal conductivity of intermetallic compounds with metallic bonding." *Materials transactions* 43.12, 3167-3176, (2002).
- [15] G. SAUTHOFF, "Intermetallic Phases as High-Temperature Materials." *ChemInform* 17.52 (1986).
- [16] R.L. Fleischer, "High-strength, high-temperature intermetallic compounds." *Journal of materials Science* 22.7, 2281-2288, (1987).
- [17] M.H. Yoo, S.L. Sass, C. Fu, M.J. Mills, D.M. Dimiduk and E.P. Goerge, "Deformation and fracture of intermetallics." *Acta metallurgica et materialia* 41.4, 987-1002, (1993).
- [18] Z. Belamri, Ph.D. dissertation, Physics department, Faculty of science, University Constantine1 (2013).
- [19] J.B. Clark, J.W. Hastie, L.H.E. Kihlberg, R. Metselaar, and M.M. Thackeray, "Definitions of terms relating to phase transitions of the solid state." *Pure Appl Chem* 66, 577-594, (1994).
- [20] B. Yang, M. Asta, O.N. Mryasov, T.J. Klemmer and R.W. Chantrell, "The nature of A1-L1 0 ordering transitions in alloy nanoparticles: A Monte Carlo study." *Acta materialia* 54.16, 4201-4211, (2006).
- [21] M. Héritier, transition de phase-généralités, Chap. 2, 46-89, (2007):.
- [22] C. H. Novion, Ph.D. dissertation, école de printemps, laboratoire Léon brillouin (CEA-CNRS), Gif-sur-Yvette, France (2007)
- [23] G. Bénard, A. Michel, J. Philibert, J. Talbot, *Métallurgie générale, Métallurgie Générale*, Masson et C^{ie}, Editeurs, Paris VI, 49-52, (1969).
- [24] J. M. Cowley, "X-ray measurement of order in single crystals of Cu₃Au." *Journal of Applied Physics* 21.1, 24-30, (1950).
- [25] C. Kittel, *Physique de l'état solide*, Dunod Université, ISBN 2-04-010611-1, 1983.
- [26] W. H. Rothery, R. E. Smallman, C. W. Haworth, *The structure of metals and alloys*, 5th edition, (1969).
- [27] A. K. Jeam, M. C. Chatrvedi, *Phase Transformation In Materials: diffusional transfrmation in solids : Short-Range Diffusion*, (1992).
- [28] V. Walls, *JD. Z Phys Chim* , 13, 657, (1984).
- [29] J.W. Cahn and J.E. Hilliard, "Free energy of a nonuniform system. I. Interfacial free energy." *The Journal of chemical physics* 28.2, 258-267, (1958).

- [30] J.M.Howe A. R. S. Gautam, , K. Chatterjee, and F. Phillipp, "Atomic-level dynamic behavior of a diffuse interphase boundary in an Au–Cu alloy." *Acta materialia* 55.6, 2159-2171, (2007).
- [31] A. K. Jena, M. C. Chantnrvedi, *Phase transformation in materials: Diffusional transformation in solids: Shurt-Range diffusion* Chap. 7, 256-270, (1992).
- [32] A. H. Lipson, *Progress in Metal Physics*, (1950).
- [33] P. Haasen, *Physical Metallurgy*, presse de l'université de Combrige, 154, (1978).
- [34] D. A. Porter, K. E. Eastoring, *Phase transformation in metals end alloys*, second edition, Chapman et Hall, London, 358-366, (1992).
- [35] Y. Adda, J.M. Dupouy, J. Philibert, Y. Quere, *Eléments de métallurgie physique –défauts cristallins*, (1977).
- [36] F. R. N. Nabarro, *Dislocations in solids*, North Holland Publishing Company, Volume II, 231, (1979).
- [37] R. W. Cahn and P. Haasen, *Physical Metallurgy*, Volume III, 237, North Holland (1996)
- [38] M. J. Marcinkowski, "Order-disorder transformations in solids, ed. H. Warlimont." (1974).
- [39] J. H. Westbrook, "Segregation at grain boundaries." *Metallurgical Reviews* 9.1, 415-471, (1964).
- [40] M. J. Marcinkowski and D. S. Miller. "The effect of ordering on the strength and dislocation arrangements in the Ni₃Mn superlattice." *Philosophical Magazine* 6.67, 871-893, (1961).
- [41] O. Dezellus, PhD dissertation, *Elaboration, microstructure et propriétés des interfaces dans les multimatériaux métalliques et céramiques*, Université Claude Bernard-Lyon I, (2010).
- [42] S. MERMOUL, Magister report, Physics department, Faculty of science, University Constantine1, (2009).
- [43] P. P. Fedorov, and S. N. Volkov. "Au–Cu Phase Diagram." *Russian Journal of Inorganic Chemistry* 61.6, 772-775, (2016).
- [44] S. Mermoul, Magister report, Physics department, Faculty of science, University Constantine1 (2009).
- [45] V. Sima, *J. Mater. Sci. Eng A* 324, 62, (2002).

- [46] P. Mašek, F. Chmelik, V. Šima, A. Brinck, and H. Neuhäuser, "Microstructure processes induced by phase transitions in a CuAu alloy as studied by acoustic emission and optical cinematography." *Acta materialia* 47.2, 427-434, (1999).
- [47] Y. Tanaka, K. I. Udoh, K. Hisatsune and K. Yasuda, "Spinodal ordering in the equiatomic AuCu alloy." *Philosophical Magazine A* 69.5, 925-938, (1994).
- [48] Y. Feutelais, B. Legendre and M. Guymont, "New enthalpies determination and in situ X-ray diffraction observations of order/disorder transitions in Au_{0.5}Cu_{0.5}." *Acta materialia* 47.8, 2539-2551, (1999).
- [49] C. E. Lekka, N. Bernstein, M. J. Mehl and D. A. Papaconstantopoulos, "Electronic structure of the Cu₃Au (111) surface." *Applied surface science* 219.1, 158-166, (2003).
- [50] J. Bénard, A. Michel, J. Philibert and J. Talbot, *Métallurgie générale*, Masson, 50 (1969)
- [51] P. Scardi and M. Leoni, "Diffraction whole-pattern modelling study of anti-phase domains in Cu₃Au." *Acta materialia* 53.19, 5229-5239, (2005).
- [52] C. S. Barrett, "MA Ph. D, TB Massalski." Ph. D Sc.(London), C graw-Hill Book company, structure of metals 300 (1966).
- [53] J. W. Matthews, S. Mader and T. B. Light, "Accommodation of misfit across the interface between crystals of semiconducting elements or compounds." *Journal of Applied Physics* 41.9, 3800-3804, (1970).
- [54] Y. Quéré, *Défauts ponctuels dans les métaux*, No. 5. Masson et Cie, 1967.
- [55] J. R. Beeler and J. A. Delaney, "Order-disorder events produced by single vacancy migration." *Physical Review* 130.3, 962, (1963).
- [56] E. W. Elcock, "Vacancy diffusion in ordered alloys." *Proceedings of the Physical Society* 73.2, 250, (1959).
- [57] J. A. Brinkman, C. E. Dixon and C. J. Meechan, "Interstitial and vacancy migration in Cu₃Au and copper." *Acta Metallurgica* 2.1, 38-48, (1954).
- [58] S. Benci, G. Gasparini and E. Germagnoli, "The influence of quenched-in vacancies on the ordering rate of the Cu₃Au alloy." *Il Nuovo Cimento* (1955-1965) 31.6, 1165-1175, (1964).
- [59] I. Tkalcec, D. Mari and R. Schaller, "Anelastic Effects of Phase Decomposition in 14-carat AuAgCu alloy." *Solid State Phenomena* 184, 277-282, (2012).

- [60] A. Prince, G. V. Raynor and D. S. Evans, Phase diagrams of ternary gold alloys, 294. Woodhead Pub Ltd (1990).
- [61] A. Prince, "Critical assessment of copper–gold–silver ternary system." *International materials reviews* 33.1, 314-338, (1988).
- [62] M. Nakagawa and K. Yasuda "A coherent phase diagram of the Au-Cu-Ag (Ag_{0.24}Cu_{0.76}) 1– x section of the Au- Cu- Ag ternary system." *Journal of the Less Common Metals* 138.1, 95-106, (1988).
- [63] G. Chen, X. Ni and T. Nsongo, "Lattice parameter dependence on long-range ordered degree during order–disorder transformation." *Intermetallics* 12.7, 733-739, (2004).
- [64] Y. Tanaka, K. I. Udoh, K. Hisatsune and K. Yasuda, *Philosophical Magazine A* 69. 5, 925-938, (1994).
- [65] M. L. Bhatia and R. W. Cahn "Lattice parameter and volume changes on disordering." *Intermetallics* 13.5, 474-483, (2005).
- [66] J. Bonneaux and M. Guymont, "Study of the order–disorder transition series in AuCu by in-situ temperature electron microscopy." *Intermetallics* 7.7, 797-805, (1999).
- [67] R. Smith and J. S. Bowles "The crystallography of the cubic to orthorhombic transformation in the alloy AuCu." *Acta metallurgica* 8.7, 405-415, (1960).
- [68] A.J. Pedraza, J. Kittl, Morphology and kinetics of the AuCu (disordered) to AuCu II transformation, *Acta Met* 24, 835, (1976).
- [69] H.I. Aaronson, K.R. Kinsman, Growth mechanisms of AuCu II plates, *Acta Met* 25, 367-376, (1977).
- [70] D. Mouani, C. Souleau and B. Legendre, "Etude du diagramme d'équilibre entre phases du système ternaire or-germanium-etain." *Journal de chimie physique* 89, 2107-2125, (1992):.
- [71] A.K. Audren, Ph.D. dissertation 6473, École Polytechnique Fédérale de Lausanne, Faculté des Sciences de Base, Institut de Physique de la Matière Condensée, Groupe de Spectroscopie Mécanique (2014).
- [72] A.K. Maier, I. Tkalcec, D. Mari and R. Schaller, "Grain boundary relaxation and grain growth in 18-carat yellow gold alloy." *Scripta Materialia* 66.6, 374-377, (2012).
- [73] I. Tkalcec, D. Mari, R. Schaller, "Anelastic effects of phase decomposition in 14-carat AuAgCu alloy", *Solid State Phenomena* 184, 277-282, (2012).

- [74] A.K. Maier, I. Tkalcec, D. Mari and R. Schaller, "Grain boundary formation stages in a deformed yellow gold single crystal studied by mechanical spectroscopy." *Materials Science and Engineering: A* 560, 466-472, (2013).
- [75] A.K. Maier, I. Tkalcec, D. Mari and R. Schaller, "Grain Boundary Relaxation in 18-carat Yellow Gold." *Solid State Phenomena* 184, 283-28, (2012).
- [76] A.K. Maier, I. Tkalcec, D. Mari and R. Schaller, "Theoretical modelling of grain boundary anelastic relaxations." *Acta Materialia* 74, 132-140, (2014).
- [77] A.K. Maier, I. Tkalcec, D. Mari and R. Schaller, "New In–Pd mechanical loss peak in ternary gold alloys." *Acta Materialia* 61.16, 6107-6113, (2013).
- [78] I. Tkalcec, D. Mari and R. Schaller, "Mechanical Spectroscopy of Ordered Binary Au-Cu." *Archives of Metallurgy and Materials* 60.3, 2093-2096, (2015).
- [79] J. Hennig, D. Mari and R. Schaller, "Stress-induced and atomic ordering in 18-carat Au–Cu–Ag alloys." *Materials Science and Engineering: A* 521, 47-51, (2009).
- [80] J. Hennig, D. Mari and R. Schaller, *Physical Review B* 79 (2009): 116-144.
- [81] C. Zener, *Phys Rev* 71, 34-8, (1947).
- [82] G. Binnig and R. Heinrich, "Scanning tunneling microscopy—from birth to adolescence." *reviews of modern physics* 59.3, 615, (1987).
- [83] J.A. Golovchenko, "The tunneling microscope: a new look at the atomic world." *Science* 232, 48-54, (1986).
- [84] https://en.wikipedia.org/wiki/Scanning_tunneling_microscope
- [85] https://en.wikipedia.org/wiki/X-ray_photoelectron_spectroscopy
- [86] D. Hamana, L. Chetibi, L. Amiour, "The apparition of a new reaction at lower temperature in equiatomic CuAu alloy" *Phase Trans* 82.10, 755-766, (2009).
- [87] *Handbook of X-Ray Photoelectron Spectroscopy*, Eds. J. Chastain, R.C. King, Jr., ULVACPHI, Chigasaki, Japan (1995).
- [88] NIST X-ray Photoelectron Spectroscopy Database, <http://srdata.nist.gov/xps/>
- [89] I. S. Golovin, A. M. Balagurov, I. A. Bobrikov, V. V. Palacheva and J. Cifre, "Phase transition induced anelasticity in Fe–Ga alloys with 25 and 27% Ga." *Journal of Alloys and Compounds* 675, 393-398, (2016).
- [90] A.K. Maier, I. Tkalcec, D. Mari and R. Schaller, "Grain boundary relaxation and grain growth in 18-carat yellow gold alloy." *Scripta Materialia* 66.6, 374-377, (2012).
- [91] J. Hennig, D. Mari and R. Schaller, *Physical Review B* 144, 116 - 79, (2009).

- [92] Y. Q. Xie, Y. F. Li, X. B. Liu, X. B. Li, H. J. Peng and Y. Z. Nie, "Systematic science of Au-Cu system based on experimental data of disordered alloys: Characteristic atom occupation patterns of Au₃Cu, AuCu₃, AuCu I and AuCu II", Transactions of Nonferrous Metals Society of China 21, 1092-1104, (2011).
- [93] A.K. Maier, I. Tkalcec, D. Mari and R. Schaller, "Grain boundary formation stages in a deformed yellow gold single crystal studied by mechanical spectroscopy." Materials Science and Engineering: A 560, 466-472, (2013).
- [94] I. Tkalcec, , D. Mari, and R. Schaller, "Mechanical Spectroscopy of Ordered Binary Au-Cu." Archives of Metallurgy and Materials 60.3, 2093-2096, (2015).
- [95] I. Lamiri, M .S. M. Abdelbaky, D. Hamana and S. García-Granda, "Metastable phase in binary and ternary 12-carat gold alloys at low temperature", Materials Research Express 5.4, 046503, (2018).

Abstract

Study of the order disorder transitions and the mechanical properties in the metallic alloys (AuCu and AuCuAg)

This work is motivated by a scientific interest in gaining a better understanding of the phase transformations that govern the mechanical properties of gold alloys due to their huge industrial importance such as their common use in jewelry applications, luxury watch making, catalyses, electronic industries ...etc...

The selected alloys fall in one of two categories of yellow gold, based on the binary system of Gold-Copper and the ternary system Gold-Copper-Silver

In this thesis, selected alloys from the two categories are studied, using two principal compositions of 12 and 18-carat. The study starts primarily by the thermal identification of the possible anomalies that could happen during the heating from the room temperature up to 973K (temperature near to the industrial use -1023K). Un expectable anomaly at low temperature has been noticed by the thermal analyses while the primary state before the heating process was the disorder. The fact that has orientate the study to the use of surface techniques in order to determine the relationship of the thermally detected anomalies with the surface aspect of the alloys. The study has lead to highlight new kind of metastable phase transition that precede the ordering reaction in gold alloys at low temperature presented in dendrite shape of precipitated phase on the surface. The participation of the silver in the alloy composition leads to accelerate the ordering reaction.

18-carat binary composition, has been treated in the thorough way in terms of structural study. Using the in-situ temperature XRD measurement with data acquisition frequency of 1 pattern/1.1min. Phase transition sequences and temperatures have been determined over the fitting of the obtained patterns and through the following of the behavior evolution of the intensities of the typical peak of every phase as well as the atomic volume occupancy.

The analysis and interpretation of the experimental data stemming from the mechanical spectroscopy reveal three important anelastic relaxations (internal dissipation processes), which dominate the mechanical loss spectrum of the binary 18-carat alloy above room temperature. A Zener relaxation, due to directional ordering of atoms in the substitutional solid solution, occurs nearby the phase transition AuCuI - AuCuII upon heating and the classic Zener relaxation peak accompanies the phase transition A1 - AuCuI + AuCuII upon cooling. A twin boundaries peak has been highlighted as typical peak of the AuCuII. Grain boundaries sliding relaxation peak has been attributed to the pure disordered phase

Keywords: 12 and 18-carat, gold, silver, copper, thermal analyses, precipitation, dendrite, mechanical spectroscopy, anelasticity, internal dissipation, Zener relaxation, twin boundary relaxation, grain boundaries sliding relaxation.

دراسة تحولات اضطراب النظام والخواص الميكانيكية في السبائك المعدنية

(AuCu و AuCuAg)

ويأتي هذا العمل بدافع علمي في اكتساب فهم أفضل للتحولات الطورية التي تحكم الخواص الميكانيكية لسبائك الذهب نظرا لأهميتها الصناعية الضخمة مثل استخدامها المشترك في صناعة المجوهرات و الساعات الفاخرة والحفارات والصناعات الإلكترونية .. الخ.

تقع السبائك المختارة ضمن فئة واحدة من فئتين من الذهب الأصفر، التي تستند الى نظام تنائي من الذهب- نحاس و النظام الثلاثي من ذهب- نحاس-فضة.

في هذه الأطروحة، تم اختيار السبائك ذات نظام تنائي الفئة المراد دراستها ، وذلك باستخدام اثنين من التراكيب الرئيسية من 12 و 18 قيراط. تبدأ الدراسة في المقام الأول عن طريق اجراء تحاليل حرارية للعينات من أجل معرفة الشدود المحتملة التي يمكن أن تحدث أثناء عملية التسخين من درجة حرارة الغرفة الى 973 K (درجة الحرارة قريبة من درجة الحرارة المستعملة في الصناعة 1023K).

لقد لوحظ الشذوذ غير متوقع عند درجة حرارة المنخفضة ، و هذا راجع لعملية التحاليل الحرارية، بينما عند الحالة الابتدائية (الاولية) قيل عملية التسخين كانت العينة غير منظمة. في الحقيقة، كان الهدف من هذه الدراسة هو التركيز على استخدام التقنيات السطحية من أجل تحديد العلاقة بين الشذوذ المكتشف الناتج عن عملية التسخين مع جانب سطح السبائك.

وقد أدت هذه الدراسة إلى تسليط الضوء على نوع جديد من الانتقال شبه مستقرة مرحلة الانتقالية التي تسبق عملية رد فعل الترتيب في سبائك الذهب عند درجة حرارة منخفضة و التي ظهرت على شكل تشعبات شجرة المترسبة على السطح. يؤدي مشاركة الفضة في تكوين تركيب السبيكة إلى تسريع رد فعل الترتيب.

بالنسبة لتركيب التنائي لـ 18 قيراط، تمت معالجتها عن طريق درجة الحرارة باستعمال جهاز انعراج الاشعة السينية وذلك بتسليط درجة حرارة في مواقع مع تسجيل الناتج الطيف خلال كل 1 دقيقة ، وهذا من أجل دراسة البنية .

يحدد طور الانتقال المتتالي و درجة الحرارة من خلال الفيتينك الاطياف المتحصل عليها و هذا خلال متابعة تطور سلوك شدة نوع القمة لكل طور بسهولة مثل حجم احتلال الذرة.

التحاليل و المناقشة لنتائج التجربة من خلال مطيافية الميكانيكية الذي اظهرت ثلاثة نتائج مهمة الاسترخاء غير مرنة (عملية التبيد الداخلي)، التي تسيطر على قلة طيف الميكانيكي لنائي السبائك 18 قيراط عند درجة حرارة الغرفة. عند استرخاء زينر، الذي ادى الى اتجاه ترتيب الذرات في استبدال المواقع في محاول الصلب، الذي يظهر تقريبا الانتقال $AuCuI - AuCuII$ عند التسخين و يصاحب قمة استرخاء زينر الكلاسيكي طور الانتقال $AuCuI + AuCuII - A1$ عند التبريد. الحد المزدوج الحدين للقمة ذو الاهمية مثل نموذج قمة $AuCuII$. انزلاق الاسترخاء القمة الذي بدوره يشير الى طور الغير منتظم النقي.

مفتاح الكلمات: 12 و 18 قيراط، ذهبي، فضة، نحاس، التحاليل الحرارية، الترسيب، تشعب شجري، مطيافية الميكانيكية، غير مرنة، التبيد الداخلي، استرخاء زينر، الحد المزدوج للاسترخاء، استرخاء انزلاق الحدود.

Résumé

Etude des transitions ordre- désordre et des propriétés mécaniques dans les alliages métalliques (AuCu et AuCuAg)

Ce travail est motivé par un intérêt scientifique à mieux comprendre les transformations de phase qui régissent les propriétés mécaniques des alliages d'or en raison de leur importance industrielle telle que leur usage commun dans l'industrie bijoutière, montres de luxe, catalyse, industries électroniques. etc...

Les alliages sélectionnés appartiennent à l'une des deux catégories d'or jaune, basées sur le système binaire Or-Cuivre et le système ternaire Or-Cuivre-Argent.

Dans cette thèse, des alliages sélectionnés des deux catégories ont été présents, en utilisant deux compositions principales de 12 et 18 carats. L'étude débute principalement par l'identification thermique des éventuelles anomalies pouvant survenir lors du chauffage de la température ambiante jusqu'à 973K (température proche de l'utilisation industrielle -1023K). Une anomalie non détectable à basse température a été constatée par les analyses thermiques dans le cas où l'état primaire avant le processus du chauffage était le désordre. Le fait qui a orienté l'étude vers l'utilisation de techniques de surface afin de déterminer la relation entre les anomalies thermiquement détectées et l'aspect de surface des alliages. L'étude a conduit à mettre en évidence un nouveau type de transition de phase métastable qui précède la réaction de mise en ordre dans les alliages d'or à basse température présentés en forme de précipitées sous forme de dendrite sur la surface. La participation de l'argent dans la composition de l'alliage conduit à accélérer la réaction de mise en ordre.

La composition binaire de 18 carats, a été étudiée d'une manière approfondie sur le plan structural. En utilisation la in-situ DRX avec une fréquence d'acquisition de données d'1 spectre / 1,1 min. Les séquences de transition de phase et les températures ont été déterminées à partir du fitting des data obtenus et à travers le suivi de l'évolution du comportement des intensités des pics typiques de chaque phase ainsi que le volume atomique normalisé.

L'analyse et l'interprétation des données expérimentales issues de la spectroscopie mécanique révèlent trois relaxations anélastiques importantes (processus de dissipation interne), qui dominent le spectre de perte mécanique de l'alliage binaire 18 carats au-dessus de la température ambiante. Une relaxation Zener, due à l'ordre directionnel des atomes dans la solution solide substitutionnelle, se produit à proximité de la transition de phase AuCuI - AuCuII lors du chauffage et le pic de relaxation Zener classique accompagne la transition de phase A1 - AuCuI + AuCuII durant le refroidissement. Un pic de des joints d'antiphase a été mis en évidence en tant que pic typique de l'AuCuII. Une pic de relaxation mécanique attribué au glissement des joints de grain dans la phase désordonnée A1.

Mots-clés: 12 et 18 carats, or, argent, cuivre, analyses thermiques, précipitation, dendrite, spectroscopie mécanique, anélasticité, dissipation interne, relaxation de Zener, relaxation des joints de macles, joints de grains

Abstract

This work is motivated by a scientific interest in gaining a better understanding of the phase transformations that govern the mechanical properties of gold alloys due to their huge industrial importance such as their common use in jewelry applications, luxury watch making, catalyses, electronic industries ...etc...

The selected alloys fall in one of two categories of yellow gold, based on the binary system of Gold-Copper and the ternary system Gold-Copper-Silver

In this thesis, selected alloys from the two categories are studied, using two principal compositions of 12 and 18-carat. The study starts primarily by the thermal identification of the possible anomalies that could happen during the heating from the room temperature up to 973K (temperature near to the industrial use -1023K). An expectable anomaly at low temperature has been noticed by the thermal analyses while the primary state before the heating process was the disorder. The fact that has orientate the study to the use of surface techniques in order to determine the relationship of the thermally detected anomalies with the surface aspect of the alloys. The study has lead to highlight new kind of metastable phase transition that precede the ordering reaction in gold alloys at low temperature presented in dendrite shape of precipitated phase on the surface. The participation of the silver in the alloy composition leads to accelerate the ordering reaction.

18-carat binary composition, has been treated in the thorough way in terms of structural study. Using the in-situ temperature XRD measurement with data acquisition frequency of 1 pattern/1.1min. Phase transition sequences and temperatures have been determined over the fitting of the obtained patterns and through the following of the behavior evolution of the intensities of the typical peak of every phase as well as the atomic volume occupancy.

The analysis and interpretation of the experimental data stemming from the mechanical spectroscopy reveal three important anelastic relaxations (internal dissipation processes), which dominate the mechanical loss spectrum of the binary 18-carat alloy above room temperature. A Zener relaxation, due to directional ordering of atoms in the substitutional solid solution, occurs nearby the phase transition AuCuI - AuCuII upon heating and the classic Zener relaxation peak accompanies the phase transition A1 - AuCuI + AuCuII upon cooling. An antiphase boundaries relaxation peak has been highlighted as typical peak of the AuCuII. Grain boundaries sliding relaxation peak has been attributed to the pure disordered phase

Keywords: 12 and 18-carat, gold, silver, copper, thermal analyses, precipitation, dendrite, mechanical spectroscopy, anelasticity, internal dissipation, Zener relaxation, twin boundary relaxation, grain boundaries sliding relaxation.